

Garcia Center for Polymers at Engineered Interfaces



AT STONY BROOK UNIVERSITY



Summer 2016



“The program has no set time limits. Research is a lifelong experience and we hope to remain a resource to our students long after ‘graduation’.”



The Garcia Center for Polymers at Engineered Interfaces was founded in 1996 and is named after the late Queens College professor Narciso Garcia, who was a pioneer in the integration of education and research. The Center focuses on the integration of materials research with tissue engineering, biomaterials, drug delivery systems, sustainable energy, nanocomposites, and recently, additive manufacturing. The Center also supports innovation through entrepreneurship and has multiple collaborations with industry and national laboratories, both in the US and abroad. For information on the numerous programs that are available please see our website at: <http://polymer.matscieng.stonybrook.edu>



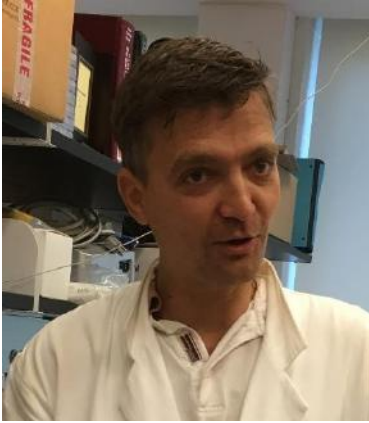
The research scholar program offers the opportunity for high school teachers and students to perform research on the forefront of polymer science and technology together with the Garcia faculty and staff. Students work as part of focus research teams and are taught to make original contributions of interest to the scientific community. In addition to entering national competitions, the students are encouraged to publish in refereed scientific journals, present their results at national conferences, and develop patents to protect their intellectual property. Our goal is to convey to the students the excitement we enjoy daily in research and provide for them a supportive network within the scientific community. Research is a lifelong experience and we hope to remain a resource to our students long after “graduation”.

Mina Rafailina

Jon Doktor

Aug. 10, 2016

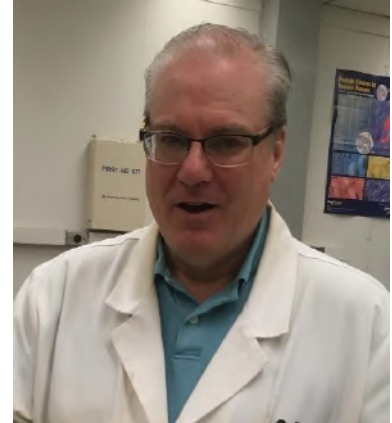
Faculty/Staff



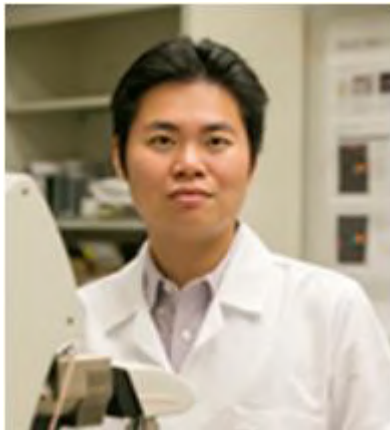
Steffen Mueller



Marcia Simon



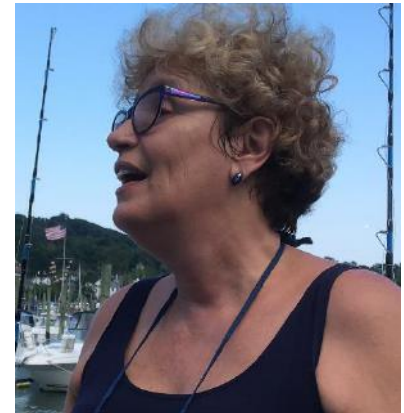
Stephan G. Walker



Chung-Chueh
(Simon) Chang



John Luckner Jerome



Adriana Pinkas-Sarafova



Dennis Galanakis



Dilip Gersappe

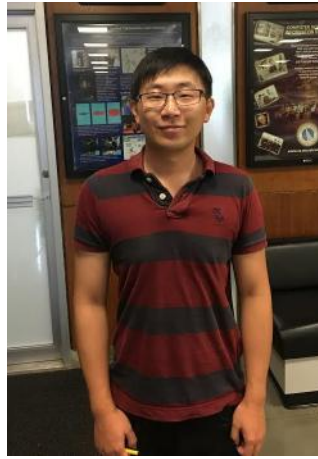


Zoe Auletta

Graduate Students



Clement Marmorat



Fan Yang



Linxi Zhang



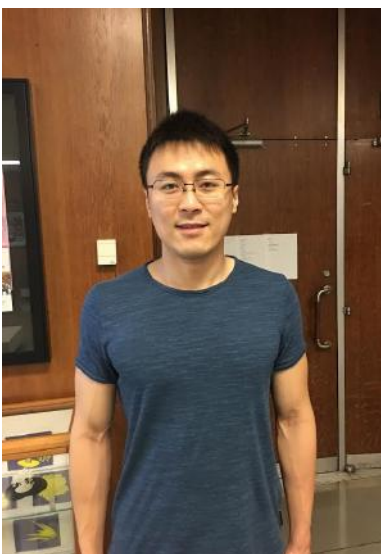
Julia Budassi



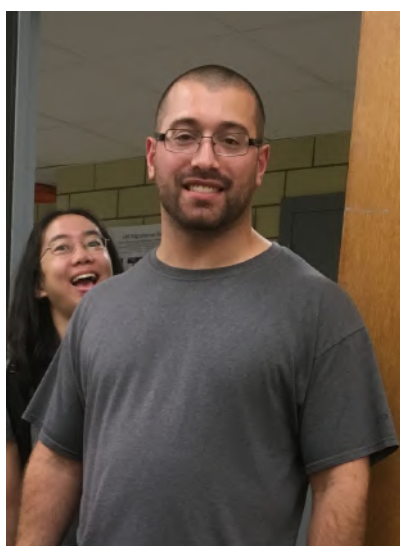
Kao Li



Yachen Chuang



Yichen Guo



Vincent Ricotta



Likun Wang

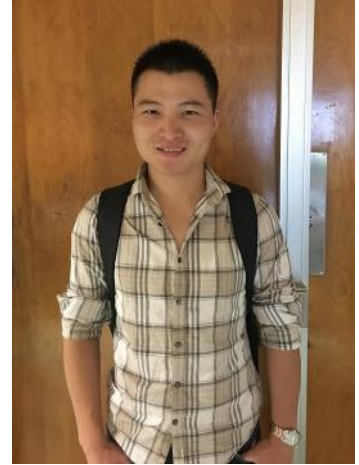
Graduate Students



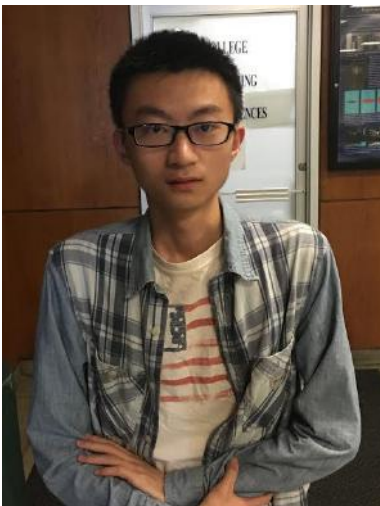
Xianghao Zuo



Yuval Shmueli



Zhenhua Yang



Juyi Li



Yuchen Zhin



Yan Xu



Hongfei Li



Kuan-che Feng



Yuan Xue

Graduate Students



Di Xu



Jiaolong



Linxi Zhang

Research Experience for Teachers (RET)



Herb Weiss



Gina Gabalski



Rebecca Isseroff

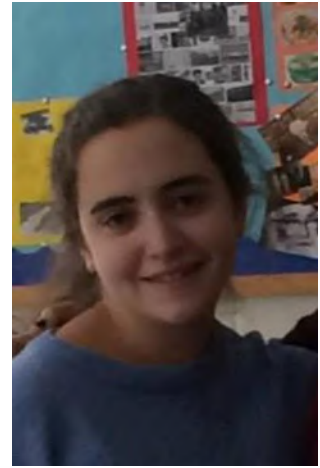
Research Experience for Undergraduates (REU)



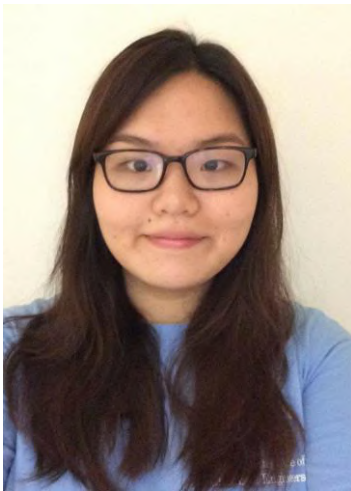
William Burnett



Gurkirat Singh



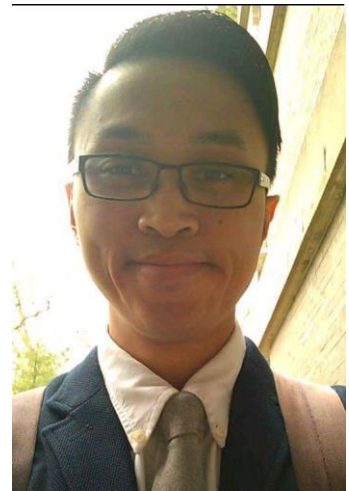
Bonnie Mendelson



Helen Liu



Junaid Khan



Donald Liu



Indeeep Singh



Landen Kwan



Simon Lin

Research Experience for Undergraduates (REU)



Matthew Brass



William Berger



Kevin Riegel



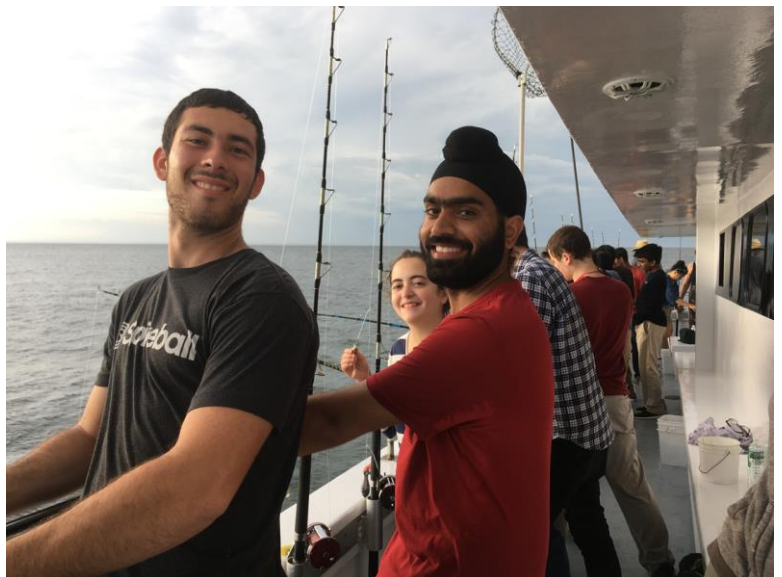
Da Qu



Abigail Wax



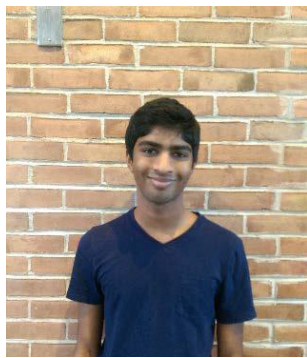
Jinyue Pan



High School Students



Somil Aggarwal



Ketan Agrawal



Sukrit Arora



Ashvik Awasti



Jesse Blatt



Katherine Cao



Antonio Carrero



Dalai Chadraa



Sharon Chao



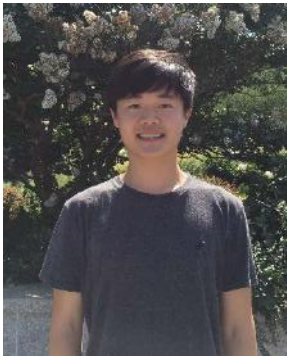
Bill Chen



Shannon Chen



Justin Chen



Mark Choi



Benjamin Dacek



Benjamin Davidson



Tiffany Ding



Jasmin Gao



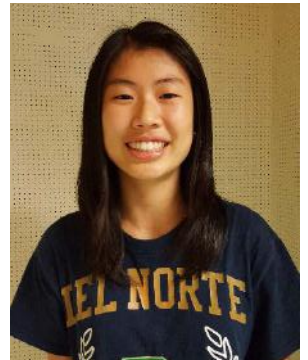
Marc Gottlieb



Allen Green



Tzvi Heimowitz



Rose Hong



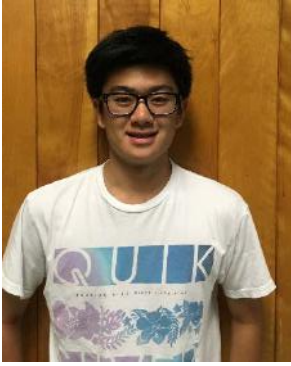
William Hu



Sharon Huang



Thomas Jiang



Michael Kao



Peyrin Kao



Maira Khan



Hari Kothapalli



Aviva Landau



Junyu Liang



Liana Lo



Trisha Madhavan



Justin Ng



Cecilla Orduna



Neha Parvathala



Vaidehi Patel



Shiv Patil



Michael Peng



Joshua Plaut



Samuel Plaut



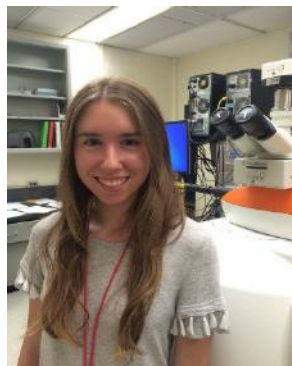
Miriam Radinsky



Paul Rhee



Adam Richter



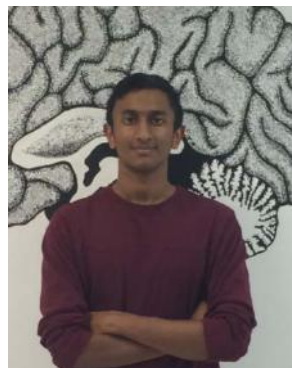
Rachel Sacks



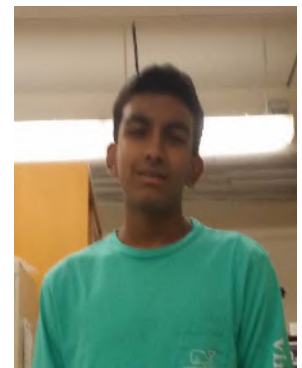
Yash Samantaray



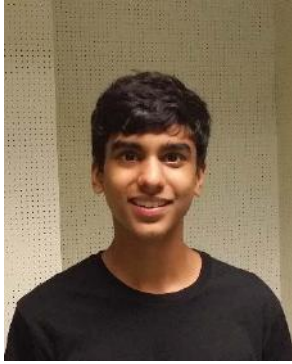
Gila Schein



Sujay Shankar



Kiran Shetty



Neal Soni



Natalie Tan



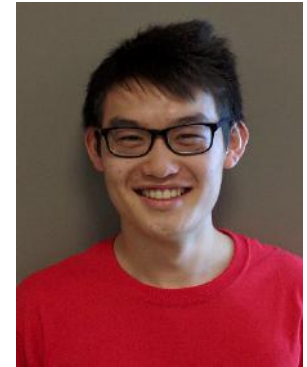
Sara Teitelman



Stefan Wan



Alexander Wang



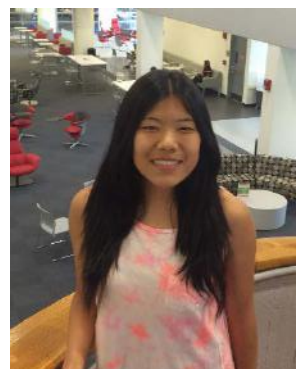
Justin Wang



Carolyn Wong



Yun Jin Woo



Alice Wu



Wilson H. Wu



Oliver Xu



Zixuan Xu



Michael Ye



Ryan Yoo



Jennifer Yu



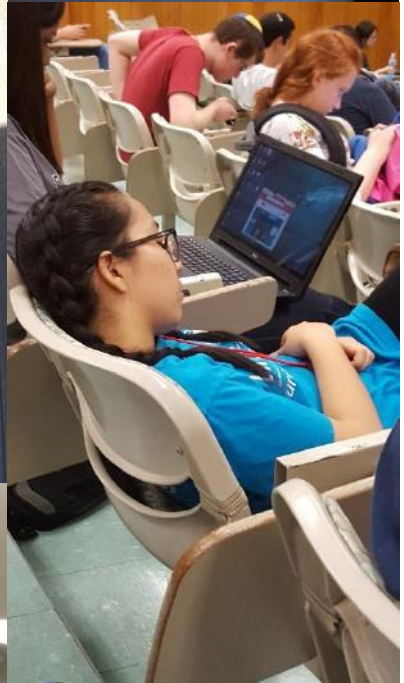
Nicholas G Zumba



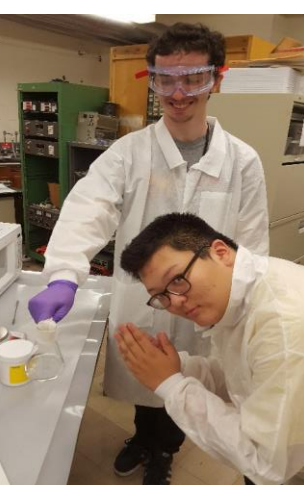
LABWORK....



SLEEPERS....



Memorable Moments....





Canoe Trip....

Fishing trip....



Visit to the American Museum of Natural History and NSLSII at BNL








Garcia: Polymers at Engineered Interfaces-2016 Summer Scholar Program Schedule of Activities



EVERY DAY STARTS WITH A GROUP MEETING

CHECK SCHEDULE DAILY!

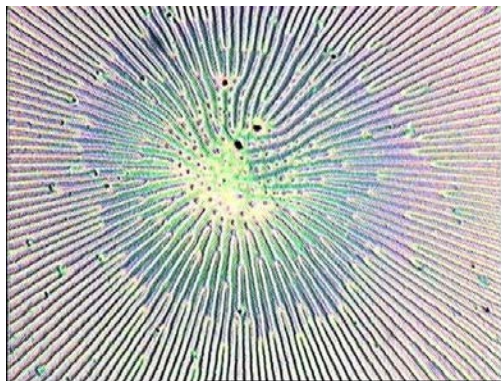
	MONDAY	TUESDAY	WEDNESDAY	THURSDAY	FRIDAY
	6/27	6/28	6/29	6/30	7/1
	<p>10:00 Welcome to Garcia</p> <p>Dr. Fotis Sotiropoulos, Dean CEAS</p> <p>Group picture: Greg Filiano, Media Relations</p> <p>10:15-10:45 Introduction</p> <p>Drs. Miriam Rafailovich and Adriana Sarafova</p> <p>10:45-11:45 3-D Printing in Neurosurgery Dr. Barry Lieber, Department of Neurosurgery</p> <p>12:00-1:30 ID cards and lunch at SAC</p> <p>1:45 Electronic Projects for Mobility Assist Gabriel Romero, Stealth Co.</p> <p>2:45-4:00 Campus Facility tour; HSC, SDM, LIRR</p>	<p>10:00 General meeting</p> <p>10:30 AM- 12:30 PM Library Resources and Intro to Excel Courses (2 Groups) Computer SINC site (room 2116); SBS SINC site (room 620)</p> <p>12:30 -1:15 Lunch</p> <p>1:30-2:15 The Science and Medicine of Blood Dr. Dennis Galanakis, MD</p> <p>2:15 -3:00 Prof. Mahn Won Kim, Physics, KAIST</p> <p>3:00-4:00 The ellipsometer: coherent and incoherent light--a hands on experience Dr. Jonathan Sokolov</p>	<p>10:00 General meeting</p> <p>10:30 Stem Cell Research Dr. Michael Hadjiargyrou</p> <p>11:30 Microbiology: bacteria in the oral cavity Dr Stephen Walker, Department of Oral Biology and Pathology</p> <p>12:30 PM Lunch</p> <p>1:15 PM - ISEF Regulations and Laboratory Ethics; Mr. Herb Weiss</p> <p>2:00 - 4:00 Facilities Tour: AFM, DSC, DMA, Cell Lab, FTIR,DLS, Zeta Potent Rheology,electrospinning Hands on safety training specific to Garcia labs with Dr. Simon Chang and Linxhi Zhang</p>	<p>10:00 General meeting</p> <p>10:30 Global Ethical Considerations in STEM: Dr. Brooke Ellison School of Health Tech and Management</p> <p>11:30 Drug Delivery Dr. Stella Tsirka, Department of Pharmacology</p> <p>12:30 Lunch</p> <p>1:15 Challenges in 3-D printing; Dr. Dan Slep Chem Cubed Co.</p> <p>2:15 (i) Magic of Graphene (ii) Keeping a Laboratory Notebook Ms. Rebecca Isseroff, Lawrence HS Science Research Coordinator</p> <p>3:15 Surface DNA Separation</p>	<p>10:00 General Meeting</p> <p>10:30 Mandatory Lab Safety Training w/ EH&S</p> <p>1:00 Pizza Lunch (Hunki's Plainview)</p> <p>1:15 Polymer rheology and spin casting Dr. Steven Schwarz, Department of Physics, Queens College</p>

<p>Week of 7/4 HOMEWORK on 7/5</p> <p>a) Quiz on safety and facilities b) Prepare ppt for journal club. Choose a research paper of interest to you. Prepare a 5 minute presentation summarizing the paper. Viewgraph 1: your name, school, title of paper, reference Viewgraph 2: Hypothesis V3: Materials/Methods V4: Results/Discussion V5: Conclusion/evaluation</p>	<p>7/4 Happy 4th of July </p>	<p>7/5</p> <p>10:00 General Meeting 10:05 Lab Safety and Facilities Quiz 10:50 Statistics part I Dr. Miriam Rafailovich 11:30 Nanotoxicology Dr. Tatsyana Mironava 12:20 Lunch 1:00 Burns and skin tissue engineering Dr. Marcia Simon, Oral Biology and Pathology, SDM 2:00 -2:30 Distribution of laboratory boxes 2:30 -4:00 Divide into groups for Journal Club Student Presentations REMEMBER: Bring box and appropriate laboratory dress on Wednesday.</p>	<p>7/6</p> <p>10:00 General Meeting Data Analysis and Statistics Part II Dr. Miriam Rafailovich 10:15 -4:00 Proper Laboratory Attire Group Experiment: Polymer Thin Film Processing: Recycling, Rheology, Determination of Mw Si Single Xtals Lab Data Analysis Polymer physics Short project descriptions: from bedbugs to solar cells 4:30 Game Night Softball: Ball fields across LIRR commuter parking </p>	<p>Dr. Jonathan Sokolov 7/7</p> <p>10:00 AM General Meeting Chemistry vs Chemical Engineering-choosing careers Dr. Carol Steiner, Chemical Engineering, City College 10:20-3:00 Group Experiment Cont: Proper Laboratory Attire Polymer Thin Film Processing: Recycling Rheology Determination of Mw Si Single Xtals Lab Data Analysis Polymer physics lecture: Short project descriptions: from bedbugs to solar cells ... -> Preparation of group ppt and lab reports. 3:00-4:00 Nano-Raman Molecular Imaging Dr. Gordon Taylor, SoMAS</p>	<p>7/8</p> <p>10:00 General meeting 10:30 Predicting Catalysis in hydrogen fuel cells using DFT: Dr. Ping Liu, BNL Chemsitry 11:30-1:30 Pizza Lunch and PPT presentations by the 7 spin casting groups. 1:30 VJ Technologies: “The Science and Technology of High Voltage and x-ray machines as it applies to applications featuring this technology”. MinhTran Weekend Homework: → Each student must submit a lab report by Midnight on Monday morning. → Remember to give proper acknowledgements to your group partners, REUs, Grads.</p>
--	---	---	---	---	---

<p>Week of 7/18</p>	<p>7/11 General meeting 10:15 Polymer Nanocomposite Research Dr. Jaeson Koo 11:15 Dental Pulp Stem Cells Dr. Adriana Sarafova 12:00 Lunch 1:00 Discussion of research topics Selection of Projects</p>	<p>7/12 General meeting 10:15 Gordon Taylor: Raham Research at SoMAS 11:15 Research at Estee Lauder 12:30 PM Lunch 1:00 Discussion of research topics Selection of Projects</p>	<p>7/13 General meeting 10:15 Intellectual Property Donna Tuminello 12:30 PM Lunch</p>	<p>7/14 General meeting 10:00 AM General meeting 10:30 AM WORK! 12:30 PM Lunch Fishing Trip</p> 	<p>7/15 10:00AM General meeting 12:30 PM Pizza Lunch 2:00 PM Dismissal</p>
	<p>7/18 General meeting 10:00 AM General meeting 10:30 AM WORK! 12:30 PM Lunch 1:30 PM Work</p>	<p>7/19 General meeting 10:00 AM General meeting CANOE TRIP!</p> 	<p>7/20 General meeting 10:00 AM General meeting 10:15 AM Richard Clark - Tissue engineering 11:00 AM WORK! 12:30 PM Lunch 1:30 PM Work</p>	<p>7/21 General meeting 10:00 AM General meeting 10:15 AM SOP Training By EHS 10:30 AM WORK! 12:30 PM Lunch 1:30 PM Work</p>	<p>7/22 10:00 AM General meeting 10:30 AM WORK! 12:00 PM Lunch BBQ</p> 

<p>Week of 7/25 Trip to BNL</p>	<p>7/25</p> <p>10:00 AM General meeting 10:30 AM WORK! 12:30 PM Lunch</p>	<p>7/26</p> <p>10:00 AM General meeting American Museum of Natural History Trip </p>	<p>7/27</p> <p>10:00 AM General meeting 10:30 AM WORK! 12:30 PM Lunch 3:30 Ice Cream and Student Presentations</p>	<p>7/28</p> <p>10:00 AM General meeting 10:30 AM WORK! 12:30 PM Lunch</p>	<p>7/29</p> <p>10:00 AM General meeting 10:30 AM WORK! 12:30 PMLunch</p>
<p>Week of 8/1</p>	<p>8/1</p> <p>10:00 AM General meeting 10:30 AM WORK! 12:30 PM Lunch 3:30 PM Ice Cream and Presentations</p>	<p>8/2</p> <p>10:00 AM General meeting 10:30 AM WORK! 12:30 PM Lunch 3:30 PM Ice Cream and Presentations</p>	<p>8/3</p> <p>10:00 AM General meeting 10:30 AM WORK! 12:30 PM Lunch 3:30 PM Ice Cream and Presentations</p>	<p>8/4</p> <p>10:00 AM General meeting 10:30 AM Dr. Debra Cinotti Admission to SOM 12:30 PM Lunch 3:30 PM Ice Cream Presentations</p>	<p>8/5</p> <p>10:00 AM General meeting 10:30 AM WORK! 12:30 PM Pizza Lunch</p>
<p>Week of 8/8</p>	<p>8/8</p> <p>10:00 AM General meeting 10:30 AM WORK! 12:30 PM Lunch</p>	<p>8/9</p> <p>10:00 AM General meeting 10:30 AM WORK! 12:30 PM Lunch</p>	<p>8/10</p> <p>Garcia Program Symposium SAC Ballroom A Stony Brook 10:00 am - 2:00 pm </p>		

Courtesy Jennifer Yu



Garcia Summer Research Symposium 2016

10:00 Student String Quartet

Professor John Luckner Jerome, Julia Budassi,
Maira Kahn, Carolyn Wong

10:10 Welcome: Professor Charles S. Taber

Interim Provost and Senior VP for Academic Affairs

10:20 Plenary Lecture: Dr. Radoslav Adzic

Senior Chemist, Chemistry Division, Brookhaven National Laboratory

Student Research Presentations

Sustainable Energy

10:30 I. Hydrogen Fuel Cells

Co- Chairs: Kevin Riegel and Indeeep (Jimmy) Singh, Stony Brook University

Coating Nafion Membranes with Gold-Palladium Nanoparticles to Improve the Performance of Polymer Electrolyte Membrane Fuel Cells.

Ryan Yoo West Ranch High School, Santa Clarita, CA

Optimizing Electrode Catalyst Efficiency and DFT Modeling of CO Oxidation in Proton Exchange Membrane Fuel Cells.

Tommy Jiang Edina High School, Edina, MN,

Stefan Wan A.W. Dreyfoos School of the Arts, West Palm Beach FLA,

Justin Wang Irvine High School, Irvine, CA

Utilizing Gold-Platinum alloy Nanoparticles to Enhance the Performance of a Proton Exchange Membrane Fuel Cell

Yash Samantaray Syosset High School, Syosset, NY,

Tzvi Heimowitz DRS Yeshiva High School for Boys, Woodmere, NY,

Aviva Landau Yeshiva University High School for Girls, Hollis, NY

Graphene Oxide Enhanced Proton Exchange Membrane Fuel Cell

Gen Yuan (Bill) Chen Prince of Wales Secondary High School, Vancouver, BC Canada

Synthesis and Characterization of Reduced Iron Graphenes

Allen Green Lawrence High School Cedarhurst, NY

10:45 II. Solar Power Generation

Co-Chairs: Jinyue Pan and Da Qu, Stony Brook University

Enhancing the Efficiency of PCDTBT:PCBM Bulk Heterojunction Organic Solar Cells Through the Use of Ternary Polymer Blends

Ketan Agrawal Columbus Academy, Gahanna, OH,

Hari Kothapalli The Roxbury Latin School, West Roxbury, MA

Optimizing the Efficiency of Solar to Hydrogen Conversion and Water Purification in a Model Irrigation System: A Comparative Analysis of Power Efficiency Commercial PVC-HFC and Self-Designed PEC-HFC Renewable Energy Technology

Antonio Carrero, Stony Brook University,

Maira Kahn H. Frank Carey High School, Franklin Square, NY

Assessing the Power Conversion Efficiency and Nanoscale Morphology of Photovoltaic Cells with High Molecular Weight Polystyrene Additives

Shiv Patil, Kiran Shetty Half Hollow Hills High School East, Dix Hills, NY

Enhancing the Efficiency of Bulk Heterojunction Polymer Solar Cells via Mechanical Chain Alignment

Dalai Chadraa Redmond High School, Redmond, WA

10:55 Dental Pulp Derived Cells

Chair: Bonnie Mendelson, University of Pennsylvania

Investigating the Effects of Nanoscale Surface Topography and Cell-Plating Density on the Proliferation and Differentiation of Dental Pulp Stem Cells

Alice Wu Half Hollow Hills High School West, Dix Hills, NY,

William Hu Saratoga High School, Saratoga, CA ,

Katherine Cao Homestead High School, Mequon WI

Comparison of Dental Pulp Cells' Response to Different PLA Composites (Molded vs. Printed)

Justin Ng, George W. Hewlett High School, Hewlett, NY

Nicholas Zumba George W. Hewlett High School, Hewlett, NY

Characterization of Injectable Enzymatically Cross-Linked Gelatin Based Hydrogels with Encapsulated Dental Pulp Stem Cells for Dental Pulp Tissue Regeneration

Neha Parvathala Desert Vista High School, Phoenix, AZ

Odontogenic Differentiation of Human Dental Pulp Stem Cells on Fibrin Gel Scaffolds for Applications in Regenerative Endodontics

Rose Hong Del Norte High School, San Diego, CA, **Jasmin Gao** Northview High School, Johns Creek, GA

11: 10 Bio Based Devices

Chair: Matthew Brass, University of Rhode Island

Synthesis of a Novel Biomaterial for Blood Vessel Constructs

Sujay Shankar A&M Consolidated High School, College Station, TX

The Effect of TiO₂ Nanoparticles on the Heat Transfer and Effectiveness of Mosquito Repellant Cream

Peyrin Kao Diamond Bar High School, Diamond Bar, CA

Synthesis of Testing Rapid Zika Biosensor by Analyte Imprinting Method on Gold Plated Silicon Wafers

Sharon Huang Morrison Academy, Taichung, Taiwan,

Trisha Madhavan Cinco Ranch High School, Katy TX,

Carolyn Wong Morristown High School, Morristown, NJ

11: 20 Modeling and Simulation

Chair: Landen Kwan, Stony Brook University

Computer Simulations of Physically Crosslinked Gels Using Classical Molecular Dynamics

Alex Wang Miramonte High School, Orinda, CA

Lattice-Boltzmann Modeling of Anode Morphologies for Lithium-Ion Cells

Wilson Wu Valley Christian High School, San Jose, CA

Lattice-Boltzmann Modeling of Water Uptake in Gecko Setae

Zixuan (Alex) Xu Shenzhen Middle School, Shenzhen, Guangdong

Nanocomposites

11:30 I. Gas Permeability:

Chair: Helen Liu Stony Brook University

Gurkirat Singh, Stony Brook University

Mechanical Properties of HIPS/C-RDP Nanocomposites

Samuel Plaut Rambam Mesivta High School, Lawrence, NY

The Effects of Cellulose Micro Particles on the Gas Permeability and Mechanical Properties of Poly(lactic) Acid

Ashvik Awasti, Princeton High School, Princeton, NJ

11:40 II. 3D FDM Printing, Biodegradable & Flame Retardant Materials

Chair: William Berger, Duke University

Graphene Nanocomposites for 3D-Printing Filaments
Justin Chen, Arcadia High School Arcadia CA

Thermal and Structural Properties of PLA/Graphene Filaments in FDM 3D Printing
Michael Ye Syosset High School, Syosset, NY,
Sukrit Arora St. Francis High School Mountain View, CA,
Ben Dacek South Side High School, Rockville Centre, NY

Investigating the Mechanical and Flame Retardant Properties of PLA-based Biodegradable Nanocomposites
Cecilia Orduna Ward Melville High School, East Setauket, NY,
Jesse Blatt Half Hollow Hills High School East, Dix Hills, NY,
Liana Lo South Side High School, Rockville Centre, NY

Investigating the Role of MoS₂ in Flame Retardant EVA
Paul Rhee, Half Hollow Hills High School East, Dix Hills, NY,
Yun Jin Woo, Half Hollow Hills High School West, Dix Hills, NY

Compatibilization of EVA/HDPE Blend Using RDP Coated Graphene
Marc Gottlieb, HAFTR High School, Cedarhurst, NY
Joshua Plaut, HAFTR High School, Cedarhurst, NY

11:55_Hydrogels and Colloids

Chair: Simon Lin, Stony Brook University

Contact Angle of Fluids on Pluronic F127 and Gelatin Hydrogels
Jennifer Yu Mission San Jose High School, Fremont, CA

Transdermal Delivery of Curcumin Using Microemulsions as Vehicles and Effect of Curcumin on Human Dermal Fibroblasts
Sara Teitelman Yeshiva University High School for Girls, Hollywood, NY

Characterization of Pluronic F127 Degradation Patterns and Drug Release to Mimic Post-laminectomy *in vivo* Conditions
Somil Aggarwal Jamesville-Dewitt High School, Fayetteville, NY,
Michael Kao Troy High School, Fullerton, CA,
Neal Soni Staples High School, Westport, CT

12:05_Separating DNA on Surfaces

Co-chairs: Demian Zuric, Macaulay Honors College at Baruch and **Donald Liu**, SBU

Utilization of Laser Interference Lithography as a Novel Method for Synthesizing Sub-micron Soft Gratings for Applying Interference Cutting Enzymes to Surface-absorbed DNA

Junyu Liang Guangdong Experimental High School, Guangzhou, Guangdong, China
Adam Richter Munster High School, Munster, IN

12:10 Nanotoxicology

Chair: Abigail Wax, University of Pennsylvania

The Effects of Titanium Dioxide Nanoparticle Exposure on the Keratinocyte and U937 Cell Susceptibility to Bacterial Infection

Natalie Tan Herricks High School, New Hyde Park, NY,

Sharon Chao Stuyvesant High School, NY, NY

The Effect of Different Concentrations of TiO₂ Nanoparticles on Dental Pulp Stem Cells (DPSCs) Plated on Thin and Thick Polybutadiene Films

Vaidehi Patel Half Hollow Hills High School East, Dix Hills, NY

Evaluating the Cytotoxic Response of Adult Human Dermal Fibroblasts to Hybrid Bismuth Oxyhalides of Varying Concentrations

Michael Peng Campbell High School, Smyrna, GA

12:20 Cells on Natural and Electrospun Fibers

Co-chairs: William Burnett Rochester Institute of Technology and **Junaid Khan** SBU

Effects of Cancerous Extracellular Matrix on Healthy Keratinocytes

Yutong (Oliver) Xu Edina High School, Edina MN

The Effect of Sulfonated Polystyrene and Graphene Oxide/Reduced Graphene Oxide Functionalized with Gold and Silver Nanoparticles on the Extracellular Matrices of Fetal Bovine and Serum Dental Pulp Stem Cells

Rachel Sacks, HAFTR High School, Cedarhurst, NY

Gila Schein, HAFTR High School, Cedarhurst, NY

A Comparison of the Biological and Mechanical Properties of Poly (4-Vinylpyridine) and Polystyrene Tissue Culture Plastic

Ben Davidson Campbell High School, Marietta, GA

Effects of Electrospun P4VP Fiber Structure and Thin Film Composition on the Biomineralization and Proliferation Rate of Dental Pulp Stem Cells

Mark Choi Mission San Jose High School, Fremont CA,

Hong-Hsuan Chen Saratoga High School, Saratoga CA

The Effect of Fibronectin and P12 on Human Dermal Fibroblast Migration on PLA and PMMA Fibrillar Substrates

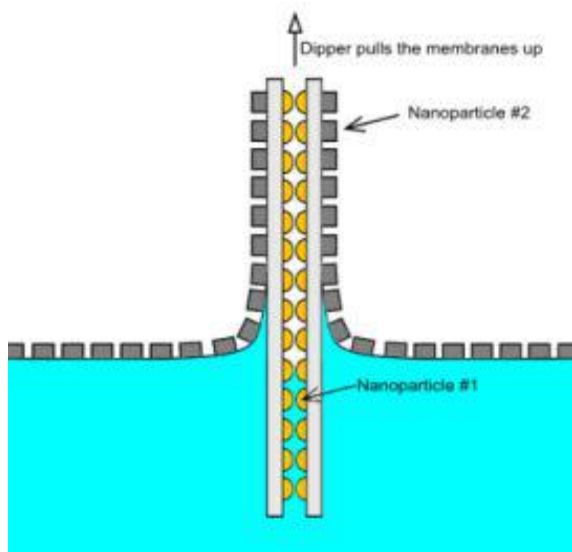
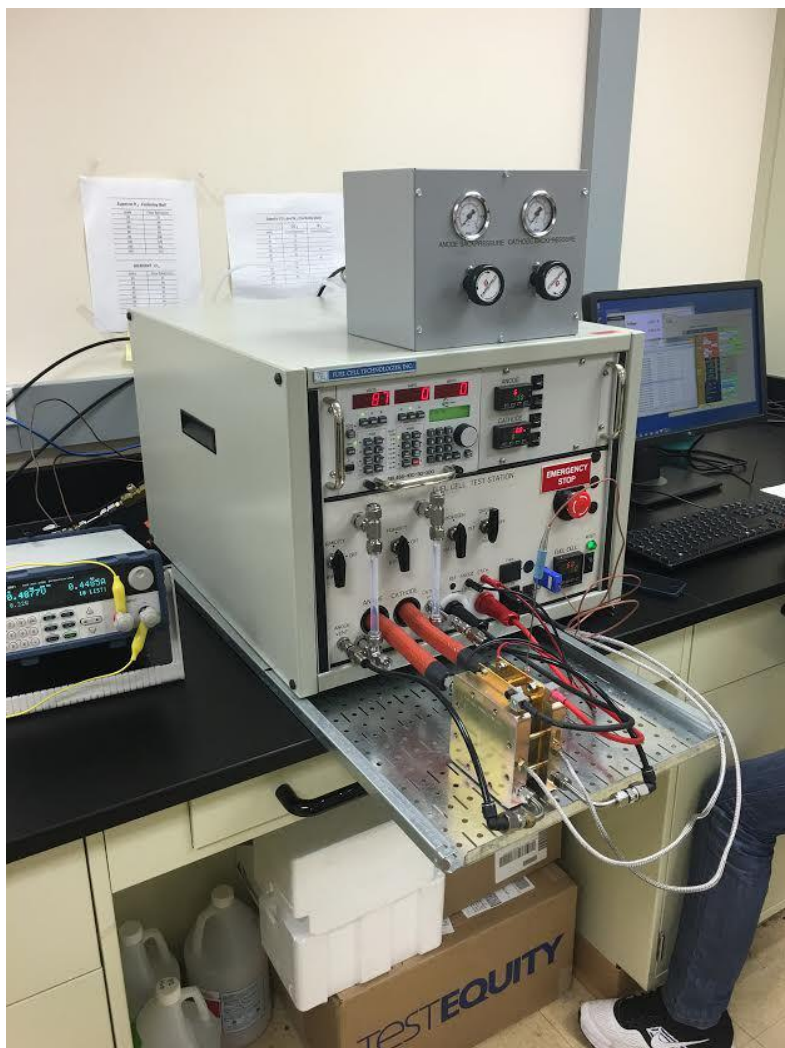
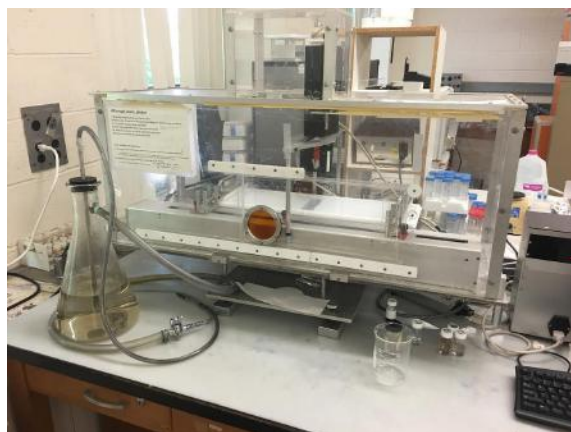
Tiffany Ding Emma Willard School, Troy, NY,

Miriam Radinsky Yeshiva University High School for Girls, Holliswood, NY

12:30 Buffet Luncheon: *Wing Wan of West Hempstead*

Session I: Sustainable Energy

**Graduate Students: Hongfei Li, Likun Wang,
Yuchen Zhin, Zhenhua Yang**

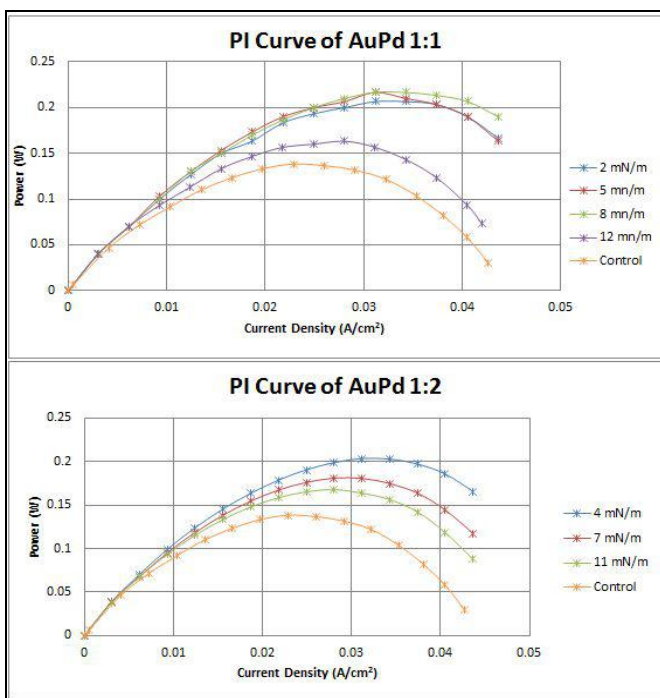


Coating Nafion Membranes with Gold-Palladium Nanoparticles to Improve the Performance of Polymer Electrolyte Membrane Fuel Cells

Ryan Yoo¹, Kevin Riegel², Hongfei Li³, Likun Wang³, Miriam Rafailovich³,

¹West Ranch High School, 26255 Valencia Blvd, Santa Clarita, CA 91381, USA; ²Stony Brook University, NY 11794, USA; ³Department of Chemical and Molecular Engineering, Stony Brook University, NY 11794, USA

Polymer electrolyte membrane fuel cells (PEMFCs) show great promise as a future leading source of renewable energy, as they are compact and leave waste only in the form of water. While the PEMFC has the potential to be a great future source of clean energy, one of the greatest obstacles to widespread PEMFC use is carbon monoxide (CO) poisoning of the electrodes. When CO forms through the reverse water gas shift reaction, it bonds with platinum present in the electrodes, halting the oxidation process and decreasing efficiency.¹ It was discovered that this degradation can be mitigated by coating the polymer membranes with gold (Au) nanoparticles, resulting in decreased degradation rates of up to 40% improvement.² To see if similar results would occur with Au alloys, this lab researched the effects of a gold-palladium (AuPd) alloy on a PEMFC.



Thiol-functionalized AuPd nanoparticles at ratios of 1:1 and 1:2 were synthesized through the two phase method.³ Three 4cm x 4cm Nafion® [117] membranes were coated with the 1:1 AuPd nanoparticle solution via a monolayer formed on the Langmuir-Blodgett Trough (KSV 3000) at various surface pressures (5 mN/m, 8 mN/m, 12 mN/m).² Results indicated increased performance with lower surface pressure, so another membrane of 1:1 AuPd was coated at a surface pressure of 2 mN/m. Three additional 4cm x 4cm membranes were then coated with the 1:2 synthesized AuPd nanoparticles at surface pressures of 4 mN/m, 7 mN/m, and 11 mN/m.

The membranes were then tested in an H-Tec Demonstration Kit, acting as an MEA (membrane electrode assembly) fuel cell. Tests of each membrane were run from 0.000 A to 0.700 A at ~0.050 A intervals, with each interval

~30 seconds long, to measure at what current a membrane generated its maximum power.

Between the two AuPd alloy ratios, 1:1 generally had better performances than 1:2, with the 1:1 alloys reaching maximum powers of .215 W, .220 W, and .221 W at 2 mN/m, 5 mN/m, and 8 mN/m, respectively—the greatest of these, the 1:1 membrane coated with a surface pressure of 8 mN/m, showed a 62.5% increase over the control. In both alloy ratios, performance was lowest with the highest surface pressures (Figure 1).

Future work would involve conducting further tests on each membrane, coating additional membranes for each alloy, synthesizing further ratios of AuPd, such as a 2:1 ratio, and researching the effects of different gases (free air vs. pure oxygen, partial CO vs. pure H₂) on performance. This last possible experiment, in addition to TEM or DFT analysis of the AuPd nanoparticles, could help in research on how to directly combat CO poisoning.

¹Baschuk, J. J., & Li, X. (2001). Carbon monoxide poisoning of proton exchange membrane fuel cells. *International Journal of Energy Research*, 25(8), 695-713

²Li, H.; Pan, C.; Zhao, S.; Liu, P.; Zhu, Y.; & Rafailovich, M. H. (2016). Enhancing performance of PEM fuel cells: Using the Au nanoplatelet/Nafion interface to enable CO oxidation under ambient conditions. *Journal of Catalysis*, 339, 31-37, doi:10.1016/j.jcat.2016.03.031

³Brust M.; Walker, M.; Bethell, D.; Schiffrin, D. J.; & Whyman, R. (1994). Synthesis of thiol-derivatized gold nanoparticles in a two-phase Liquid-Liquid system, *J. Chem. Soc., Chem. Commun.*, 1994,(7), 801

Optimizing Electrode Catalyst Efficiency and DFT Modeling of CO Oxidation in Proton Exchange Membrane Fuel Cells

Tommy Jiang, Edina High School, 6754 Valley View Rd., Edina, MN
Stefan Wan, A. W. Dreyfoos School of the Arts, 501 S Sapodilla Ave., West Palm Beach, FL
Justin Wang, Irvine High School, 4321 Walnut Ave., Irvine, CA
Landen Kwan, Stony Brook University, Stony Brook, NY

Hongfei Li, Department of Materials Science & Engineering, Stony Brook University, Stony Brook, NY
Likun Wang, Department of Materials Science & Engineering, Stony Brook University, Stony Brook, NY
Miriam Rafailovich, Department of Materials Science & Engineering, Stony Brook University, Stony Brook, NY

Growing concerns about the use of fossil fuels demand innovative technologies for viable, alternative energy sources. Proton exchange membrane fuel cells (PEMFCs), a zero-emission fuel source incorporating reverse electrolysis to power a load, present a practical solution. In general, PEMFCs exhibit superb performance with much higher efficiency than fossil fuels, but their vulnerability to carbon monoxide (CO) poisoning inhibits their applications in transportation and general infrastructure^[1]. The objective of this study is to examine electrode and membrane enhancement for increased CO tolerance in PEMFCs. We integrated a theoretical investigation of CO oxidation using the density functional theory with a permutation of laboratory tests involving modifications of both electrodes and membranes. Density functional theory (DFT) has received considerable attention in the fields of physical chemistry and materials science for its ability to accurately model the electronic structure of atoms and many-body systems. We used DFT to model various nanoparticles and their effects on CO oxidation in order to minimize CO poisoning. By varying catalyst materials and methods of preparation, the modeling results help find the most efficient usage of catalyst, thereby providing practical direction for laboratory testing.

Modifications of electrodes and membranes were conducted in the laboratory with an isothermal curve developed to determine the optimal target pressure for coating the Au alloys onto the Nafion® membranes. By varying the pressure on the Langmuir-Blodgett trough (LB trough), a monolayer of Au alloys or graphene oxide (GO) was created onto the membrane for use in the PEMFC. GO-coated commercial electrodes were also created through use of the LB trough. To overcome the problem of uneven distribution of catalyst on commercial electrodes, gas diffusion electrodes were synthesized through spraying Pt/C ink onto carbon cloth at the same catalyst loading with commercial electrodes. GO-coated ink-sprayed electrodes were prepared by applying a separate layer of GO ink through spraying. Results indicated that ink-sprayed gas diffusion electrodes with a normal membrane produced more power than their commercial counterparts (0.19W vs. 0.15W), likely due to the fact that the ink-sprayed gas diffusion electrodes provided a more homogenous layer of catalyst than the commercial electrodes. With commercial electrodes, Au alloy and GO enhanced membranes elevated power output to 0.22W and 0.27W, respectively. GO-coated electrodes with commercial membranes demonstrated similar enhancements to GO-coated membranes with commercial electrodes (0.27W) (Fig. 1). However, ink-sprayed electrodes did not increase power output with Au alloy and GO enhanced membranes due to the instability of the catalyst ink when exposed to Au alloys or GO membranes, suggesting that improvement of the durability of the ink catalyst in a hydrated environment is a technical issue to be solved in future research.

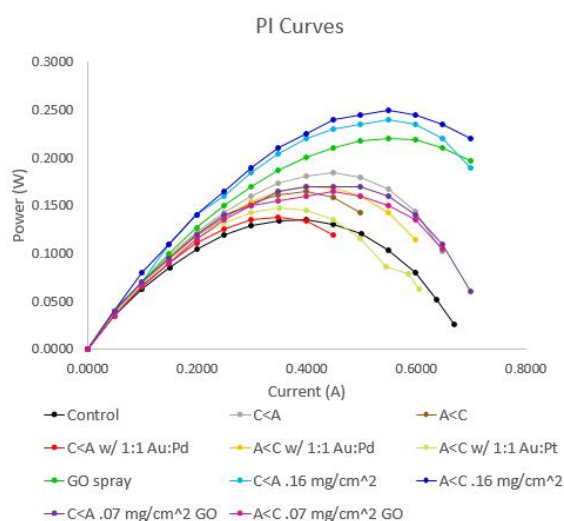


Fig 1. PI curves for all MEA combinations

System	a.u.	eV
Au shell	-1625.927075	-44243.10163
Pt	-118.9618662	-3237.07134
CO	-113.156465	-3079.100568
Au-CO	-1739.149432	-47323.99519
Pt-CO	-232.3697493	-6323.013248
Pt@Au	-1745.166827	-47487.73452
Pt@Au-CO	-1858.338262	-50567.24244
Calculation	eV	
Au-CO - Au shell - CO	-1.7929893	
Pt-CO - Pt - CO	-6.84134037	
Au@Pt CO - Au@Pt - CO	-0.40735547	

Fig 2. Total and binding energies for CO oxidation

Au nanoparticles are known to enhance CO oxidation^[2]. The enhancement of CO oxidation with alloyed Au nanoparticles was investigated using DFT calculations in Gaussian 03. Alloys of Pt@Au₁₂ and Pd@Au₁₂ were tested to see whether their binding energies when associated to CO were lower than that of CO bonded to a bare Au₁₂ shell. In order to evaluate these energies, thirteen molecular models were optimized to their lowest total energies. To calculate binding energy, total energy of the system was subtracted from that of the bare cluster and CO. Results showed that Pt-Au nanoparticles decreased CO binding energy by 1.39 eV, a significant decrease from the original -1.79 eV CO binding energy when bonded with Au nanoparticles (Fig. 2). Pd-Au nanoparticle results are yet to be completed.

[1] Bruijn, F. D., Papageorgopoulos, D., Sitters, E., & Janssen, G. (2002). The influence of carbon dioxide on PEM fuel cell anodes. *Journal of Power Sources*, 110(1), 117-124. doi:10.1016/S0378-7753(02)00227-6
[2] Phala, N. S., Klatt, G., & Steen, E. V. (2004). A DFT study of hydrogen and carbon monoxide chemisorption onto small gold clusters. *Chemical Physics Letters*, 395(1-3), 33-37. doi:10.1016/j.cplett.2004.07.065

Utilizing Gold-Platinum Alloy Nanoparticles to Enhance the Performance of a Proton Exchange Membrane Fuel Cell

Yash Samantaray¹, Tzvi Heimowitz², Aviva Landau³, Indeeep Singh⁴, Kevin Riegel⁴, Likun Wang⁴, Hongfei Li⁴, Miriam Rafailovich⁴

¹Syosset High School, Syosset, NY 11791; ²DRS Yeshiva High School For Boys, Woodmere, NY 11598; ³Yeshiva University High School For Girls, Hollis, NY 11423; ⁴Department of Materials Science and Engineering, State University of New York at Stony Brook, Stony Brook, NY 11794

With ever increasing demands for forms of clean renewable energy, PEM (proton exchange membrane) fuel cells have gained interest in the past few years. In these fuel cells, energy is created from hydrogen gas with the only byproduct being water.¹ Over time, carbon monoxide from the air and what is formed in the fuel cell from the reverse water gas shift reaction bonds with platinum, blocking its ability to catalyze reactions at the anode and cathode.² This CO contamination decreases the efficiency of PEM fuel cells, making it harder to implement these fuel cells as long-term sources of energy.² It has been found that coating the membrane with gold nanoparticles reduces CO poisoning by up to 50%.¹

Hydrophobic, thiol-functionalized gold-platinum nanoparticles at ratios of 1:1 and 2:1 were synthesized through the modified two-phase Brust Method.^{1,3} Six Nafion® 117 membranes were coated with the AuPt alloy nanoparticles using a Langmuir Blodgett Trough (KSV 3000). Three were coated with AuPt 1:1 nanoparticles at different surface pressures using the LB trough. The three surface pressures were 2 mN/m, 5 mN/m, and 8 mN/m. All three coatings had a monolayer of nanoparticles. Another three were coated with AuPt 2:1 nanoparticles at surface pressures of 5 mN/m, 8 mN/m, and 11 mN/m. This time, the membranes coated with a surface pressure of 5 mN/m and 8 mN/m had monolayers of nanoparticles, however the membrane coated with a surface pressure of 11 mN/m had a multilayer of nanoparticles. This was done to test the difference in efficiency between a monolayer and a multilayer of nanoparticles on the membrane.

After coating, the membranes were then tested in a single stack hydrogen fuel cell (H-Tec Demonstration Kit). Tests were run with multiple currents ranging from 0.000 A to 0.700 A at 0.050 A intervals and used to calculate the maximum power for each membrane. The voltage was measured as the current increased (Figure 1).

The Nafion® membrane coated with AuPt 1:1 nanoparticles at a surface pressure of 2 mN/m showed the greatest increase in power output over the control with a

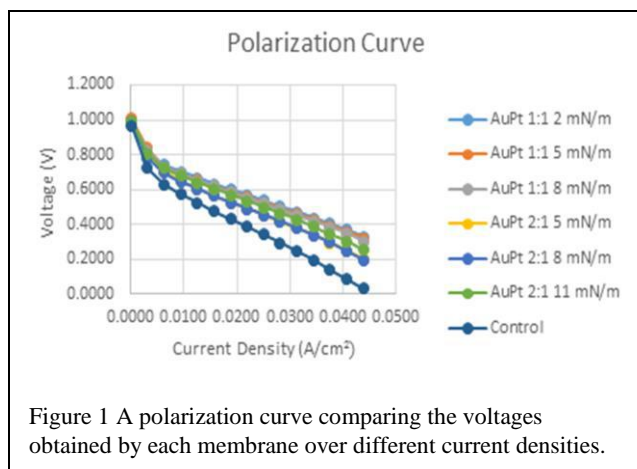


Figure 1 A polarization curve comparing the voltages obtained by each membrane over different current densities.

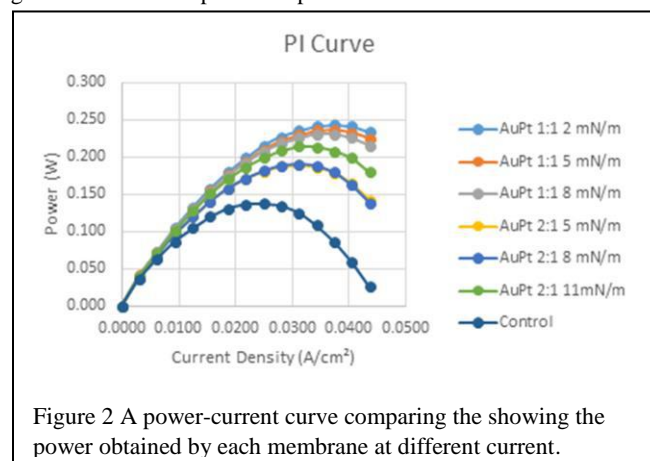


Figure 2 A power-current curve comparing the showing the power obtained by each membrane at different current.

maximum power of 0.244 W, which was a 76.8% increase over the control (Figure 2). Overall, the AuPt 1:1 nanoparticles showed a higher enhancement of the maximum power obtained by the PEM fuel cell when compared to the AuPt 2:1 nanoparticles.

In the future, more trials will be completed, and particles in a 1:2 ratio will be synthesized and used to coat membranes. Certain other conditions during the fuel cell testing will be altered, such as using pure oxygen instead of air to see if the AuPt is catalyzing the water gas shift reaction or assisting the catalysis reactions in the anode and cathode. Additionally, the particles will be viewed using a TEM to see the morphology of the gold-platinum alloy nanoparticles.

1. Li, H., Pan, C., Zhao, S., Liu, P., Zhu, Y., & Rafailovich, M. H. (2016). Enhancing performance of PEM fuel cells: Using the Au nanoplatelet/Nafion interface to enable CO oxidation under ambient conditions. *Journal of Catalysis*, 339, 31-37. doi:10.1016/j.jcat.2016.03.031
2. Baschuk, J. J., & Li, X. (2001). Carbon monoxide poisoning of proton exchange membrane fuel cells. *International Journal of Energy Research*, 25(8), 695-713.
3. Brust M.; Walker, M.; Bethell, D.; Schiffrin, D. J.; & Whyman, R. (1994). Synthesis of thiol-derivatised gold nanoparticles in a two-phase Liquid-Liquid system, *J. Chem. Soc., Chem. Commun.*, 1994,(7), 801

Graphene Oxide Enhanced Proton Exchange Membrane Fuel Cell

Gen Yuan (Bill) Chen¹, Hongfei Li², Likun Wang², Miriam Rafailovich², Helen Liu³

1. Prince of Wales Secondary School 2250 Eddington Drive, Vancouver, BC, Canada;
2. Department of Material Science and Engineering, SUNY Stony Brook, NY 11794;
3. SUNY Stony Brook, NY 11794;

As the detrimental effects of fossil fuel on the environment are becoming more evident and predictable, demands for alternative energy with low emission and high efficiency has been on the rise. Hydrogen fuel cell has emerged as a promising area of development with high theoretical efficiency limits and practically zero emission. However, costs of manufacturing and poor actual performance has rendered its cost per unit of energy higher than other types of energy sources, marking the difficulties to compete with existing unsustainable energy resources.

We hoped to address these problems through improving the performance of Proton Exchange Membrane Fuel Cell (PEMFC), a type of fuel cell applicable to various everyday energy needs due to its low operation temperature and the excellent mechanical stability of its polymer electrolyte. However, it presents a set of challenges: namely the demand of extremely high purity fuel source and difficulty in proper hydration of the membrane. Its need for high purity fuel source stems from the well-known poisoning phenomenon of the Pt catalyst by CO. CO concentrations as low as 10ppm can significantly reduce the efficiency of the fuel cell by adsorbing to Pt catalysts and occupying its active sites. The requirement for high purity fuel source further contributes to cost. The polymer electrolyte in PEMFC also requires proper hydration to achieve full performance as its proton conductivity is greatly affected by dehydrations.

We hypothesized that graphene oxide could improve the performance fuel cells due to its high water uptake potential, proton conductivity^[1] and theorized CO oxidation potential^[2], all of which could improve the performance of H₂/O₂ PEMFCs.

Graphene Oxide (GO) powder is purchased (Graphene Supermarket) and dissolved in various solvents (Methanol/DI water, Isopropanol/DI water, DMF). Solutions were sonicated, stirred overnight and further sonicated before use. Attempts to obtain isothermal curve for each solutions using LB trough (KSV 5000) and Tensiometer attached to Wilhelmy plate were made but pressure failed to build due to GO flakes sinking beneath the subphase surface. The surface pressure was however maintained at 1mN/m and Nafion™ 117 membranes were coated anyways at 1mN/m target surface pressure without further attempts to alter surface morphology. The membranes were then tested in H-tech PEMFC kit with open air environment at cathode and pure Hydrogen fed into anode. Polarization curves and power performance curves were collected. These were compared and fuel cell coated with graphene oxide dissolved with isopropanol was found to have the best performance with as much as 81% improvement in maximum power over control (Fig.1). GO was also coated onto electrodes using the same LB method and similar improvement in performance was recorded.

The hypothesis of improved performance through CO oxidation was tested by replacing the open air environment at cathode with high purity oxygen. An improvement of more than 40% (Fig.2) in the absence of CO indicates the incompleteness of the CO oxidation model. Other hypotheses must be tested in the future to find the exact mechanism for the improvement in performance and durability should also be investigated.

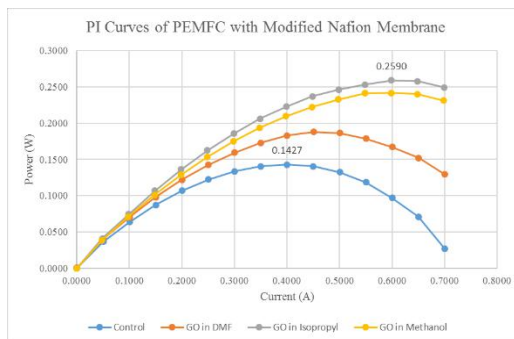


Figure 1 Power Performance Curves (PPC) of membranes coated with GO in various solvents

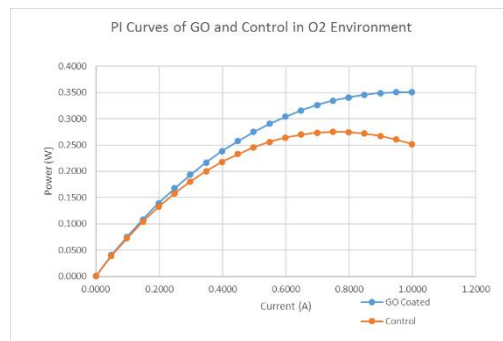


Figure 2. PPC of control and coated membrane in pure O₂ environment: Note the difference in performance

[1]Surana, K., Singh, P. K., Bhattacharya, B., Verma, C., & Mehra, R. (2015). Synthesis of graphene oxide coated Nafion membrane for actuator application. *Ceramics International*,41(3), 5093-5099. doi:10.1016/j.ceramint.2014.12.080

[2]Jia, T., Lu, C., Zhang, Y., & Chen, W. (2014). A comparative study of CO catalytic oxidation on Pd-anchored graphene oxide and Pd-embedded vacancy graphene. *Journal of Nanoparticle Research J Nanopart Res*, 16(2). doi:10.1007/s11051-013-2206-0

Synthesis and Characterization of Reduced Iron Graphenes

Allen Green¹, Rebecca Isseroff¹, Simon Lin², Dr. Miriam Rafailovich³

¹Lawrence High School, Cedarhurst, NY 11581

²State University of New York at Stony Brook, Stony Brook, NY, 11794

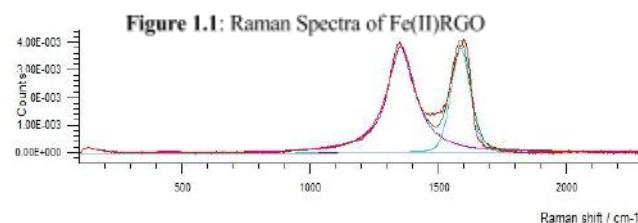
³Department of Material Science and Engineering, State University of New York at Stony Brook, Stony Brook, NY, 11794

The applications of metal nanoparticles in graphene are being investigated for their catalytic ability and drug-delivery potential. Previous research focused primarily on gold, silver, and platinum; but to date, no extensive research has been conducted on iron nanoparticles in graphene. Our project set out to synthesize reduced iron graphenes using three different sources of iron: 1) Iron (II) sulfate, 2) Iron (III) sulfate, and 3) Iron pentacarbonyl. We then characterized them by their Raman spectra.

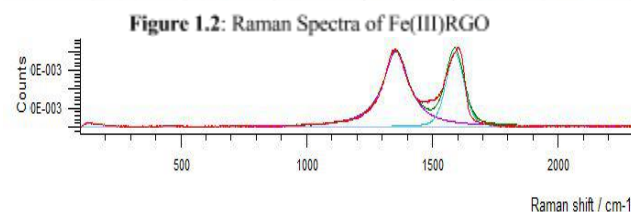
Graphene oxide (GO) was synthesized using a modified Hummer's method by dissolving graphite in sulfuric acid (H_2SO_4) and oxidizing it with potassium permanganate ($KMnO_4$) and sodium nitrate ($NaNO_3$).¹ Once the graphene oxide was extensively washed and then dried into flakes, a 1mg/ml solution was made in distilled water, sonicated and then centrifuged to remove impurities. The metal salts iron (II) sulfate ($FeSO_4$) and iron (III) sulfate ($Fe_2(SO_4)_3$) were added to respective GO solutions at a concentration of 0.2 mmol and left to stir overnight. The next day the solution was reduced using sodium borohydride ($NaBH_4$) at a concentration of 12 mmol and again stirred overnight. The individual solutions were then applied and dried multiple times onto glass slides and three different points on each slide were analyzed using a Renishaw InVia Raman Spectrometer.

The results of the Raman spectra showed that there were significant differences between the D and G peaks of regular reduced graphene oxide (RGO) and both reduced iron graphenes. However, there were no significant differences between the two reduced iron graphenes (Fe(II)RGO/Fe(III)RGO). When compared to regular RGO, the iron sample's D and G peaks had more area than the peaks of RGO. The iron samples had a higher D peak than G peak with a D to G peak ratio of 1.02 for both samples (**Figure 1**) while the regular RGO had a higher G peak with a D to G peak ratio of 0.97 (**Figure 2.1**). The regular graphene oxide (GO) we also tested had a D to G peak ratio of 0.95 (**Figure 2.2**).

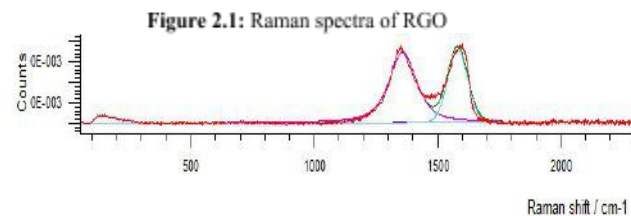
Future work includes determining the magnetic character using Mossbauer; analyzing the size of the nanoparticles by Scanning Electron Microscopy; and applications in hydrogen fuel cells as well as dental pulp stem cell differentiation.



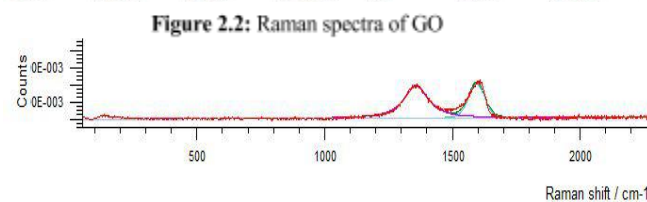
Curve Name	Centre	Width	Height	% Gaussian	Type	Area
Curve 1	1355.67	131.109	0.00392265	0	Mixed	0.007051
Curve 2	1590.31	88.5165	0.0030534	81.2528	Mixed	0.395465



Curve Name	Centre	Width	Height	% Gaussian	Type	Area
Curve 1	1355.67	122.303	0.0041641	0	Mixed	0.799975
Curve 2	1590.55	84.9396	0.00408716	71.2315	Mixed	0.420111



Curve Name	Centre	Width	Height	% Gaussian	Type	Area
Curve 1	1359.94	131.929	0.00359127	35.0065	Mixed	0.66025
Curve 2	1583.54	96.2756	0.00368904	100	Mixed	0.378061



Curve Name	Centre	Width	Height	% Gaussian	Type	Area
Curve 1	1359.42	114.457	0.00393489	10.5948	Mixed	0.683286
Curve 2	1596.04	74.7363	0.00416253	82.3759	Mixed	0.358908

¹ Hummers, W. S., & Offeman, R. E. (1958, September 25). Preparation of Graphitic Oxide. *J. Am. Chem. Soc. Journal of the American Chemical Society*, 80(6), 1339-1339. doi:10.1021/ja01539a017

Enhancing the Efficiency of PCDTBT:PCBM Bulk Heterojunction Organic Solar Cells Through the Use of Ternary Polymer Blends

Ketan Agrawal¹, Hari Kothapalli², Zhenhua Yang³, Yuchen Zhou³, and Miriam Rafailovich³

¹ Columbus Academy, Gahanna, OH 43230, ² The Roxbury Latin School, West Roxbury, MA 02132, ³ Department of Materials Science, SUNY Stony Brook, Stony Brook, New York 11790

Organic solar cells have numerous potential advantages over their inorganic counterparts, including their flexibility, semitransparency, and cost-effectiveness, making them promising candidates for the alternative energy generation.¹ One method of improving the efficiency of bulk heterojunction (BHJ) solar cells is incorporating a third polymer into the Poly[N-9'-heptadecanyl-2,7-carbazole-alt-5,5-(4',7'-di-2-thienyl-2',1',3'-benzothiadiazole)] (PCDTBT):1-[3-(Methoxycarbonyl)propyl]-1-phenyl-[6.6]C₆₁ (PCBM) standard blend, such as an additional electron donor in order to broaden the ultraviolet-visible (UV-Vis) absorption spectrum, or a non-photoactive, insulating polymer in order to stimulate favorable phase separation in the active layer.² The columnar nanostructure created by inert polymers such as polystyrene has been shown to improve the power conversion efficiency (PCE) due to increased interfacial area and charge transport.³

Our work, therefore, was twofold. Initially, we introduced a second electron donor, Poly[2,6-(4,4-bis-(2-ethylhexyl)-4H-cyclopenta [2,1-b;3,4-b']dithiophene)-alt-4,7(2,1,3-benzothiadiazole)] (PCPDTBT). We prepared 6:6:24, 5:5:20, and 1:5:20 mg/mL ratios of this PCPDTBT:PCDTBT:PCBM blend. While light absorption certainly increased in these ternary blends, each resulted in significantly decreased power conversion efficiencies (PCEs) when compared to the control solar cells comprised of a PCDTBT:PCBM blend in 6:24, 5:20, and 5:20 mg/mL ratios, respectively, possibly due to increased exciton recombination and unfavorable interaction between the two donors.⁴

Thus, to enhance the morphology in the active layer of our PCDTBT:PCBM solar cells, we replaced PCPDTBT with a non-photoactive polymer, with the intention of creating the aforementioned columnar nanostructure. The two inert polymers tested were Styrene Acrylonitrile Resin (SAN) for its exceptional solubility in chlorobenzene and its similarities to Polystyrene and Polylactic Acid (PLA) for its crystallinity. As with PCPDTBT, we experimented with multiple ratios to optimize active layer morphology and thus attain greater cell performance. First, we used a 4:4:16 mg/mL ratio for both the SAN:PCDTBT:PCBM and PLA:PCDTBT:PCBM cells. Although we achieved much more promising PCE results with both of these blends than we had with the PCPDTBT:PCDTBT:PCBM blend, Atomic Force Microscopy (AFM) imaging revealed that the concentrations of SAN and PLA both had to be reduced. With this ratio, the active layers of both the SAN and PLA infused cells demonstrated bicontinuous phase separation, which displays relatively large polymer clusters that reduce the contact area between electron donor (PCDTBT) and acceptor (PCBM). To obtain a more favorable "island" morphology, we accordingly created a 1:4:16 mg/mL SAN:PCDTBT:PCBM blend and both a 0.5:4:16 mg/mL and 1:4:16 mg/mL PLA:PCDTBT:PCBM blend. Of all the ternary polymer blends we tried, the 1:4:16 mg/mL PLA:PCDTBT:PCBM and 1:4:16 mg/mL SAN:PCDTBT:PCBM blends exhibited the highest overall cell performance with peak PCEs of 2.94% and 2.91%, respectively. These figures represent a 83.8% and 81.9% power conversion efficiency increase, respectively, over the 4:16 mg/mL PCDTBT:PCBM control solar cell, which demonstrated a peak PCE of 1.60%. Therefore, in the future, we aim to optimize the concentrations of PLA and SAN in their respective blends, possibly using molecular dynamics to optimize columnar structure in the active layer of the solar cell.

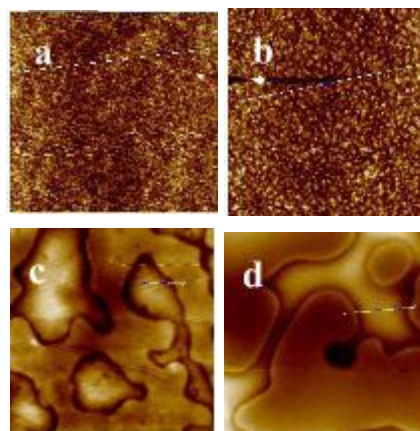


Figure 1: AFM image of (a) 5:20 mg/mL PCDTBT:PCBM, (b) 1:5:20 mg/mL PCPDTBT:PCDTBT:PCBM, (c) 4:4:16 mg/mL SAN:PCDTBT:PCBM and (d) 4:4:16 mg/mL PLA:PCPDTBT:PCDTBT:PCBM thin films

[1] Scharber, M. C., Sariciftci, N.S. "Efficiency of bulk-heterojunction organic solar cells." *Progress in Polymer Science*. 38(12), 1929-1940. <http://dx.doi.org/10.1016/j.progpolymsci.2013.05.001>

[2] Ameri, T., Khoram, P., Min, J., Brabec, C. J. "Organic Ternary Solar Cells: A Review." *Advanced Materials*. 25(31), 4245-4266. <http://dx.doi.org/10.1002/adma.201300623>

[3] Pan, C., Li, H., Akgun, B., Satijia, S. K., Zhu, Y., Xu, D., Ortiz, J., Gersappe, D., Rafailovich, M. H. (2013). "Enhancing the Efficiency of Bulk Heterojunction Solar Cells via Templated Self-Assembly." *Macromolecules*, 46(5), 1812-1819. <http://dx.doi.org/10.1021/ma302458d>

[4] Yang, M., Chen, W., Dou, L., Chang, W., Sheng, D., Bob, B., Li, G., Yang, Y. "High-performance multiple-donor bulk heterojunction solar cells." *Nature Photonics*. 9(3), 190-198. <http://dx.doi.org/10.1038/nphoton.2015.9>

Optimizing the Efficiency of Solar to Hydrogen Conversion and Water Purification in a Model Irrigation System: A Comparative Analysis of Power Efficiency Commercial PVC-HFC and Self-Designed PEC-HFC Renewable Energy Technology

Antonio Carrero¹, Dr. John Jerome², Maira Khan³, Dr. Miriam Rafailovich⁴

¹*Stony Brook University, Stony Brook, NY*, ²*Suffolk Community College, Selden, NY*, ³*H. Frank Carey High School, Franklin Square, NY*

In an effort to supply the global demand for renewable energy, many methods have been developed in recent years to provide efficient and cost effective energy for commercial and sustainable development systems, the two most commonly used being photovoltaic (PVC) and hydrogen fuel cell (HFC) technology. However, current photovoltaic systems only use about 10-15% of energy harvested while hydrogen fuel cell technology still remains too costly to be used in wide scale applications¹. Thus, this research aimed to optimize the efficiency of a through the synthesis of a commercial PVC-HFC water purification and renewable energy system through the use of purchasable parts as well as a novel photocatalytic (PC) - HFC water purification and energy generation system using GO and Graphene on a PCB membrane.

Using a digital power rating meter in the STAR photovoltaic water purification system provided by NexTek Power Technologies Inc., power generated by the solar cell was recorded daily over a 14 day period. These power ratings were correlated with temperature and cloud coverage to determine the total power obtained by the solar cell for future comparison in solar to hydrogen conversion (Figure 1). This solar power system was connected to an irrigation system to model power usage.

To set up the PC-HFC system filters were first created. Graphene oxide was added to 5 mL of water in a sample vial and sonicated. Standard commercial screen mesh was cut into ~13 cm circles using scissors to create 12 circles. Forceps were used to place two Sterlitech polycarbonate (PCB) membrane filters into two separate petri dishes. Pipettes were used to cover these filters in the graphene oxide solution. This process was repeated to construct graphene filters. These filter along with a plain PCB filter were inputted in a gauntlet found in the STAR solar system. Water was run through the filter and the output of each filter was collected using sample vials. These filters have yet to be tested for antibacterial and photocatalytic (Figure 2) properties.

Future work will mainly involve determining power losses during inversion and gains in efficiency through the use of a commercial fuel cell system. This system will be compared to the novel photocatalytic hydrogen system for efficiency and cost. Water purification technology in the STAR system and PC-HFC system will also be compared to determine the feasibility of both dual-purpose methods.

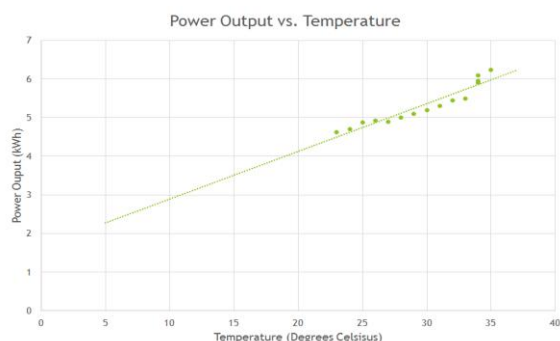


Figure 1

Power harvested by STAR solar cell

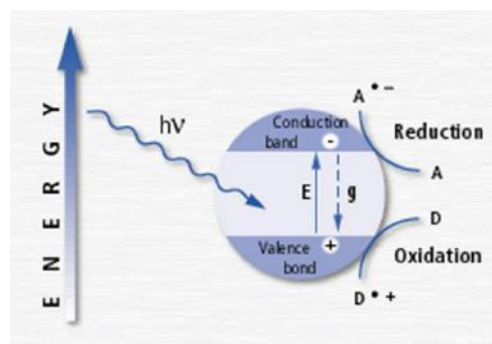


Figure 2

Photocatalytic process used for H₂ production

¹Tributsch, H. (2008). Photovoltaic hydrogen generation. *International Journal of Hydrogen Energy*, 33(21), 5911-5930. doi:10.1016/j.ijhydene.2008.08.017

Assessing the Power Conversion Efficiency and Nanoscale Morphology of Photovoltaic Cells with High Molecular Weight Polystyrene Additives

Shiv Patil¹, Kiran Shetty¹, Zhenhua Yang², Yuchen Zhou², Miriam Rafailovich²

¹Half Hollow Hills High School East, Dix Hills New York 11746

²Department of Materials Science, Stony Brook University, Stony Brook, New York

As the reserves of nonrenewable energy diminish at unprecedented rates, more researchers look toward renewable and sustainable sources of energy. The polymer photovoltaic cell (OPV) is one of the most promising technologies in bringing about low cost energy production and offers many unique benefits, including flexibility, semi transparency, low manufacturing costs, and integration into a variety of products. Polystyrene (PS) was explored as a means to optimize the PCE of polymer photovoltaic cells through the morphological modification of the polymer active layer^[1].

For this study, the morphology of the Bulk Heterojunction (BHJ) cell was altered. In a BHJ cell, the electron donor polymer and electron acceptor polymer are mixed together in order to promote charge transfer and surface contact. PCDTBT, an electron-rich polymer with high absorption power, served as the polymer donor while PCBM, a polymer with a high affinity for electrons, served as the polymer acceptor. The added PS had a high molecular weight since, as shown by previous studies, the addition of polymers with high molecular weight increased the PCE of the polymer solar cell^[2].

The composition of the active layer was modified in each trial by adding a different concentration of PS:PCDTBT:PCBM solution in chlorobenzene (CB). However, the amount of PCDTBT:PCBM added was kept at a 1:4 ratio. The amount of PS added was 2.5% of the total mass of PCDTBT:PCBM in each trial. Each sample had a volume of 1ml. The PCE, Short Circuit Current (Jsc), Open Current Voltage (Voc), and Fill Factor (FF) were analyzed and compared to the control sample without PS additive.

With the addition of PS, the morphology of the active layer changes from a bulk heterojunction structure to an ordered heterojunction structure (Figure 1). The increase in surface area permits a greater number of electron-hole transfers, the driving force of the OPV. The PS additive OPV had a PCE nearly double that of the control sample, with a highest recorded measurement of 3.26% while the control had a highest PCE of 1.6%. It was concluded that 20 mg/ml solution PS:PCDTBT:PCBM was the most efficient concentration to use since the average efficiency, Jsc, Voc, and FF were all greater than any other concentration.

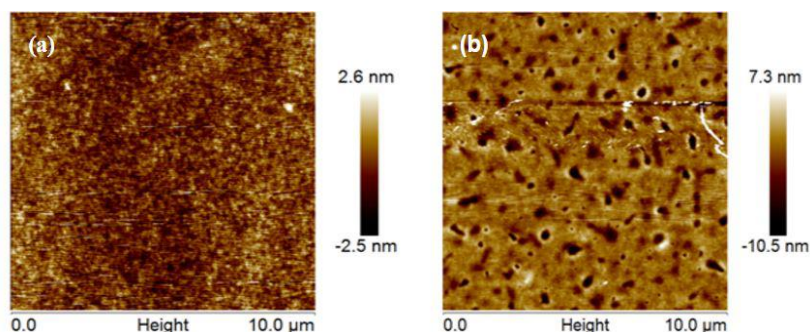


Figure 1a: the morphology of the control group **Figure 1b:** Phase separation is visible with the addition of polystyrene in the sample

References

- [1]Huang, Y., Wen, W., Mukherjee, S., Ade, H., Kramer, E. J., & Bazan, G. C. (2014). High-Molecular-Weight Insulating Polymers Can Improve the Performance of Molecular Solar Cells. *Adv. Mater. Advanced Materials*, 26(24), 4168-4172. doi:10.1002/adma.201400497
- [2] Xiao, Z., Sun, K., Subbiah, J., Qin, T., Lu, S., Purushothaman, B., . . . Wong, W. W. (2015). Effect of molecular weight on the properties and organic solar cell device performance of a donor-acceptor conjugated polymer. *Polym. Chem.*, 6(12), 2312-2318. doi:10.1039/c4py01631a

Enhancing the Efficiency of Bulk Heterojunction Polymer Solar Cells via Mechanical Chain Alignment

Dalai Chadraa, Redmond High School, Redmond, WA

Jinyue Pan, Stony Brook University, Stony Brook, NY

Zhenhua Yang, Dept. of Materials Science, Stony Brook University, Stony Brook, NY

Dr. Miriam Rafailovich, Stony Brook University, Stony Brook, NY

Solar cells provide a sustainable alternative to meet energy demands, but standard solar cells are financially straining to manufacture. Organic photovoltaic (PV) solar cells are a potential solution to current energy challenges as the costs associated with manufacturing are substantially cheaper. If organic solar cells can be improved to match the performance of standard commercial solar cells, there will be greater incentive to expand reliance on sustainable energy sources.

Bulk heterojunction (BHJ) polymer solar cells were the focus of this study. The main component of a BHJ solar cell is an active layer composed of a mix between an organic electron donor and electron acceptor. Mixing the two substances increases mutual surface exposure which improves the transfer of electrons.^[1] Mechanical chain alignment can be achieved through rubbing the surface of the active layer. Previous studies have shown that rubbing the surface of the active layer of a solar device composed of Poly(3-hexylthiophene-2,5-diyl) (P3HT) and Phenyl-C61-butyric acid methyl ester (PCBM) can improve the out-of-face hole charge mobility and therefore improve the power conversion efficiency.^[2] In this study, in addition to using the traditional polymer donor P3HT, we introduced Poly[N-9'-heptadecanyl-2,7-carbazole-alt-5,5-(4',7'-di-2-thienyl-2',1',3'-benzothiadiazole)] (PCDTBT) as a new electron donor to the device to explore whether the effect of rubbing could be generalized to other solar cell devices.

Standard devices were developed using different concentrations of P3HT:PCBM and PCDTBT:PCBM blends dissolved in Chlorobenzene (CB) and spin coated at 2000 rpm onto TiO₂ coated ITO glass. The active layer was either non-rubbed or rubbed 3 times. Solar performance was evaluated using a solar simulator with an AM1.5G filter under light with an intensity of 100 mW/cm². In order to analyze the morphological characteristics of the PCDTBT:PCBM active layer before and after rubbing, the film was examined using Atomic Force Microscopy (AFM).

As the concentration of the PCDTBT:PCBM solution increased, there was a clear trend showing the PCE decreasing from 2.30% at 4:16 mg/ml to 0.584% at 6:24 mg/ml. This trend disappeared after the film was rubbed. PCE for rubbed films actually increased by a factor 1.042 from 4:16 mg/ml to 5:20 mg/ml. The solar cells consisting of 4:16 mg/ml and 5:20 mg/ml of PCDTBT:PCBM experienced a significant increase in efficiency, by 11.7% and 49.7% respectively. The effect for the 6:24 mg/ml film was insubstantial. This trend indicates the presence of a sweet-spot for magnifying the effect of rubbing which diminishes when the PCBM:PCDTBT ratio was altered beyond a certain point. AFM reveals that, at the nanoscale level, rubbing homogenizes the distribution of the film, diminishing the magnitude of peaks and ridges. Rubbing also straightened the structure, possibly improving the absorbance of light polarized parallel to the direction of rubbing. Collectively, rubbing the active layer film of an organic solar cell produces significant improvements in efficiency.

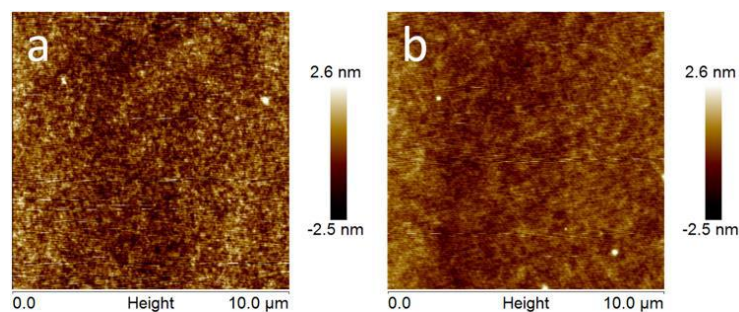
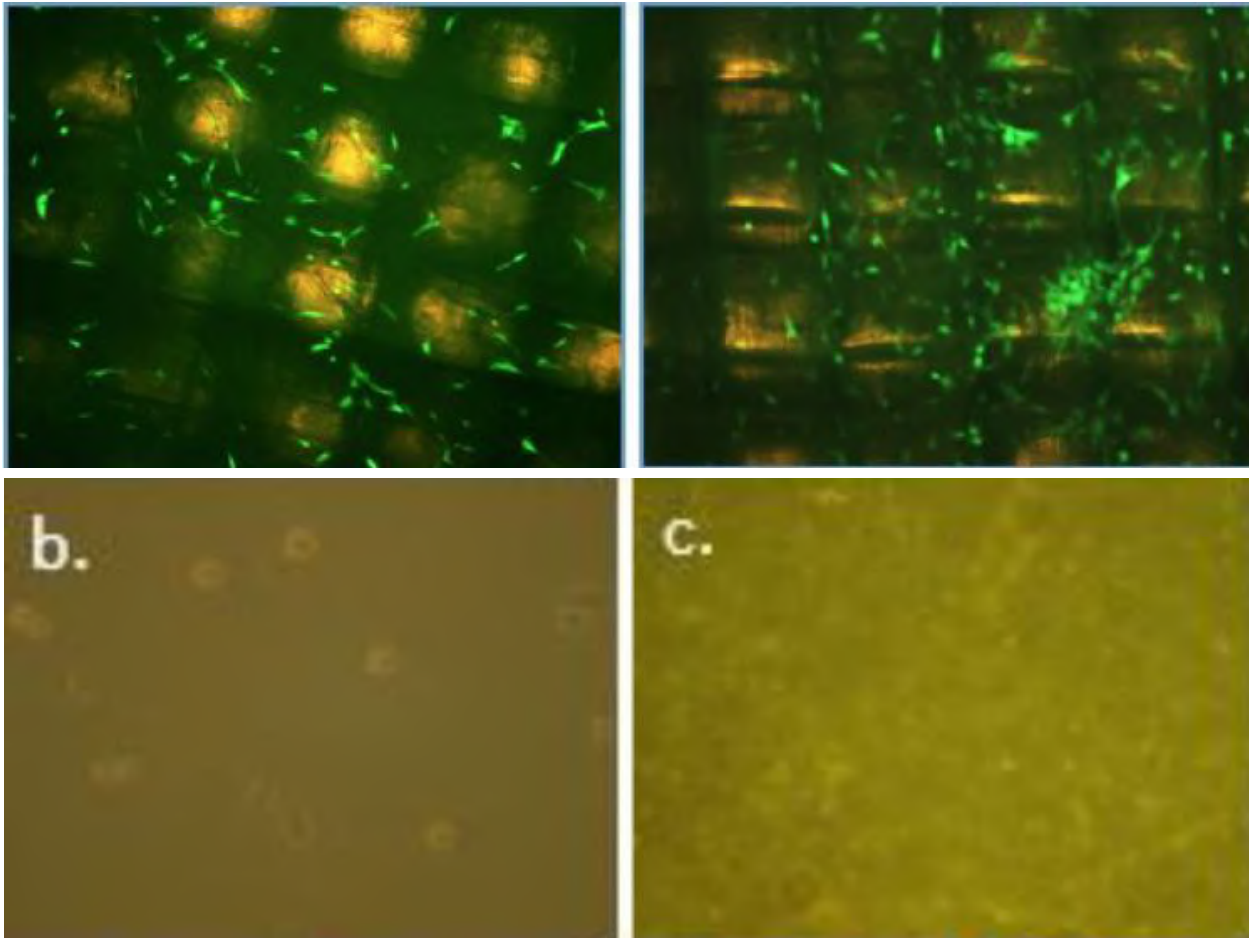


Figure 1. Atomic Force Microscope image of (a) non-rubbed 6:24 mg/ml PCDTBT:PCBM film and (b) rubbed 4:16 mg/ml PCDTBT:PCBM film

-
- [1] Scharber, M. C., and N. S. Sariciftci. "Efficiency of Bulk-heterojunction Organic Solar Cells." *Efficiency of Bulk-heterojunction Organic Solar Cells*. Elsevier, Dec. 2013. Web. 07 Aug. 2016.
- [2] Kajiya, Daisuke, Shuhei Ozawa, Tomoyuki Koganezawa, and Ken-Ichi Saitow. "Enhancement of Out-of-plane Mobility in P3HT Film by Rubbing: Aggregation and Planarity Enhanced with Low Regioregularity." *J. Phys. Chem. C The Journal of Physical Chemistry C* 119.15 (2015): 7987-995. Web.

Session II: Dental Pulp Stem Cells

Graduate Students: Kuan-che Feng, Ya-chen Chuang, Clement Marmorat



Characterization of a Novel, Spin-casted PLA/Polystyrene Scaffold to Investigate the Effects of Nanoscale Surface Topography and Cell-Plating Density on the Proliferation and Differentiation of Dental Pulp Stem Cells

Alice Wu¹, William Hu², Katherine Cao³, Kuan-Che Feng⁴, Adriana Pinkas-Sarafova⁴, Miriam Rafailovich⁴

¹Half Hollow Hills West, Dix Hills, NY 11746; ²Saratoga High School, Saratoga, CA 95070;

³Homestead High School, Mequon, WI 53092; ⁴Department of Materials Science and Engineering, Stony Brook, NY 11794

Dental pulp stem cells (DPSCs) have the ability to proliferate and differentiate into various cell types, lending themselves to immense promise in medicine and tissue regeneration. Physical features within the microenvironment of growing cells, such as topographical size, shape, and geometric arrangement, along with the cell plating density¹ of the substrate they reside upon, have demonstrated significant influence over decisive cell behaviors, including adhesion, orientation, proliferation, and differentiation². Thus, we developed a protocol for the creation of nanoscaled topography using spin-casted poly-lactic acid (PLA) and polystyrene (PS) thin films on silicon wafers. Following the characterization of these substrates, DPSCs were plated to observe the regulative effects of nanoscaled scaffolds on stem cell fate, as well as determine the optimal plating density for DPSC proliferation.

To create the surfaces, polymer solutions of pure PLA, medical-grade PLA, and PS with 25k, 45.8k, and 123k molecular weight were prepared in chloroform solvent. The PLA and PS solutions were combined in volume ratios of 1:1, 1:3, and 3:1 and spin-casted onto silicon wafers. The samples were then annealed for three days, before they were placed in toluene solution to dissolve the polystyrene and create different nanoscale topographies. Atomic force microscopy was conducted to characterize the surfaces by the magnitude of their topographical features and the overall roughness of the surface. The controls were designated as pure PLA and medical-grade PLA without polystyrene, and two other surfaces of pure PLA with PS and medical-grade PLA with PS were chosen for plating. However, because of the differing polymeric interactions at the surface of the substrates, the medical-grade PLA surfaces were characterized by holes (Fig. 1A), while the pure PLA surfaces were characterized by bumps (Fig. 1B). Following AFM analysis, DPSCs were plated on the spin-casted surfaces and analyzed using confocal microscopy after 1, 3, and 5 days.

In regards to the early stages of cell proliferation, topography seemed to have a lesser effect at higher plating densities compared to lower plating densities. Moreover, starting on day 3, cells plated at the lower density began proliferating at a significantly faster rate than cells plated at the higher density, with an average proliferation rate of 5.33 cells/min compared to 3.225 cells/min (Fig. 2). The relatively slower proliferation rates of PLA 1:PS 25k 1 and M-PLA 1:PS 123k 1, demonstrate that ridge topography may inhibit cell proliferation at lower plating densities. Because the data collected on Day 1 is inconsistent with the data collected on Days 3 and 5, more trials studying the early stages will need to be conducted to verify the results. After 28 and 42 days, SEM and RNA analysis will be conducted to study the differentiation of DPSCs in their later stages.

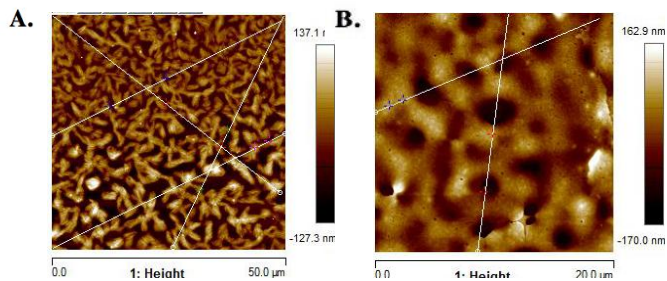


Figure 1. AFM Images of PLA 1:PS 25k 1 (left) and M-PLA 1:PS 123k 1 (right)

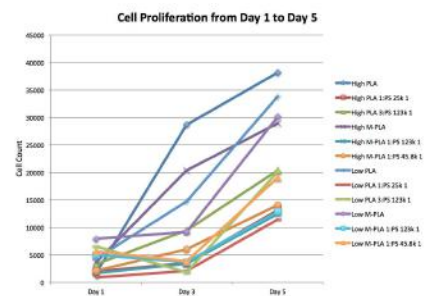


Figure 2. Graph of cell count on each recorded day

¹ Kanafi, Mohammad Mahboob, Rajarshi Pal, and Pawan Kumar Gupta. "Phenotypic and functional comparison of optimum culture conditions for upscaling of dental pulp stem cells." *Cell biology international* 37.2 (2013): 126-136.

² Nguyen, Anh Tuan, Sharvari R. Sathe, and Evelyn KF Yim. "From nano to micro: topographical scale and its impact on cell adhesion, morphology and contact guidance." *Journal of Physics: Condensed Matter* 28.18 (2016): 183001.

Comparison of Dental Pulp Stem Cells Response to Different PLA Composites (Molded vs 3D Printed)

Justin Ng¹, Nicholas Zumba¹, Kuan-Che Feng², Yichen Guo², Yuval Smueli², Dr. Adriana Pinkas-Savafova², Dr. Miriam Rafailovich²

¹George W Hewlett High School, Hewlett, NY 11577; ²Department of Material Science and Engineering, Stony Brook University, Stony Brook, NY 11790

Poly(lactic acid), or PLA, is a widely available biodegradable polyester commonly used in 3D printing. Created from organic plant products, such as corn starch, it is considered environmentally friendly in comparison to other plastics. In addition, its deviance from traditional polyesters includes its thermoplastic characteristics, as it can be melted and remolded without suffering significant differences in its chemical properties¹. PLA sees potential in application for tissue engineering. This experiment compares different PLA composites through scaffold preparation methods to create an environment for dental pulp stem cells (DPSC) attachment, proliferation and differentiation.

Molded samples of pure PLA and commercial PLA are compared with versions 3D printed at 210°C to understand the impact additives in commercial PLA have on DPSC growth. In addition, the flame retardant resorcinol bis(diphenyl phosphate) (RDP) was molded into two samples of PLA, one containing 2% RDP, and the other with 10% RDP treated clay.

Scanning electron microscopy (SEM) was conducted (Fig. 1) to evaluate the topography of the scaffolds. In addition, contact angle for all scaffolds were measured to characterize hydrophobicity. Overall, the SEM results for the molded samples had flat surfaces, and only showed few rough patches at a low nanoscale. 3D printed scaffolds, on the other hand, had many more inconsistencies and rough surfaces at the micro and milliscale. Contact angle of all samples laid within the hydrophilic level, ranging between 56° and 72°, suggesting that the hydrophobicity is not a factor towards the surface of the scaffold, but rather a characteristic of PLA.

The DPSC were plated in Alpha MEM medium, plus 10% Fetal Bovine Serum at an initial 9×10^3 cells per cm^2 . After day 1, the medium was changed with Alpha MEM, 10% FBS, ascorbic acid and β -glycerophosphate, and changed every other day until the end of the experiment. The cells were counted using a Countess II automated cell counter, and visualized with a fluorescent microscope (Fig. 2).

Cell plating efficiency measured found molded commercial PLA to have the highest efficiency of 48%, while clay treated PLA had the lowest efficiency at 8%. Overall, 3D printed scaffolds had low efficiencies compared to their molded counterparts. Calculating cell doubling time showed that molded clay PLA had the shortest time with a minimum of 11 hours, while the longest was commercial PLA with a maximum of 34 hours. Further studies on the biomineralization and cell differentiation of the DPSC on each scaffold in their early and late stages must be conducted in order to uncover more information that may explain the significant difference in cell plating efficiency and doubling time.

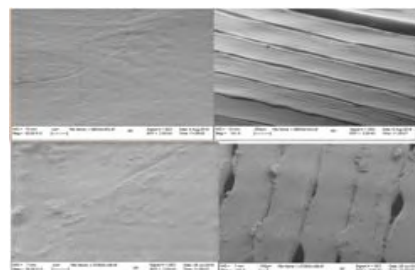


Figure 1. SEM images of 3D Printed Pure PLA (Top) and Commercial PLA (Bottom) at different magnifications (Left to right: 30,000x and 150x)

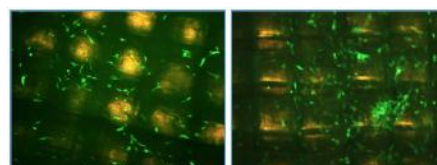


Figure 2. Images of scaffolds with cells for 3D Printed Commercial PLA (Left) and 3D Printed Pure PLA (Right) (From Day 1 of August 1st experiment at 4x magnification)

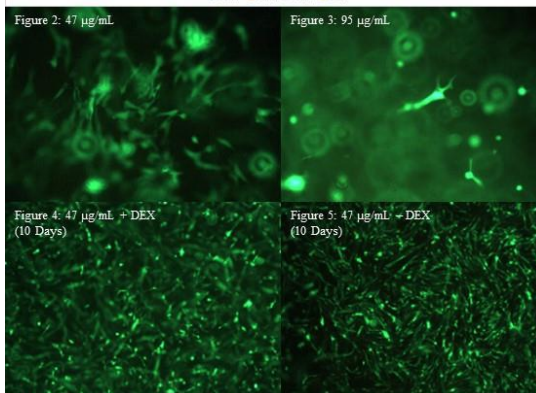
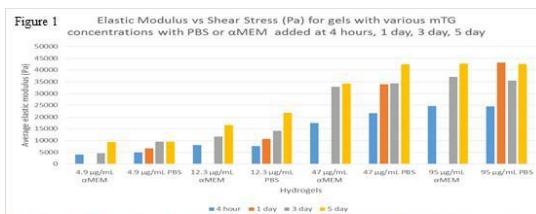
¹Yuanyuan Chen, Luke M. Geever, John A. Killion, John G. Lyons, Clement L. Higginbotham & Declan M. Devine (2016) Review of Multifarious Applications of Poly(Lactic Acid), Polymer-Plastics Technology and Engineering, 55:10, 1057-1075, DOI:10.1080/03602559.2015.1132465

Characterization of Injectable Enzymatically Cross-Linked Gelatin Based Hydrogels with Encapsulated Dental Pulp Stem Cells for Dental Pulp Tissue Regeneration

Neha Parvathala¹, Bonnie Mendelson², Clement Marmorat³, Adriana Pinkas-Sarafaova³, Miriam Rafailovich³, Marcia Simon⁴
Desert Vista High School, Phoenix, AZ 85048¹, University of Pennsylvania, Philadelphia, PA², Department of Material Science and Engineering, SBU, Stony Brook, NY 11794³, Department of Oral Biology and Pathology, SDM, Stony Brook, NY 11794⁴

Gelatin based hydrogels are ideal constructs for encapsulated cell growth because they possess characteristics similar to cells' extracellular matrix and are biodegradable. They can also be used in injectable cell delivery applications; they must be cross-linked with microbial transglutaminase (mTG), an enzyme that links amino acids of the gelatin protein together, enabling the gel to polymerize at body temperature when injected^{1,2}. Human dental pulp stem cells (DPSCs) are easily accessible stem cells with high proliferative and multi-lineage differentiation potential, and can be induced to undergo odontogenic differentiation³. In this study, we examined hydrogels with different concentrations of mTG to find a concentration that both allows the DPSCs to move through the hydrogel and polymerizes in optimal time for injection or bioprinting applications. We will also evaluate the ability of DPSCs to differentiate when embedded in mTG cross-linked hydrogels. The strain of human DPSCs used in this study was AV1-GFP, a strain that was genetically engineered to express green fluorescent protein, which was useful for cell visibility during fluorescence microscopy.

Hydrogels dissolved in solvents PBS, DMEM (Dulbecco's Modified Eagle Medium), and DMEM + 10% FBS (Fetal Bovine Serum) were prepared with varying concentrations of mTG. The hydrogels prepared in media did not cross-link as well as the hydrogels prepared in PBS, so all of the subsequent hydrogels were prepared as 10% gelatin PBS weight/volume solutions. Next, hydrogels with mTG concentrations 95 $\mu\text{g/mL}$, 47 $\mu\text{g/mL}$, 12.3 $\mu\text{g/mL}$, and 4.9 $\mu\text{g/mL}$ were prepared. Half of the hydrogels were hydrated with PBS, while half were treated with αMEM (Minimum Essential Medium Eagle). The strengths of the PBS-treated hydrogels and the αMEM -treated hydrogels were compared to determine whether the presence of media affects hydrogels' mechanical properties, as media provides increased target sites for the mTG enzyme. The strengths were tested at 4 hours, 3 days, and 5 days to observe the kinetics of the mTG enzyme. Hydrogel strengths were assessed through rheology with a Bohlin Gemini HR rheometer, and a general increasing trend was observed from 4 hours to day 5 in all of the hydrogels. (Fig. 1)



Hydrogels with DPSCs embedded in them at low density (1×10^5 cells/mL) and high density (5×10^5 cells/mL) were prepared with mTG concentrations of 95 $\mu\text{g/mL}$ and 47 $\mu\text{g/mL}$, and their strengths were tested and compared to those of hydrogels without cells at 1 day, 5 days, and 12 days. The low density and high density concentrations of DPSCs did not show significant effects on the hydrogel strengths, and though the strengths of the 95 $\mu\text{g/mL}$ and 47 $\mu\text{g/mL}$ mTG hydrogels were different on day 1, by day 12, the strengths were similar. However, when the 95 $\mu\text{g/mL}$ and 47 $\mu\text{g/mL}$ mTG hydrogels with low density DPSCs were imaged at 8 days with fluorescent microscopy, the DPSCs in the 47 $\mu\text{g/mL}$ mTG hydrogels were more elongated and numerous (Fig. 2 & 3), so 47 $\mu\text{g/mL}$ mTG was used as the hard gel composition for subsequent hydrogels with DPSCs embedded.

To investigate the proliferation and differentiation ability of DPSCs embedded in and plated on cross-linked gelatin based hydrogels, hydrogels with mTG concentrations 47 $\mu\text{g/mL}$ and 4.9 $\mu\text{g/mL}$ were prepared with DPSCs embedded at low density (1×10^5 cells/mL) or plated on the hydrogel. Half of the hydrogels were treated with non-induction media (αMEM , 10% FBS, ascorbic acid, and β -glycerol phosphate), and the other half were treated with induction media (αMEM , 10% FBS, ascorbic acid, β -glycerol phosphate, and dexamethasone). The induction media included dexamethasone, a glucocorticoid steroid known to stimulate odontogenic differentiation³. Only minor differences in cell morphology between hydrogels with and without dexamethasone were observed when the hydrogels were imaged with fluorescence microscopy at 5 days and 10 days, which was expected as 5 and 10 days may be too early in the differentiation process. (Fig. 4 & 5) The biomineralization and the gene expression of the DPSCs will be characterized through confocal microscopy, SEM, and RT-PCR as end-point analysis.

¹ Irvine, S.A., Agrawal, A., Lee, B.H. et al. (2015). Printing cell-laden gelatin constructs by free-form fabrication and enzymatic protein crosslinking. *Biomed Microdevices* 17: 16. doi:10.1007/s10544-014-9915-8

² Kuwahara, K., Yang, Z., Slack, G. C., et al. (2010). Cell Delivery using an Injectable and Adhesive Transglutaminase-Gelatin Gel. *Tissue Engineering Part C* 16 : 4. doi: 10.1089=ten.tec.2009.0406

³ Bhatnagar, D., Bherwani, A. K., Simon, M., Rafailovich, M. H. (2015). Biomineralization on enzymatically cross-linked gelatin hydrogels in the absence of dexamethasone. *Journal of Materials Chemistry B*, 3, 5210-5219. doi:10.1039/c5tb00482a

Odontogenic Differentiation of Human Dental Pulp Stem Cells on Fibrin Gel Scaffolds for Applications in Regenerative Endodontics

Rose Hong¹, Jasmin Gao², Clement Marmorat³, Kuan-che Feng³, Dr. Marcia Simon⁴, Dr. Dennis Galanakis⁵,
Dr. Gurtej Singh⁵, Dr. Miriam Rafailovich³

¹Del Norte High School, San Diego, CA 92127, ²Northview High School, Johns Creek, GA 30024, ³Department of Materials Science and Engineering, SBU, Stony Brook 11794, ⁴School of Dental Medicine, SBU, Stony Brook, NY 11794, ⁵School of Medicine, SBU, Stony Brook, NY 11794

With over 16 million endodontic procedures performed annually in the United States alone, dental trauma is a pressing issue.¹ However, current endodontic therapies fail to continue root development and strengthen the root structure because dental pulp is extracted, thereby compromising the long-term structural integrity of teeth.² This is crucial in young children, who develop immature necrotic permanent teeth and risk tooth loss if their apices fail to develop and close. As a result, regenerative endodontics, a field aimed to restore the root canal and surrounding tissue, has recently gained prominence over traditional apexification. However, pulp revascularization, which involves blood clot induction from the periapical region, is relatively new and has uncertain success rates.¹ Because DPSCs are easily accessible, demonstrate clonogenic ability, display rapid proliferation rates, and can differentiate into odontoblastic cell lineages, they are a promising cell source for dental tissue regeneration.³ Additionally, since fibrin gels exhibit outstanding biocompatibility, promote cell adhesion, and degrade controllably, they serve as suitable scaffolds for minimally invasive cell delivery methods.⁴ With these facts in mind, we investigated the ability of fibrin gel scaffolds to proliferate and differentiate DPSCs for the odontogenic regeneration of a functional pulp-dentin complex.

We first varied the concentration of the fibrin gel to determine the most suitable concentration for plating hDPSCs. We made gels from EVICEL[®] Fibrin Sealant (Human) with concentrations of 7.5 mg/mL fibrinogen (FBG) and 54.0 IU/mL thrombin and 12 mg/mL FBG and 85.5 IU/mL thrombin diluted in phosphate-buffered saline (PBS). We also tested purified FBG and recombinant thrombin donated by the SBU Blood Bank with concentrations of 1 mg/mL FBG, 2 mg/mL FBG, and 4 mg/mL FBG, each with 1 IU/mL thrombin, 10 mg/mL FBG, 15 mg/mL FBG, and 20 mg/mL FBG, each with 2 IU/mL thrombin. Through rheology, we found that the fibrin gels made from EVICEL[®] and the 1 mg/mL, 2 mg/mL, and 4 mg/mL FBG fibrin would be too weak to potentially differentiate hDPSCs. On the other hand, we discovered that the 10 mg/mL FBG and 15 mg/mL FBG fibrin gels had enough strength to proliferate hDPSCs at an elastic modulus of 11.8 kPa and 3.1 kPa, respectively (Figure 1a).

In the next stage, we plated hDPSCs on 10 mg/mL FBG fibrin gels at a cell density of $2.5 \times 10^3/\text{cm}^3$. After 50 hours, the cells appeared to be highly confluent and had a high cell plating efficiency of 97% (Figure 1b-c). We then plated hDPSCs on 15 mg/mL FBG fibrin gels and tissue culture plastic (TCP) at a cell density of $1.6 \times 10^3/\text{cm}^3$. On day 1, dexamethasone (DEX), a corticosteroid known to induce differentiation, was added to half of the fibrin gels as a positive control. On day 2, confocal microscopy of fibrin gels and TCP with and without DEX demonstrated that the morphology between the fibrin gel and TCP appeared to have no difference that was statistically significant as seen in Fig. 1d-g, indicating that the fibrin gel induced proliferation of DPSCs in a similar way as the status quo method of using TCP. The end point analysis by confocal microscopy, SEM and RT-PCR for detection of odontogenic markers will be performed at 28 days for additional evaluation of the fibrin gels.

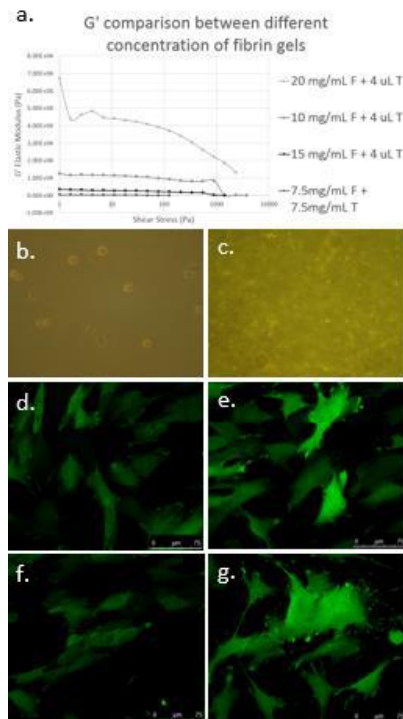


Fig. 1 | a. Graph of elastic modulus of different concentrations; b. microscope image of 10 mg/mL fibrin gel 50 minutes after plating; c. microscope image of 10 mg/mL fibrin gel minus dex 50 hrs after plating; confocal image of d. fibrin gel #5 minus dex, e. tissue culture plate #5 minus dex, f. fibrin gel #6 plus dex, g. tissue culture plate #6 plus dex. Cells were observed under fluorescence confocal microscope at 40x magnification on day 2

¹Kim, S. G., Zhou, J., Ye, L., Cho, S., Suzuki, T., Fu, S. Y., ... Mao, J. J. (2012). Regenerative Endodontics: Barriers and Strategies for Clinical Translation. *Dental Clinics of North America*, 56(3), 639–649. <http://doi.org/10.1016/j.cden.2012.05.005>

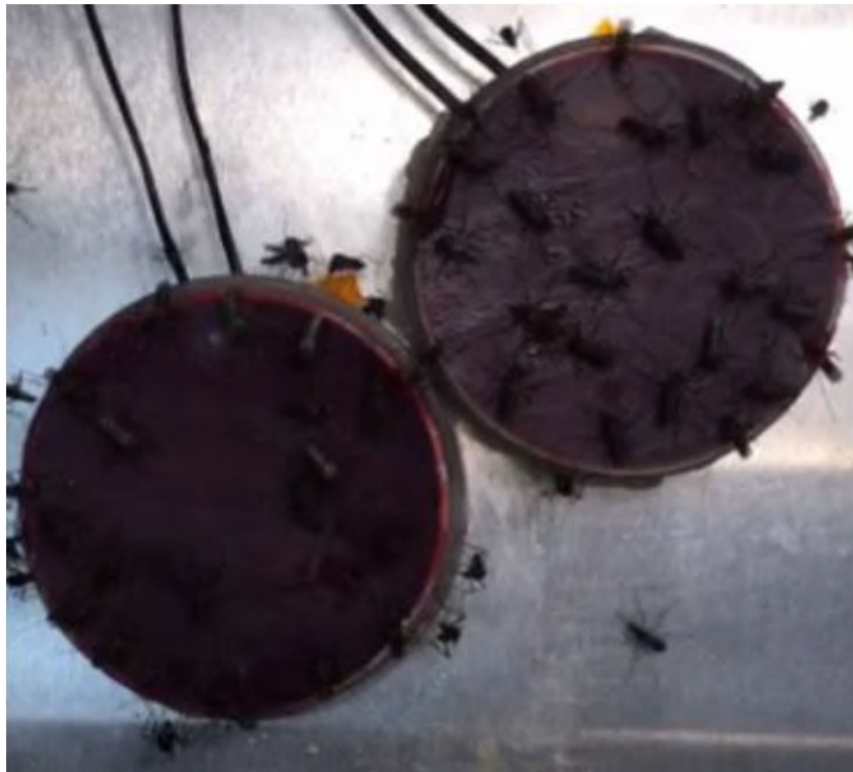
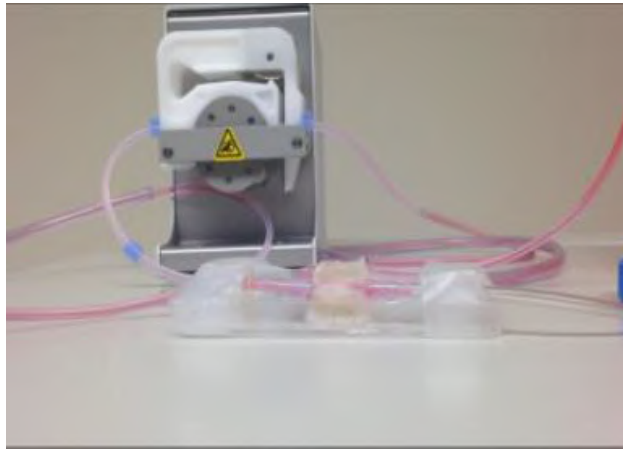
²Ray HA, Trope M. (1995). Periapical status of endodontically treated teeth in relation to the technical quality of the root filling and the coronal restoration. *Int Endod J* 28:12-18.

³Paduano F, Marrelli M, White LJ, Shakesheff KM, Tatullo M (2016) Odontogenic Differentiation of Human Dental Pulp Stem Cells on Hydrogel Scaffolds Derived from Decellularized Bone Extracellular Matrix and Collagen Type I. *PLoS ONE* 11(2): e0148225. doi:10.1371/journal.pone.0148225

⁴S. Jockenhoovel, G. Zund, S. P. Hoerstrup et al., "Fibrin gel—advantages of a new scaffold in cardiovascular tissue engineering," *European Journal of Cardio-Thoracic Surgery*, vol. 19, no. 4, pp. 424–430, 2001.

Session III: Bio Based Devices

Graduate Students: Vincent Ricotta



Synthesis of a Novel Biomaterial for Blood Vessel Constructs

Sujay Shankar¹, John Cordero², Dr. Gurtej Singh², Clement Marmarot³, Dr. Miriam Rafailovich³

¹A&M Consolidated High School, College Station, TX 77840, ²Stony Brook Medicine, Stony Brook NY 11794, ³Department of Materials Science and Engineering, Stony Brook University, Stony Brook NY 11794

Coronary Artery Bypass is among the most common surgical procedures in the United States and all over the world¹. Currently, bypass surgery is executed by removing an artery or vein from somewhere in the body and implanting that vessel into the site of injury. This procedure is time-consuming and expensive, and often fails in the long-term. This research aims to combat these concerns and eliminate surgical hazards by developing a new material for hydrogel vascular grafts, specifically those small in diameter, for direct implantation into the sites of injury. We use a design system to screen for potential polymer blends that can be used to create tough hydrogel systems. The designed blends must be mechanically robust, elastic, and cytocompatible to prove effective in cardiologic applications.

In this research, we use two polymers, gelatin and collagen, to generate a durable hydrogel with enhanced properties. Due to its strong mechanical properties and cell binding motifs, gelatin is an ideal material for the scaffold. A mature tissue, collagen, was used to coat the lumen of the blood vessel graft. Collagen's high cell viability and tissue regeneration capabilities made it an optimal polymer for the scaffold. Both gelatin and collagen were adhered to each other using fibrin, a natural protein that holds blood vessels together. The purpose of using these materials was to mimic the layered structure of blood vessels and provide a natural environment for cells.

Before experiments with vascular grafts, rheology was performed on the hydrogels to evaluate their mechanical and hydration properties [Figure 1]. This data shows that gelatin exhibits much higher strength and elasticity than collagen. Additionally, fibrin is observed to have little effect on the strength and flexibility of both gelatin and collagen.

The hydrogel scaffolds were created in the following layering order (bottom to top): Gelatin, Fibrin, and Collagen [Figure 2]. A 5 mm plastic tube mold was used to form the half-lumen shape. The gels were prepared using a specific concentration 3 ml of 20% gelatin, 450 ul of fibrin, and 2 ml collagen. Two half-lumen gels were placed on top of one another to form a full lumen gel. This hydrogel was connected with plastic tubing on both sides and media was pipetted through the gel. No leaks were observed. However, when the setup was connected to a perfusion pump, there were many leaks caused by weak fibrin glue and slippery collagen [Figure 3].

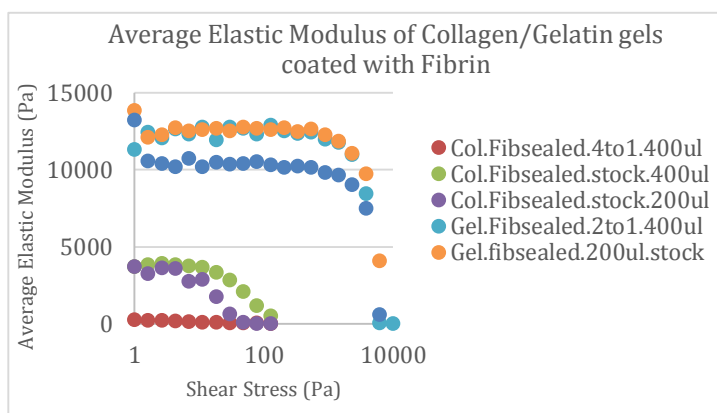


Figure 1. Rheology of Collagen and Gelatin Hydrogels with Fibrin

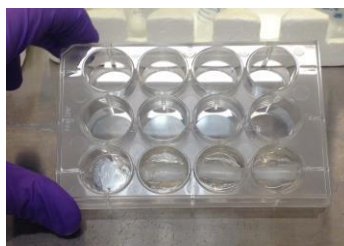


Figure 2. Half lumen wells

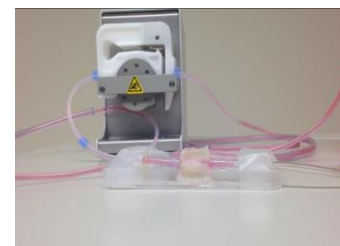


Figure 3. Media Perfusion

The entire experiment was run multiple times with different concentrations and amounts, decreasing the amount of collagen each time. A final hydrogel with 2.75 ml of 15% gelatin, 450 ul fibrin, 300 ul collagen, and 4mm diameter lumen worked most successfully. Afterward, endothelial cells were added to the media and passed through the vessel graft. After 48 hours of constant flow, the graft was removed and cross sections were made on the material. Cell studies are yet to be performed on the scaffold. In the end, a successful proof of concept model was established.

Future research on this project will focus on cellular studies. Endothelial cells and Myofibroblasts will be directly seeded on the material and their behavior will be observed. Mechanical properties can be further studied with rheology on each individual layer of the scaffold. Finally, work on 3D bioprinting and molding can be done to fabricate a complex construct for long-term medical applications.

[1] Liu, Y., Sakai, S., & Taya, M. (2016). Engineering tissues with a perfusable vessel-like network using endothelialized alginate hydrogel fiber and spheroid-enclosing microcapsules. *Heliyon*, 2(2). doi:10.1016/j.heliyon.2016.e00067

The Effect of TiO₂ Nanoparticles on the Heat Transfer and Effectiveness of Mosquito Repellent Cream

Peyrin Kao^{1,4}, Matt Brass^{2,4}, Ginna Gabalski^{3,4}, Harry Shan He⁴, Dr. Miriam Rafailovich⁴

¹Diamond Bar High School, 21400 Pathfinder Rd, Diamond Bar, CA 91765

²University of Rhode Island, 45 Upper College Rd, Kingston, RI 02881

³East Meadow High School, 101 Carman Ave, East Meadow, NY 11554

⁴Garcia MRSEC at Stony Brook University, 100 Nicolls Road, Stony Brook, NY 11790

Mosquitos are the primary transmitter of many dangerous diseases, including the Zika virus, which currently affects over 1.5 million people in Brazil alone.^[1] Effective mosquito control is essential to the prevention and eradication of these diseases. Previous research has determined that infusing Estee Lauder mosquito cream with 10% TiO₂ rutile nanoparticles helps decrease the number of mosquitoes likely to bite. The objective of this project was to investigate how TiO₂ and the cream work to mask body temperature and physically block the mosquito's proboscis, therefore providing two forms of protection against mosquitoes.

A heat test experiment was used to investigate how long and how effectively the cream could mask body temperature. A Petri dish covered with a lambskin membrane and injected with 37°C blood was used to simulate human skin. In order to provide a control, only half of the dish was covered with cream; over a period of two hours, the difference in temperature between the sides of the skin with and without cream was compared using an infrared heat gun. The results of this comparison are shown in Figure 1, suggesting that the creams with 10% TiO₂ rutile nanoparticles are the most effective, masking body temperature for up to two hours.

In order to determine the effectiveness of various types of creams and thicknesses, live female mosquitoes were released in a cage and allowed to feed on lambskin Petri dishes for about 20 minutes. The type and thickness of the cream varied in each of the four trials. Afterwards, the mosquitoes were frozen and counted to determine how many showed evidence of blood ingestion. The results, shown in figure 2, suggest that a thick coat of 10% TiO₂ rutile nanoparticles was the most effective against mosquitoes.

Over the 20-minute feeding period, the Petri dishes were filmed so that the number of mosquitoes on the dish at any moment could be counted. These results are shown in Figure 4, showing that a thicker layer of cream with rutile was the most effective at repelling mosquitoes.

The next step in this research project is to determine the role of TiO₂ in impeding the feeding mechanism of the mosquito; that is, investigating how many mosquitoes from the test were stopped from feeding due to the nanoparticles. The nanoparticles are difficult to detect, although confocal microscopy may be able to show the TiO₂ on the proboscis of the mosquitoes.

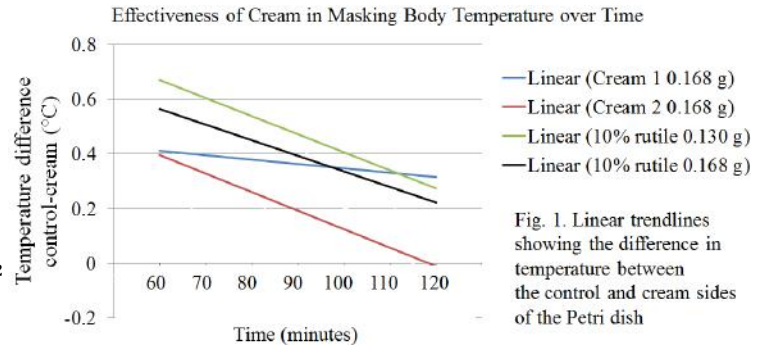


Fig. 1. Linear trendlines showing the difference in temperature between the control and cream sides of the Petri dish

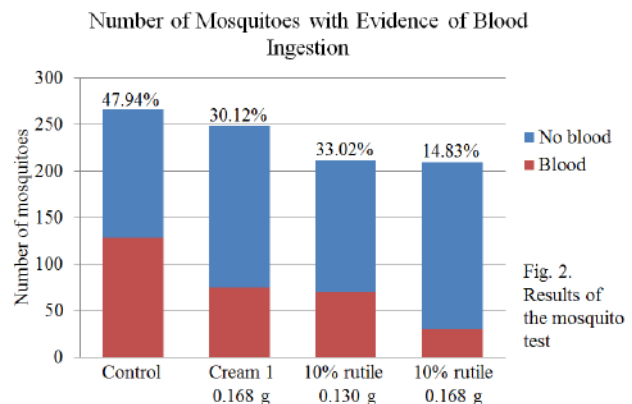


Fig. 2. Results of the mosquito test

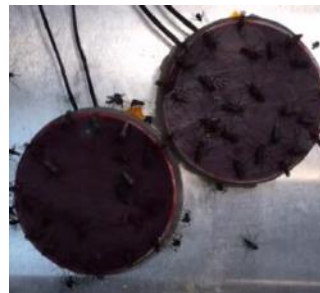


Fig. 3. Footage of the mosquito test with no cream applied on the lambskin

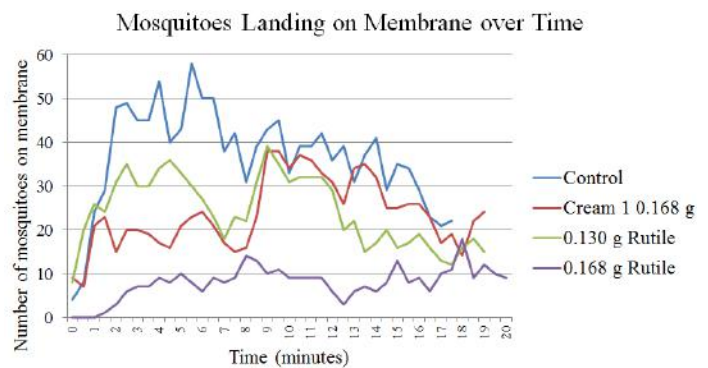


Fig. 4. Number of mosquitoes on the membrane over the 20-minute feeding period

References:

[1] Dasti, J. I. (2016, July). Zika virus infections: An overview of current scenario. *Asian Pacific Journal of Tropical Medicine*, 9(7), 601-605. doi:10.1016/j.apjtm.2016.05.010//

Synthesis and Testing of Rapid Zika Biosensor by Analyte Imprinting Method on Gold Plated Silicon Wafers

Sharon Huang¹, Trisha Madhavan², Carolyn Wong³, Vincent Ricotta⁴, Miriam Rafailovich⁴

¹Morrison Academy, Taichung, Taiwan; ²Cinco Ranch High School, Katy, Texas; ³Morristown High School, Morristown, New Jersey; ⁴Department of Materials Science & Engineering, Stony Brook University, Stony Brook, New York

There is a need for rapid methods of diagnosing Zika, as symptoms of Zika patients are similar to those of the common flu and dengue virus. Current diagnostic tools involve the amplification of viral RNA, which take hours or even days to provide conclusive results. The intent of this project was to develop a rapid biosensor for this purpose using self-assembled monolayers and potentiometric technology.

Biosensors were created by method of imprinting where both the analyte and self-assembled thiol monolayers (SAM) were adsorbed onto a gold surface. The analyte was then washed off, leaving a cavity specific to both the size and the surface functional groups of the macromolecules. When the biosensor is exposed to controlled amounts of the analyte, the target macromolecule bonds to the imprinted cavities, creating an open circuit potential (OCP) difference that can be detected in a buffer solution with an Ag/AgCl reference electrode and potentiometer.

In accordance with previous studies¹, gold-plated silicon wafers were cut in sizes of 1.3-1.5 cm x 2.5 cm., sonicated in ethanol for 5 minutes, and dried under nitrogen gas. The wafers were covered in Teflon tape with a hole punched exposed circular imprinting area of diameter 1.2 cm (Figure 1). After rinsing in ethanol, the wafers were placed in a scintillation vial containing a thiol solution of the analyte for 2.5 hours. For imprinting, two analytes were used, hemoglobin and fibrinogen. After imprinting, the wafers were rinsed in ethanol and placed in a 1 M NaCl solution for 1 hour to remove the imprinted macromolecules. The wafers were then rinsed with ethanol before testing.

Hemoglobin was first used an analyte to evaluate the viability of biosensor, since the size of hemoglobin (5nm in diameter) is comparatively smaller than that of most viruses (30-100nm)¹. Results of hemoglobin testing, shown in Figure 2, show that the biosensor was effective in detecting small analytes. Current research focuses on the use of lentivirus and Zika virus as the analytes.



Figure 1. Teflon tape revealing 12mm diameter hole for imprinting

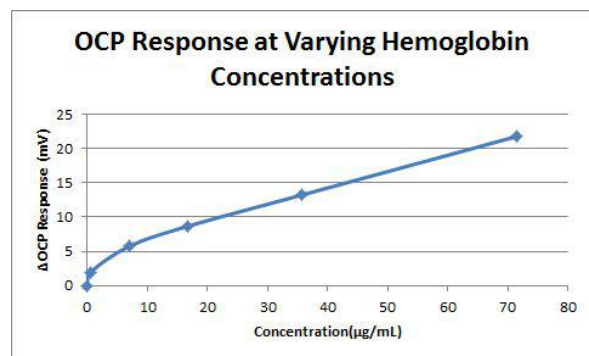
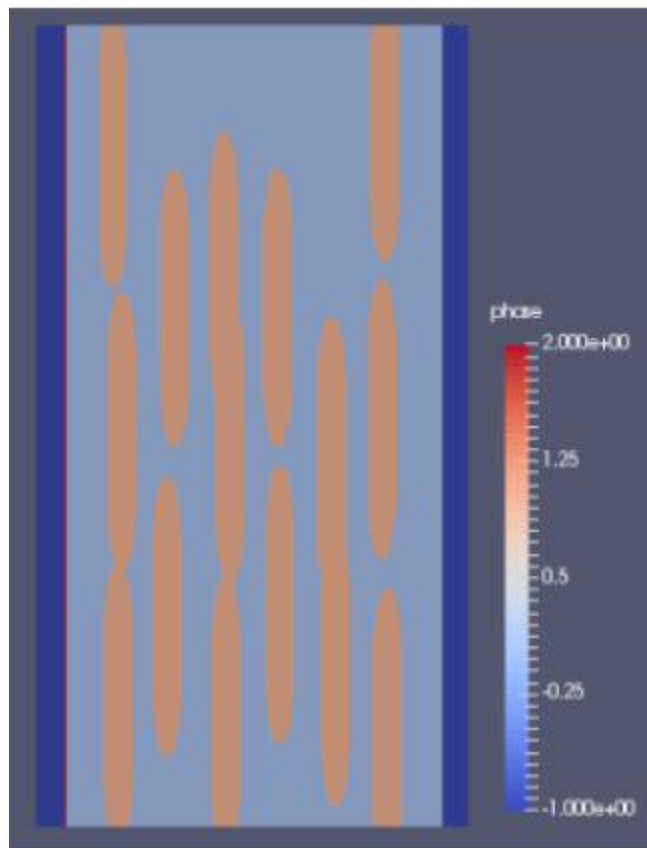
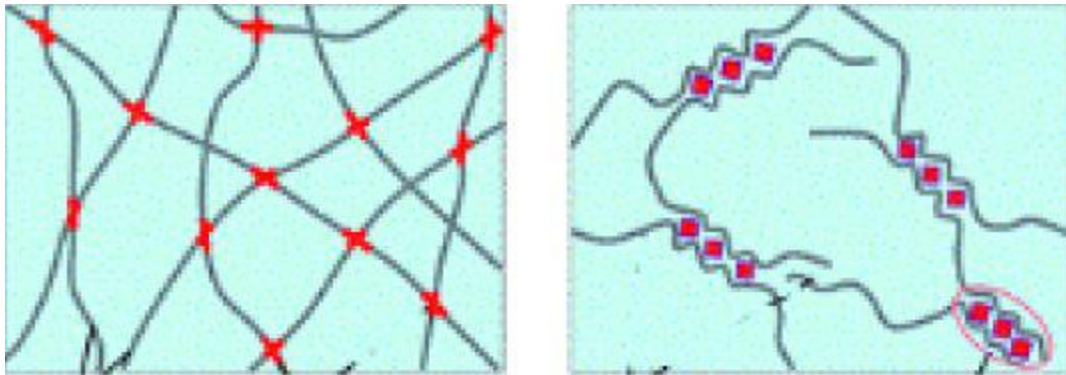


Figure 2. OCP difference over increasing hemoglobin concentrations

¹ Y. Yu, Q. Zhang, C. Chang, Y. Liu, Z. Yang, Y. Guo, Y. Wang, D. Galanakis, K. Levon and M. H. Rafailovich, Analyst, 2016, DOI: 10.1039/C6AN01157H.

Session IV: Modelling and Simulation

Graduate Students: Di Xu, Jiaolong Jiang



Computer Simulations of Physically Crosslinked Gels Using Classical Molecular Dynamics

Wang, Alex¹; Xu, Di²; Gersappe, Dilip²; Rafailovich, Miriam²

¹ Miramonte High School, 750 Moraga Way, Orinda, CA 94563

² Department of Materials Science and Chemical Engineering, Stony Brook University, 100 Nicolls Road, Stony Brook, NY 11790

Physically crosslinked gels are characterized by the attachments between the polymer chains. Rather than chemical bonds between monomers, the chains are bound by filler particles. This attraction creates the necessary gel network.^[1] (Figure 1) Gels are used for many different purposes, both naturally and synthetically. For example, the human body produces gels in the forms of cartilage, blood clots, mucin, and vitreous humor in the eye. Synthetic uses include soft drug delivery systems, contact lenses, wound dressings, hemocompatible surfaces for medical devices, and scaffolds in tissue engineering.^[2] Each of these applications of gels requires a different set of properties of the gel (e.g. a gel made to deliver a drug to a patient should degrade much more rapidly than one used to support a long-term medical device). As such, it is important to understand fully the effects of significant changes on such properties.

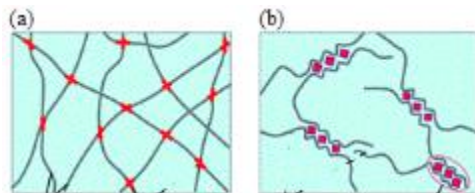


Figure 1. A visual representation of the difference between (a) chemically crosslinked and (b) physically crosslinked gels.^[1]

However, many of these properties are difficult to control and to measure physically. Thus, we use the Large Atomic/Molecular Massively Parallel Simulator (LAMMPS) to model the gel. LAMMPS uses molecular dynamics to simulate atoms. Molecular dynamics is a computer simulation method that calculates the interactions and trajectories of individual atoms with classical physical laws. The interactions between atoms are described by potential curves such as the Lennard-Jones potential.^[3] In our particular simulation, we used molecular dynamics to measure the effect of varying the volume fraction of rod-like filler in a physical gel on the gel's resulting percolation. The particles that comprise the polymer and the filler are randomly generated in a 30 unit cube simulation box for each simulation. (Figure 2) The solvent is implicit rather than explicit to save time and memory. The resulting loss of hydrodynamic information was not significant enough to warrant the extra complications.

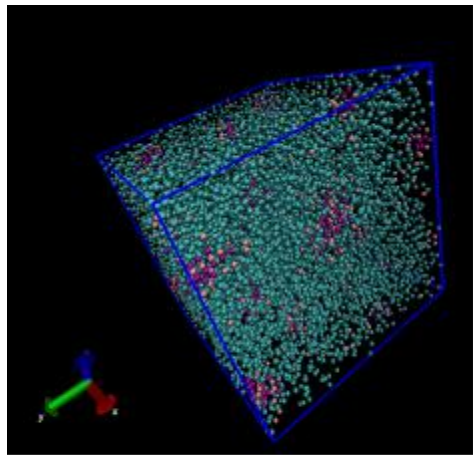


Figure 2. A visualization of the simulated gel in VMD. Filler rods are shown in magenta, end monomers in pink, and other monomers in turquoise.

After running the simulations, we analyze the data output to determine whether the gel percolates. We examine the stress autocorrelation (SAC) function output to achieve this goal. As the concentration of filler in the system increases, the value of the SAC function over time increases as well. A dramatic increase in the function corresponds to a change from a fluid-like substance to a solid-like substance.

^[1] Raghavan, S. R., & Douglas, J. F. (2012). The conundrum of gel formation by molecular nanofibers, wormlike micelles, and filamentous proteins: Gelation without cross-links? *Soft Matter*, 8(33), 8539. doi:10.1039/c2sm25107h

^[2] Qiu, Y., & Park, K. (2001). Environment-sensitive hydrogels for drug delivery. *Advanced Drug Delivery Reviews*, 53(3), 321-339. doi:10.1016/s0169-409x(01)00203-4

^[3] Haile, J. M. (1992). *Molecular dynamics simulation: Elementary methods*. New York: Wiley.

Lattice Boltzmann Modeling of Water Uptake in Gecko Setae

Zixuan Xu¹, Jiaolong Jiang², Dr. Dilip Gersappe², and Dr. Miriam Rafailovich²

1. Shenzhen Middle School, Shenzhen, Guangdong; 2. Department of Materials Science and Engineering, Stony Brook University, Stony Brook, NY, 11790

Geckos are able to attach and detach their adhesive toe pads in milliseconds under perhaps the most severe conditions of any adhesive applications due to uniform microarrays of hair-like setae covering their toe pads. Gecko setae have unique properties that differentiates from conventional artificial adhesive in the way that setae are non-sticky by default and does not stay dirty. The component making up gecko setae is a lipid layer, β -keratin and the matrix. It is known that water is likely to alter adhesion energies and surface geometry when presented in both hydrophilic and hydrophobic surfaces. However, it has been a difficulty to predict the effect of water on gecko adhesion due to the complexity of the system¹. In 2005, a study by Huber et al, confirmed that humidity has a significant effect on gecko adhesion by measurements of spatula adhesion using AFM. Thus the effect of water on gecko setae has been a interesting research area. The objective of this study is to examine the process of how water is absorbed by geckos. Since most properties of the gecko setae remains unknown, this study also examines how different parameters such as the partition coefficient between keratin and matrix and the diffusion coefficient of matrix may affect the process of water uptake in gecko.

The Lattice Boltzmann method is employed to simulate the water diffusion from outer environment into gecko setae in the y-z cross section. The morphology of gecko setae is generated based on transmission electron microscopy images. The gecko setae has permeable materials consists of fiber-like matrix embedded into keratin with a lipid layer on the outside (Figure 1). The Bhatgner-Gross-Krook (BGK) operator and Fick's laws of diffusion are used to solve the Navier-Stokes Equation for advection-diffusion, which is the dynamics of the fluid in this system. Solutions to Fick's laws are approximated by using the central finite differences method². Since water is diffused into the system and water cannot diffuse out of the system, a modified bounce back boundary condition is applied in the space outside the system. The bounce back boundary is modified so that the node on the interface cannot access the neighbor nodes, thus water is not able to escape the system.

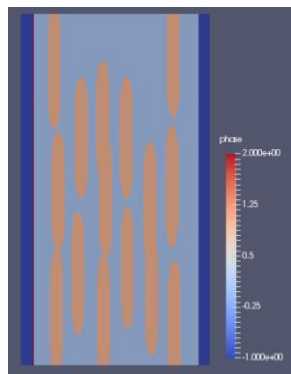


Figure 1. Morphology of the y-z cross section of gecko setae

reaching maximum concentration but matrix has not 3) water is infinitely close to saturation and the water concentration starts reaching saturation. It is found that the partition coefficient, defined as the ratio of maximum concentration of keratin over matrix, has no effect on the first process, but has a significant limiting effect on the second and third process (Figure 2). Further development includes the study of the influence of the matrix diffusion coefficient on the system.

Reference

[1] Autumn, K. (2006), Properties, Principles, and parameters of the gecko adhesive system.

[2] Chopard, B., Falcone, J.L., and Latt, J. (2009), The Lattice Boltzmann Advection-Diffusion Model Revisited, The European Physical Journal Special Topics, 171, 245-249. Doi: 10.1140/epjst/e2009-01035-5

Since it would take a large amount of time to simulate the whole process, the water absorption process is simulated in three segments: 1) when the system starts absorbing water and both the concentration of water in keratin and matrix haven't reach near their maximum concentration 2) when the water concentration starts

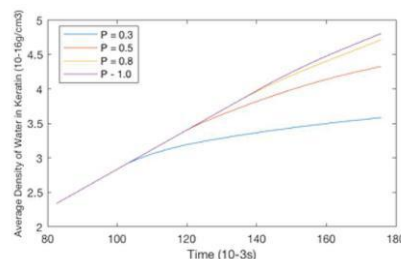
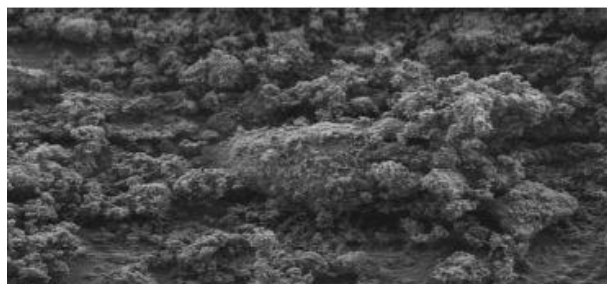
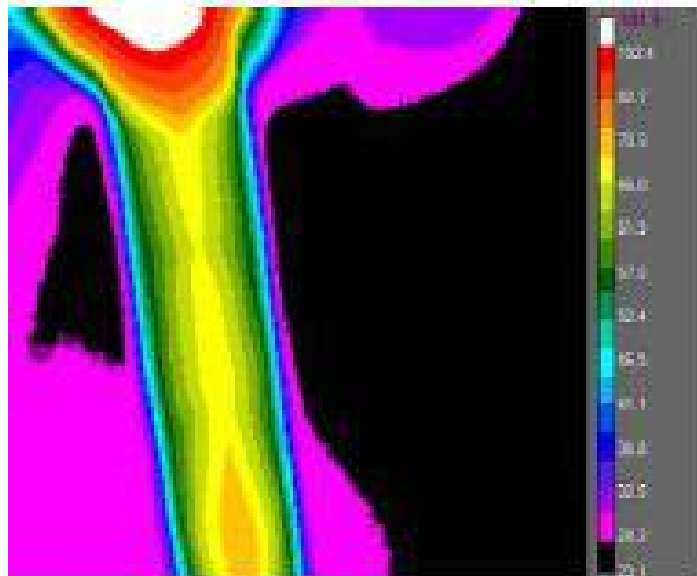
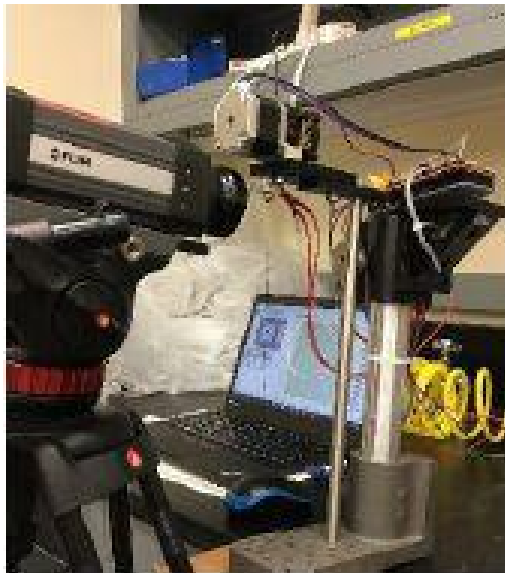
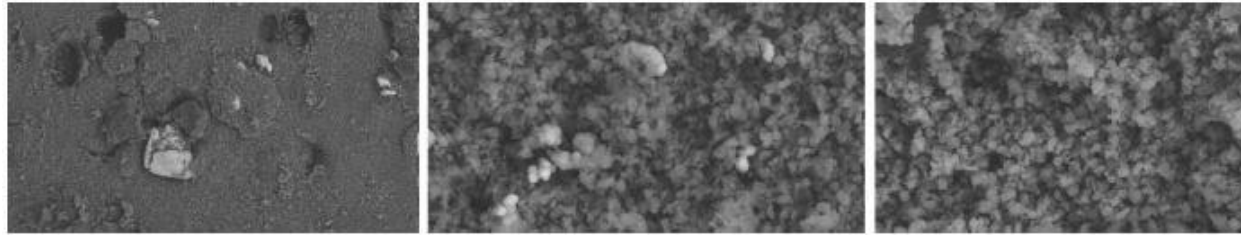


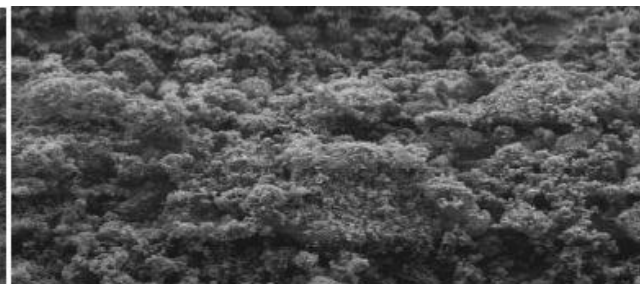
Figure 2. Average density change in keratin over time in the second process

Session V: Nanocomposites

Graduate Students: Xianghao Zuo, Yichen Guo, Yuan Xue, Yuval Shmueli



WD = 8 mm
Mag = 10.00 K X
File Name = 080216-033.tif
30°
Signal A = SE2
EHT = 1.50 kV
Date : 2 Aug 2016
Time : 15:05:22



WD = 8 mm
Mag = 10.00 K X
File Name = 080216-017.tif
30°
Signal A = SE2
EHT = 2.50 kV
Date : 2 Aug 2016
Time : 16:31:31

Lattice Boltzmann Modelling of Graphite Anode Morphologies for Lithium-Ion Cells

Wilson Wu¹, Jiaolong Jiang², Dr. Dilip Gersappe², and Dr. Miriam Rafailovich²

¹Valley Christian School, San Jose, CA

²Stony Brook University, Stony Brook, NY

In recent years, lithium-ion rechargeable batteries have seen use in an increasingly wide variety of applications, from consumer electronics (e.g. smartphones, laptops) to electric vehicles. These batteries are typically composed of one or more lithium-ion cells, consisting of an anode, cathode, and electrolyte. Currently, by far the most widely used anode material for these cells is graphite, with two main motivations for this. Firstly, it preserves structural stability while intercalating Li^+ ions, allowing it to maintain capacity across a greater number of charge-discharge cycles¹. Secondly, by intercalating the Li^+ ions, graphite prevents the formation of lithium dendrites, which are problematic as they potentially grow to a length spanning the distance between the two electrodes, causing a short circuit within the cell¹.

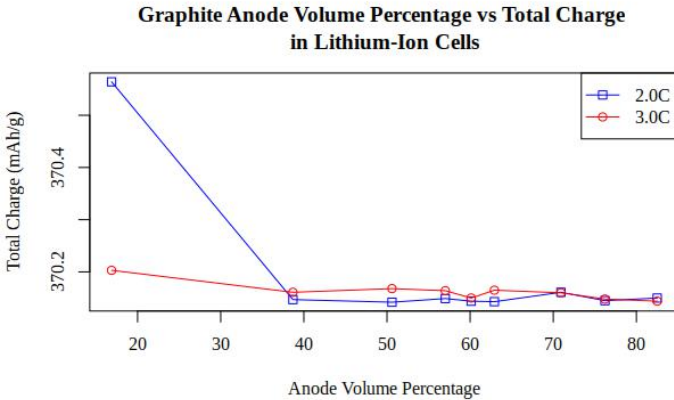


Figure 1: Cell total charge at various anode volume percentages for charging currents of 744.0 and 1116.0 mA g^{-1}

well as the Palabos library, which provided existing implementation of the Lattice-Boltzmann methods and support for parallelization. A data processing functional was created which generated anode morphologies of a target volume percentage consisting of randomly placed non-overlapping spheres of random radius, and these morphologies were used in the simulation. The Li-ion cell simulation was run with a charging current of 372.0, 744.0, and 1116.0 mA g^{-1} , using anode morphologies ranging in volume percentage from 15% to 85%. Simulation parameters, such as final total charge or number of time steps until completion, were recorded. This data suggests that the density of particles within the anode morphology does not much effect the charging of the cell, as can be seen in Figure 1, implying a lower anode density, which reduces material consumption while maintaining performance, would be optimal for most applications.

One issue preventing the development of Li-ion batteries with higher capacities or shorter recharge times is an existing limit in the rate of Li^+ ion intercalation within graphite. If this rate is exceeded, Li^+ ions flowing from the cathode plate onto the surface of the anode instead of intercalating within it, leading again to the problem of dendrite formation². To study this problem, and how morphology of the graphite anode may affect it, the Lattice-Boltzmann methods (which model fluids as momentum distribution functions on a lattice³) were used to implement a three-dimensional computer model of a Li-ion cell. The C++ programming language was used for this purpose, as

¹J. B. Goodenough, K. Park, The Li-Ion Rechargeable Battery: A Perspective. *J. Am. Chem. Soc.* 135(4), 1167-1176 (2013)

²J.-M. Tarascon, M. Armand, Issues and Challenges Facing Rechargeable Lithium Batteries *Nature* 414, 359-367 (2001)

³S. Succi, *The Lattice Boltzmann Equation, for Fluid Dynamics and Beyond* (Oxford University Press, 2001)

Mechanical Properties of HIPS/C-RDP Nanocomposites

Sam Plaut Rambam Mesivta High School, Lawrence, NY 11559
Xianghao Zuo Material Science Department, Stony Brook University

In recent years, polymers have become a popular type of material in a variety of fields for their various physical properties. One way they're commonly used is in wiring. In order to prevent air from oxidizing metal wires, industries wrap them in polymers which restrict airflow. However, other mechanical properties are also important toward creating a more efficient wire coating. In order to retain these specific properties nanocomposites composed of High Impact Polystyrene (HIPS) and sodium-RDP Nanoclay were synthesized at varying percentages ranging from 100:2 to 100:8.

An array of tests were performed to best determine how adding different ratios of C-RDP changed the mechanical and gas diffusion properties of what once was pure HIPS. The Gas Permeability results indicate that the RDP nanoclay addition to HIPS worked exceedingly well at increasing the time it takes for the oxygen to pass through (figure 1).

It was hypothesized that the results were promising due to the specific arrangement of nanoparticles in the nanocomposite. Using Scanning Electron Microscopy it was concluded that the RDP nanoclay dispersed in the ideal mannerism forming multi-level parallel rectangular prisms.

A Differential Scanning Calorimetry test (DSC) was then also performed to determine the Glass Transition Temperature (T_g), and found that the T_g remained at a relatively constant temperature (figure 2). This means that the nanocomposite will be able to withstand relatively the same heat levels emitted from the wires as the pure HIPS.

Tensile test results demonstrate the changes in the mechanical properties of HIPS when the C-RDP is added. The Tensile Strength, and Elongation percentage of the sample slightly declined with the inclusion of the nanoclay. This decrease when adding nanoclays is very common and known to happen. However, the decline quickly steadies off and becomes nearly constant. This is a remarkable improvement to typical additions of nanoclays to polymers due to the general inability to take control of the changing properties. The Young's Modulus increases with the incorporation of the C-RDP and remains practically identical with higher concentrations.

The inclusion of RDP nanoclay will always change its mechanical properties, but the ability to steady the change is key. Even so, the extraordinary reduction of airflow is the main focus, and the deduction of physical properties does not by its own nature take away from the nanocomposite's ability to exceed in its practical applications.

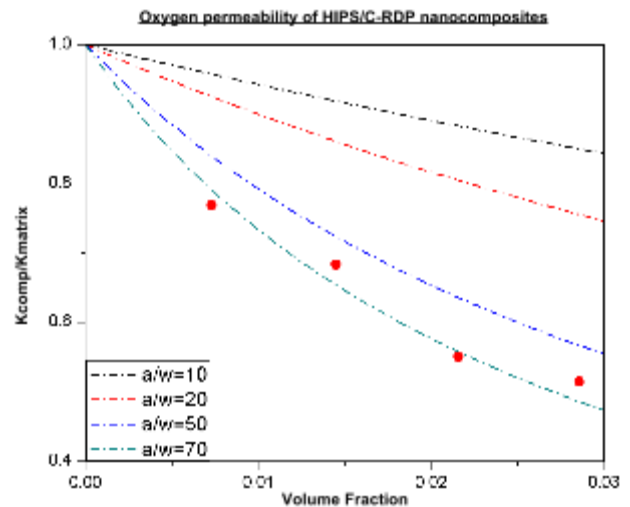


Figure 1: Oxygen diffusion of HIPS/C-RDP nanocomposites

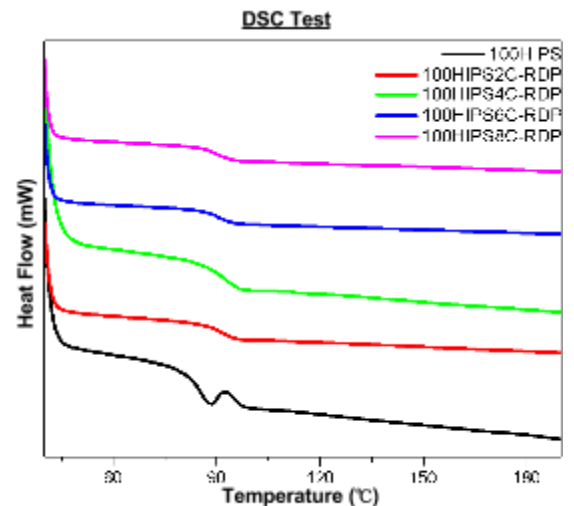


Figure 2: DSC test for HIPS/C-RDP nanocomposites

[1] Yichen Guo, Kai Yang, Xianghao Zuo, Yuan Xue, Clement Marmorat, Ying Liu, Chung-Chueh Chang, Miriam H. Rafailovich. Effects of clay platelets and natural nanotubes on mechanical properties and gas permeability of Poly (lactic acid) nanocomposites. Polymer 83 (2016) 246-259.

[2] L.E. Nielsen, J. Macromol. Sci. Part A 1 (1967) 929-942.

The Effects of Cellulose Micro Particles on the Gas Permeability and Mechanical Properties of Poly(lactic) Acid

Ashvik Awasti, Princeton High School, Xianghao Zuo, Dept. of Materials Science, Stony Brook University

Poly(lactic) Acid (PLA) is a biodegradable polymer that is used in commercial plastics. Environmental concerns dictate that new plastics be biodegradable so that they do not contribute to global pollution because there has already been so much of it (1). This concern means that any attempts to enhance the mechanical properties of PLA must also be done with biodegradable materials. Cellulose is one of the most common biodegradable materials, and in this project branched micro cellulose was used to attempt to enhance PLA (Figure 2). This research sought to determine whether adding cellulose micro particles to PLA could create a micro-composite that had better mechanical properties than pure PLA while not hindering PLA's gas permeability.

The results of the gas permeability testing show that addition of cellulose micro particles does not have a negative effect on the micro-composite's gas diffusion rate (Figure 1). Unlike clays that create barriers in polymer matrices, cellulose micro particles have long branched chains. When these chains are mixed with the polymer matrix, it aids the polymer matrix in maintaining its gas permeability properties. The results of the tensile strength testing show that adding micro cellulose can help maintain the tensile strength, elongation, and Young's Modulus of the micro-composite. The results of the impact strength testing shows that addition of cellulose to PLA increases the impact strength (Figure 1). This means that the mechanical properties of PLA are improved upon addition of cellulose micro particles. Differential Scanning Calorimetry and Scanning Electron Microscopy were also conducted.

This research can be applied to the food packaging industry. First, the micro-composites that were made were completely biodegradable. This would eliminate much of the waste that currently adds to the plastic pollution in the world. Secondly, PLA already has wide applications in the food packing industry because of its good gas permeability properties. Our material does not significantly detract from these properties, and will enhance the mechanical properties of PLA. This means that our material could be applied in the food packaging industry as our material has the gas permeability properties desired by the industry, and also has better mechanical properties than the PLA that is already widely used in the industry.

Percentage of Cellulose	Time for gas diffusion(m in)	Gas Transmission Rate (cm ³ (STP)*cm/cm ² *s*cmHg)	Mean Impact Strength (J/m)
0	7.03	8.30x10 ⁻¹¹	24.23
2	4.58	1.27x10 ⁻¹⁰	33.10
4	4.60	1.27x10 ⁻¹⁰	31.26
6	4.56	1.28x10 ⁻¹⁰	31.10
8	5.55	1.05x10 ⁻¹⁰	32.70

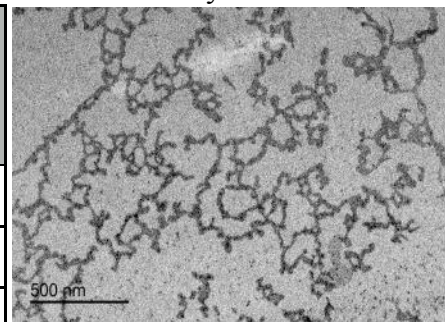


Figure 2. TEM image of branched cellulose

Figure 1. Comparison of percentage of cellulose vs. Gas Diffusion Time, Oxygen Gas Transmission Rate, and Impact Strength

(1) Large-scale production, properties and commercial applications of poly lactic acid polymers Polym. Degrad. Stab., 59 (1-3) (1998), pp. 145-152

Graphene Nanocomposites for 3D-printing Filaments

Justin Chen, Arcadia High School, Arcadia, CA 91007

Yichen Guo, Stony Brook University, Stony Brook, NY 11790

William Berger, Duke University, Durham, NC 27708

Although 3D printing has recently become popular for prototyping and hobbyist use, its usefulness in industry is currently limited, as 3D-printed materials have relatively poor mechanical properties. A common method of 3D printing is fused deposition modeling (FDM), which layers filaments in the printing process. Earlier studies by Q. Sun et al. (2008) have shown that the mechanical weakness of FDM-printed structures are largely caused by poor thermal properties, which hinder heat-based polymer sintering and cause weak bond strength between filaments.¹

Graphene nanoplatelets (GNP), nanoparticles made from several small layers of graphene, inherits many properties of two-dimensional graphene, including high thermal conductivity. Thus, a polymer nanocomposite with GNP will also have improved thermal properties, allowing for greater bond strength between filaments in the FDM process and therefore a better printing material. Graphene-based nanocomposite also have other applications, such as in heat boilers. The high thermal conductivity allows it to be a suitable non-corrosive and cost-effective replacement for traditional metal boilers.²

We created graphene nanocomposites of varying concentrations for polylactic acid (PLA) and acrylonitrile butadiene styrene (ABS), two materials commonly used for FDM filaments. We then performed thermal conductivity tests on the samples. As can be seen on the Figure 1a, the thermal conductivity of the PLA samples steadily increases with higher GNP concentrations, while the ABS sample initially increases greatly, but eventually levels off at very high concentrations of graphene. Using a differential scanning calorimeter, we created a plot of the heat flow for the samples, seen in Figure 2b. While the glass transition temperatures, represented by the dips in the graph, remain constant for PLA, the temperature steadily increases for higher concentrations of GNP for ABS. The glass transition temperature of ABS is consistent with polystyrene, showing that the graphene is likely mixing more effectively with the styrene component of the ABS copolymer. This may explain the levelling off the thermal conductivity values in ABS at higher GNP concentrations, as the styrene monomers may be saturated with graphene.

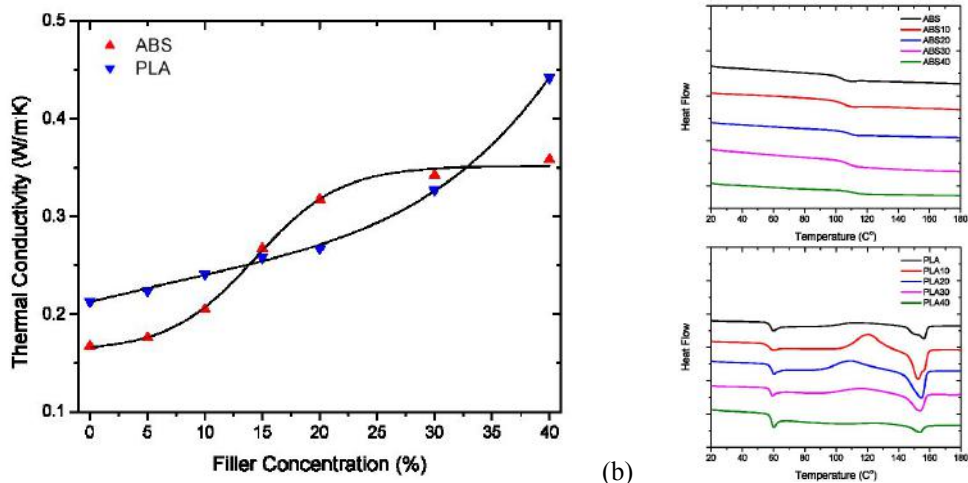


Figure 1. (a) Thermal conductivity plot for ABS and PLA with varying amounts of GNP; the dips in the graph show the glass transition temperature.

Further Izod impact strength tests showed only a minor decrease in impact strength for PLA nanocomposites. The impact strength of ABS initially decreases with the adding of GNP, but the impact strength of higher graphene concentrations remains relatively constant. Thus, the toughness of these materials is not significantly affected by the addition of graphene.

Overall, adding graphene to PLA and ABS produces a material with vastly improved thermal conductivity. This change allows for improved bonding strength between the FDM printing filaments, creating a printed product with better mechanical properties. The toughness of the material does decrease with the addition of GNP, but the effect is minor. Thus, graphene nanoplatelets hold much potential for the future of many technologies, especially 3D printing, and may play a key role in transitioning 3D-printing technology into mass industrial use.

¹ Q. Sun, G.M. Rizvi, C.T. Bellehumeur, P. Gu (2008). Effect of processing conditions on the bonding quality of FDM polymerfilaments, *Rapid Prototyping Journal*, 14 (2), 72-80.

² K. Yang, M. Endoh, R. Trojanowski, R. P. Ramasamy, M. M. Gentleman, T. A. Butcher, M. H. Rafailovich (2015). The thermo-mechanical response of PP nanocomposites at high graphene loading. *Nanocomposites*, 1, 126-137.

Thermal and Structural Properties of PLA/Graphene filaments in FDM 3D Printing

Michael Ye¹, Sukrit Arora², Ben Dacek³ and Yuval Shmueli⁴

1. Syosset High School, Syosset, NY 2. St. Francis High School, Mountain View, CA 3. South Side High School, Rockville Centre, NY 4. Stony Brook University, Stony Brook, NY

3D printing is a rapidly growing technology that has applications in a variety of fields. Fused deposition modeling (FDM) is common printing technique used in industrial manufacturing as well as rapid prototyping due to its effectivity and affordability [2]. This form of additive manufacturing is based on the melting and deposition of thermoplastic polymers. Polylactic acid (PLA) is one of the most common polymer being printed in this technique. PLA is also biodegradable and thus has numerous biomedical applications. However, its thermal and mechanical properties require improvement in order to maintain long-term high performance [3].

Graphene is a nano-filler additive that possesses unique structural features and physical properties; graphene sheets have excellent mechanical strength, electrical conductivity, and thermal stability [3]. These qualities make graphene a strong candidate as an additive to enhance PLA.

The main objectives of this project were to determine the impact of graphene on the thermal profile of the polymer during extrusion, the graphene percentage that would optimize thermal conductivity of PLA without sacrificing printability, and the effect of graphene on inter-layer polymer chain diffusion and crystallinity. Nanocomposite filaments of PLA with graphene at concentrations of 0%, 1%, 3%, 5%, 10%, and 20% were made. Each nanocomposite was pelleted and then extruded into filament. The filaments were printed through a fixed FDM extrusion system at 185°C, 200°C, 215°C, and 230°C, and at 1500 mm/min, 2500 mm/min, 3500 mm/min for each temperature. A FLIR thermal imaging camera was used to record the thermal profile of each filament during extrusion (figure 1). Select printed samples were further analyzed using an optical microscope and a scanning electron microscope to observe the dispersion of graphene within the PLA and the morphology of the printed filaments.

It was found from the thermal movies that higher concentrations of graphene correlated with higher internal temperatures and greater internal temperature consistency during extrusion (figure 2). Images from the scanning electron microscope showed that setting higher temperatures for printing resulted in smoother extruded filament (figure 3). Both the scanning electron microscope and the optical microscope showed that the graphene was dispersed evenly throughout the PLA.

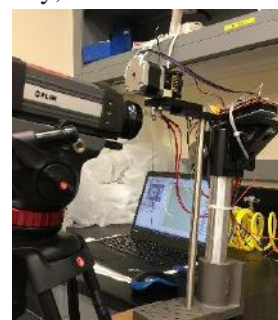


Figure 1. FLIR thermal imaging camera and fixed extrusion system

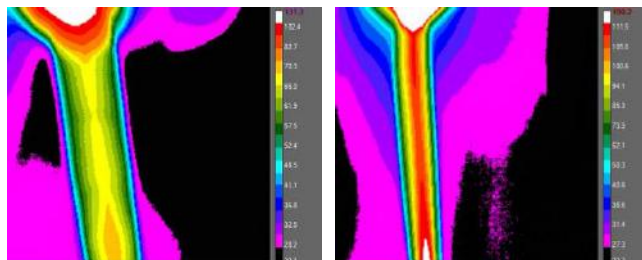


Figure 2. Comparison between temperature range and consistency between pure PLA (left) and PLA with 20% graphene (right). Both were extruded 2500 mm/min at 230 °C.



Figure 3. Comparison between SEM images of PLA with 10% graphene extruded 2500 mm/min at 185 °C (left) and at 230 °C (right). (Magnification: 150x)

References:

- [1] Gross, B.C., Erkal, J.L., Lockwood, S.Y., Chen, C., & Spence, D.M. (2014). Evaluation of 3D printing and its potential impact on biotechnology and the chemical sciences. *Analytical Chemistry*, 86(7), 3240-3253.
- [2] Wendel, B., Rietzel, D., Kühnlein, F., Feulner R., Hülder, G., & Schmachtenberg, E. (2008). Additive Processing of Polymers. *Macromolecular Materials and Engineering*, 293(10), 799-809.
- [3] Kim, I.H., & Jeong, Y.G. (2010). Polylactide/exfoliated graphite nanocomposites with enhanced thermal stability, mechanical modulus, and electrical conductivity. *Journal of Polymer Science, Part B: Polymer Physics*, 48(8), 850-858.

Investigating the Role of MoS₂ in Flame Retardant EVA

Da Qu¹, Paul Rhee², Yun Jin Woo³, Yuan Xue⁴

¹SUNY Stony Brook University, Stony Brook, NY 11794, ²Half Hollow Hills High School East, Dix Hills, NY 11746, ³Half Hollow Hills High School West, Dix Hills, NY 11746, ⁴Department of Material Science and Engineering, Stony Brook University, NY 11794

Majority of wire casing today is made with polyvinyl chloride, which, when burned, releases dioxin¹. Dioxin is hazardous to human health and is also a known carcinogen. Previous experiments done by Yuan Xue suggests a possible replacement could be nanocomposite material made with 60% EVA(ethylene vinyl acetate), 2% GNPs(Graphene), 36% ATH(aluminum trihydroxide) and 2% MoS₂(molybdenum dioxide). This material was V0 grade under the UL 94 vertical flame test and has ideal mechanical properties needed for wire casing. The goal of our experiment is to investigate the effect of molybdenum and sulfide on flame retardancy as well as other mechanical properties.

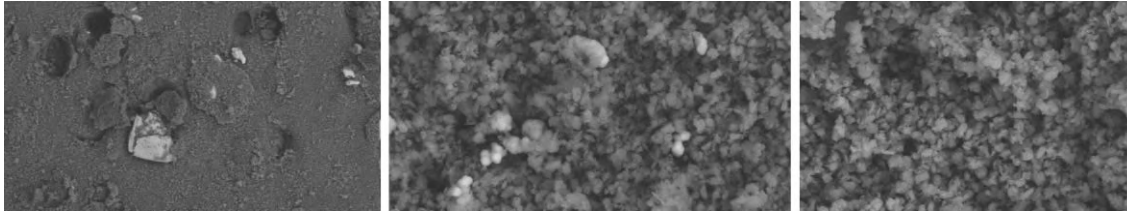


Figure 1: SEM imaging of MoO₃(left), ZnS(middle) and MoS₂(right).

To determine which component of the MoS₂ was responsible for flame retardancy, we isolated the molybdenum and the sulfide by using MoO₃ and ZnS blends. Both failed to reach a V0 grade when tested with the UL-94 vertical flame test. This shows that neither the sulfide nor the molybdenum alone was responsible for the V0 grade in the MoS₂ polymer. Further investigations with SEM-EDX imaging revealed that in the MoO₃ had become concentrated on the surface of the molybdenum blend, rendering the inside of the material flammable. The MoS₂ blend had the best dispersion and had little MoS₂ present on the char(Figure 1). Thus we concluded that the MoS₂ blend works because MoS₂ does not rise to the surface during flame exposure.

Our mechanical data showed that at -50°C, EVA-ATH-GNPs-MoS₂ maintained 82% of the impact strength of EVA-ATH. Tensile data also showed that the elongation of our blend was 400%, compared to pure EVA's 800%. Comparing EVA-ATH-GNPs-MoS₂ to pure EVA, the limiting oxygen index was increased by 19.6%, the average heat release rate was decreased by 59.55%, the peak heat release rate was decreased by 79.88%, and total smoke release was increased by 39.55%. While the MoS₂ blend released heat at a considerably slower rate, it released only 14.49% less total heat, indicating a lengthened heat release time. Also, while the smoke release can help suffocate the flame, the leading cause of death during a fire is smoke asphyxiation. Future work involves finding appropriate balances between these elements for different applications.

[1]Conesa, J.A., Egea, S., Moltó, J., Ortuño, N. & Font, R. (2013) *Decomposition of two types of electric wires considering the effect of the metal in the production of pollutants.*

Compatibilization of EVA/HDPE Blend using RDP Coated Graphene

Marc Gottlieb¹, Joshua Plaut¹, Yuan Xue², Miriam Rafailovich²

¹Hebrew Academy of the Five Towns and Rockaway, Cedarhurst, NY

²Dept. of Materials Science and Engineering, Stony Brook University

Polymer blends are a huge new area of interest in the field of materials science. There are many advantages to creating materials by mixing polymers; however when the polymers are incompatible, they will be immiscible and have phase separation. Therefore, fillers are often used as an additive to improve the compatibility of the two polymers to be miscible. Graphene as a filler has been proved to enhance the compatibility of certain polymers to have increased mechanical properties¹. In this experiment we make use of RDP(Resorcinol bis [diphenyl] phosphate) coated GNP(graphene nanoparticles) as a filler to improve the compatibility of EVA(ethylene vinyl acetate) and HDPE(high impact polyethylene). The goal of this experiment was to measure and evaluate whether sample blends of EVA and HDPE combined with RDP-coated graphene nanoparticles, as opposed to non-coated graphene nano-particles, had improved properties of impact strength and tensile strength.

The samples we made were nanocomposites of: EVA and HDPE in a 30-70 ratio mixed with 1, 3, 5, 10, and 15% RDP-coated GNP (the EVA/HDPE blend was added to supplement the RDP-GNP to 50g). The samples were combined in a Brabender at high heat and then molded at high heat to form five molds for each concentration for the impact and tensile testers. EVA-HDPE, GNP, and RDP-GNP were looked at using the SEM (scanning electron microscopy). Raman spectroscopy was also performed on the RDP-GNP, pure RDP, and pure GNP. Last year, a similar experiment was done instead with GNP that was not coated with RDP.

The samples with RDP coated GNP produced different results than the standalone GNP. With GNP as a filler, the 15% Graphene had the highest impact strength. However, with the RDP-GNP filler, the 3% RDP-GNP had the highest impact strength. In fact, the impact strength was slightly higher than that of the 15% graphene. This means that our blend could produce favorable properties despite using less graphene.

As shown in figure 2, the RDP-GNP has a more uniform surface than the GNP as a result of the RDP coating.

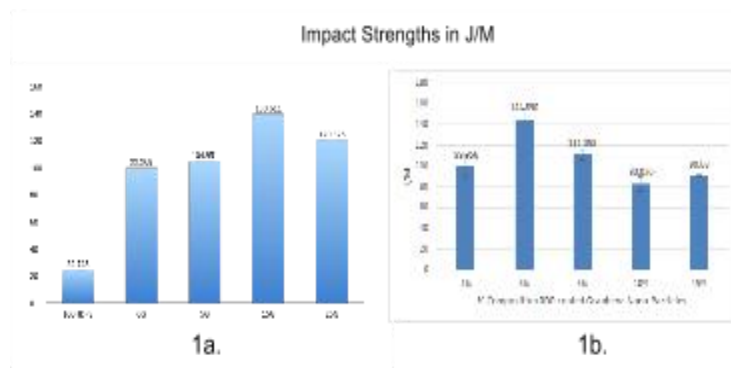


Figure 1. Image 1a. Shows impact strengths with GNP. Image 1b. Shows the impact strengths with RDP-GNP.

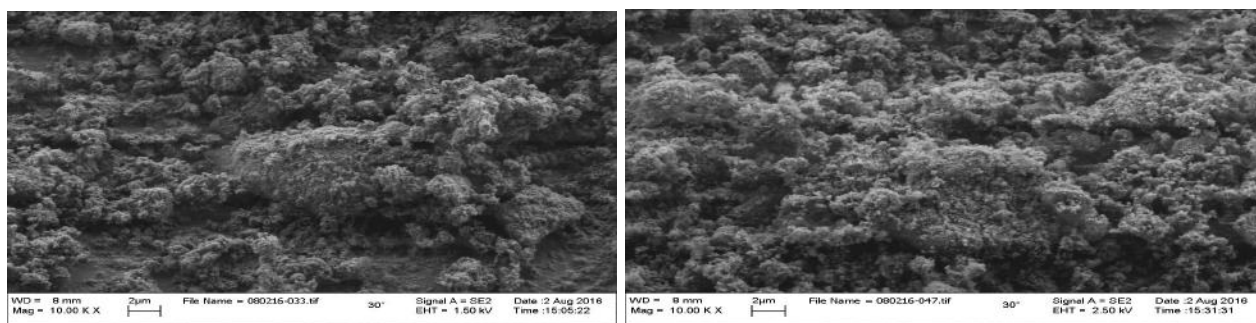
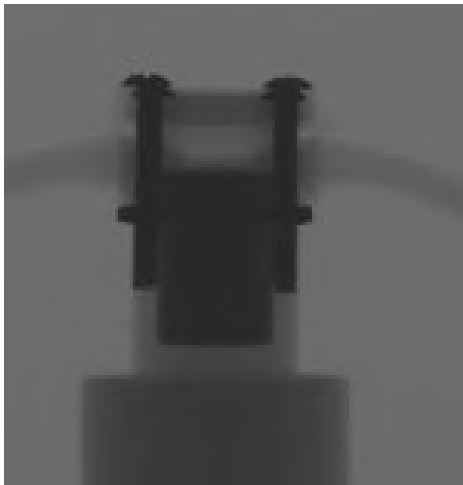


Figure 2. SEM images of RD¹P-GNP and GNP

¹ Xing, W., Wu, J., Huang, G., Li, H., Tang, M., Fu, X. (2013). Enhanced Mechanical Properties of Graphene/Natural Rubber Nanocomposites at Low Content. Polymer International, 63 (9), 1674-1681.

Session VI: Hydrogels and Colloids

Graduate Students: Clement Marmorat, Juyi Li



Contact Angle of Fluids on Pluronic F127 and Gelatin Hydrogels

Jennifer Yu¹, Bonnie Mendelson², Clément Marmorat³

¹Mission San Jose High School, Fremont, CA 94539; ^{2,3}SUNY Stony Brook, Stony Brook, NY 11794

Gelatin is an animal-derived protein that crosslinks to form a hydrogel with the addition of water. Microbial transglutaminase (MTG) is an enzyme that catalyzes crosslinking in gelatin and helps stabilize its structure. Gelatin hydrogels are often used for the 3D printing of scaffolds in order to create artificial organs and blood vessels. It is known that contact angle may be modeled for various substances as a function of time¹; however the contact angles on gelatin are not well understood. Poloxamer 407 (trade name Pluronic F127) forms a micellar hydrogel. Gelatin and Pluronic F127 solutions were used to study the coffee ring effect, which happens when a solution of solids in liquid is left to evaporate.

Gelatin hydrogels were prepared with 10% weight/volume in deionized water. Some hydrogels also had the addition of MTG in a 1:3 and 1:200 mass ratio of MTG to gelatin and were incubated at 37°C. Contact angle goniometry was performed with deionized water on these hydrogels after full swelling. This was repeated for completely desiccated gelatin of the same three types. It was observed that hydrophobicity of gelatin increases with relative presence of MTG, with the 1:3 crosslinked gel being the most hydrophobic. Contact angles of liquid gelatin

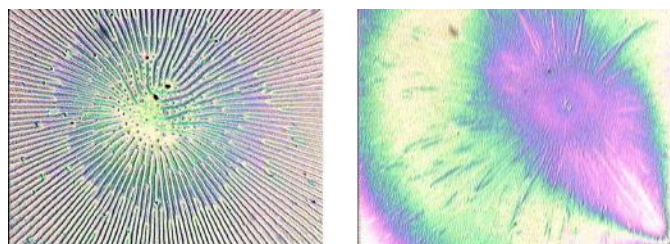


Figure 1. 5x magnified photos of stain left by Pluronic F127 solution on pure silicon (right) and polystyrene-coated silicon (left).

solution on gelatin hydrogel were also studied and showed to be much larger for cooler solutions. This suggests a dependence on viscosity, known to affect contact angle through previous studies².

Drying of 1% gelatin and Pluronic F127 solution in deionized water was also studied. Pluronic F127 evaporated much more quickly than did the gelatin solution on a silicon wafer surface. The Pluronic F127 maintained the shape of a spherical cap; however,

the shape of the gelatin solution changed to a jagged shape from a cap shape after a certain point. Optical microscopy and atomic force microscopy were then used to analyze the stains left by the two solutions. It was found that the gelatin solution produced a circular film surrounding precipitated crystals, while the Pluronic F127 solution stain was in a mesh formation. Further analysis revealed that, on silicon coated with polystyrene, Pluronic F127 stains are arranged in a radial pattern.

Future research may involve investigating the coffee ring effect of different protein solutions and determining the contact angles of gelatin solution on crosslinked hydrogel at specific temperatures of the liquid. Additionally, a better method of performing contact angle goniometry on gelatin is needed.

[1]: Boulogne, F., Ingremau, F., Limat, L., & Stone, H. A. (2016). Tuning the Receding Contact Angle on Hydrogels by Addition of Particles. *Langmuir*, 32(22), 5573-5579. doi:10.1021/acs.langmuir.6b01209

[2]: Al-Shareef, A., Neogi, P., & Bai, B. (2016, July 11). Wetting kinetics of polymer solutions and force-based contact angles. *AIChE Journal*, 62(7), 2533-2541. doi:10.1002/aic.15213

Transdermal Delivery of Curcumin Using Microemulsions as Vehicles and Effect of Curcumin on Human Dermal Fibroblasts

Sara Teitelman¹, Juyi Li², Nissim Garti³, Marcia Simon⁴, Miriam Rafailovich²

¹Yeshiva University High School for Girls, Holliswood, NY 11423

²Department of Materials Science and Engineering, Stony Brook University, Stony Brook, NY 11794

³Casali Institute of Applied Chemistry, The Hebrew University of Jerusalem, Jerusalem 91904, Israel

⁴School of Dental Medicine, Stony Brook University, Stony Brook, NY 11794

Curcumin, a bright yellow component of turmeric, has been shown to exhibit therapeutic potential in various diseases including cancer, diabetes, and AIDS¹. Curcumin acts by attacking multiple inflammation pathways to restore the body to a normal inflammation balance. However, curcumin has a low bioavailability due to rapid metabolism, poor absorption, and rapid systemic elimination². As a result, various methods have been directed at increasing the bioavailability of curcumin; one such method is using microemulsions as vehicles for delivery of curcumin to cells.

Microemulsions are optically clear, thermodynamically stable, isotropic liquid mixtures of oil, water, surfactant, and frequently a cosurfactant³. Upon the addition of a surfactant to an immiscible mixture of oil and water, droplets of water can be interspersed throughout oil (W/O ME) or droplets of oil can be interspersed throughout water (O/W ME). Microemulsions can be used as vehicles for delivering hydrophobic drugs such as curcumin to cells. This project focuses on determining the way in which microemulsions deliver curcumin to cells transdermally and the ways in which curcumin affects cells.

Three solutions were prepared to test the difference between empty vehicles, curcumin-loaded vehicles, and curcumin administered directly to cells: A solution composed of the surfactant Tween 80 and the cosurfactant propylene glycol, a solution containing Tween 80, propylene glycol, and curcumin, and a solution of powdered curcumin dissolved in dimethyl sulfoxide (DMSO). To prepare the cells for the samples, a cell-free collagen gel and a collagen gel containing a solution of one million human dermal fibroblasts were prepared. 500 μ l of the cell-free collagen was added to each well, followed by 1 ml of the cell-containing gel and 2 ml of media. Next, 2 μ M and 5 μ M concentrations of the three solutions were added to their corresponding wells. Controls containing media and controls containing DMSO were also set up. On Day 0, the gels were removed from two of the control wells and placed in tubes containing collagenase solution; the tubes were then placed in an incubator shaker to dissolve the gels and the cells were counted using a hemocytometer. The rest of the cells were counted on Day 1.

The results of the experiment (Figure 1) were compared with the results of a previous experiment done using tissue culture plates instead of collagen gels (Figure 2). The difference in the data in Figures 1 and 2 indicates that curcumin is more sensitive to collagen gel than tissue culture plates; therefore, collagen gel will be used for future experimentation since it is a more accurate representation of human skin. In addition, the data reveals that the cells that received curcumin in a microemulsion exhibited less cell growth than the cells that received curcumin in DMSO, indicating a difference between curcumin administered directly to cells and curcumin delivered to cells in vehicles.

Future research will focus on using RT-PCR to determine the effects of curcumin on DNA. In addition, another experiment will be performed in which cells will be placed at the bottom of wells and an insert will be placed on top of them; collagen gel and the samples will be added on top of the insert. The samples' ability to penetrate the collagen gel and insert to reach the cells will be observed.

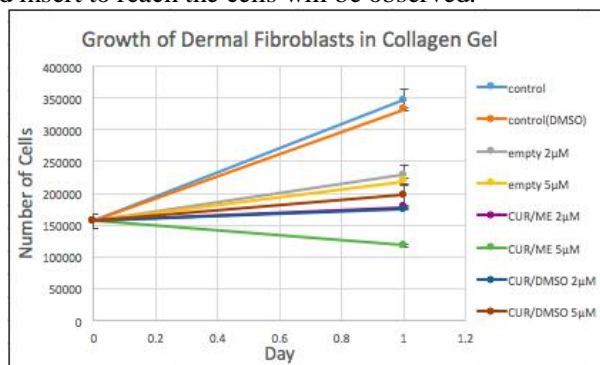


Figure 1: Graph showing the growth of dermal fibroblasts in collagen gel

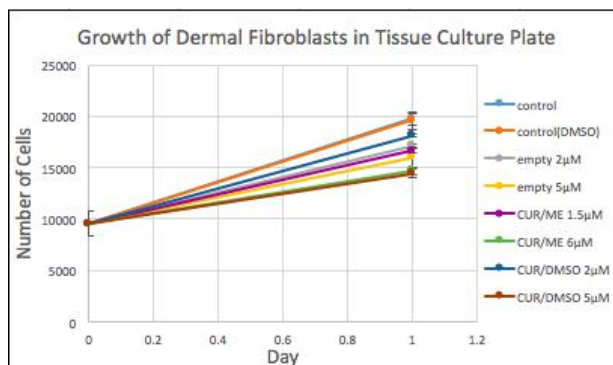


Figure 2: Graph showing the growth of dermal fibroblasts in tissue culture plates (experiment done by Juyi Li)

¹Aggarwal, B.B. & Harikumar, K.B. (2009). Potential Therapeutic Effects of Curcumin, the Anti-inflammatory Agent, Against Neurodegenerative, Cardiovascular, Pulmonary, Metabolic, Autoimmune and Neoplastic Diseases. *The International Journal of Biochemistry & Cell Biology*, 41(1), 40-59. doi:10.1016/j.biocel.2008.06.010

²Gupta, S.C., Patchva, S., & Aggarwal, B.B. (2013). Therapeutic Roles of Curcumin: Lessons Learned from Clinical Trials. *The AAPS Journal*, 15(1), 195-218. doi:10.1208/s12248-012-9432-8

³Narang, A.S., Delmarre, D., & Gao, D. (2007). Stable drug encapsulation in micelles and microemulsions. *International Journal of Pharmaceutics*, 345(1-2), 9-25. doi:10.1016/j.ijpharm.2007.08.057

Characterization of Pluronic F127 Degradation Patterns and Drug Release to Mimic Post-laminectomy *in vivo* Conditions

Somil Aggarwal¹, Michael Kao², Neal Soni³, Clement Marmorat⁴, Miriam Rafailovich⁴

¹Jamesville-Dewitt High School, Fayetteville, NY 13078, ²Troy High School, Fullerton, CA 92833, ³Staples High School, Westport, CT 06880, ⁴Department of Materials Science and Engineering, SBU, Stony Brook, NY 11794

(mention some stupid stat on FBSS) Previous and ongoing studies have presented hydrogels, particularly poloxamers, as excellent materials to be used in various biomedical applications from cell proliferation to molecular release systems. The remarkable aspect of poloxamers such as BASF-produced Pluronic® F127 lies in their thermoresponsive sol-gel transition, enabling them to easily change from liquid to gel form in a unique thermo-reversible process. Biocompatible, non-cytotoxic, non-cell adhesive, and biodegradable, Pluronic® F127 has been shown to be a viable candidate for lumbar post-microdiscectomy and post-laminectomy epidural scarring prevention, a recurring feature in failed back surgery syndrome (FBSS) patients previously diagnosed with spinal stenosis¹. Specifically, F127 may be used as a barrier to be placed in the laminal area, obstructing scar tissue growth and preventing epidural fibrosis. F127's kinetic stability makes it an effective drug delivery agent as well, and drug release was also tested under flow using vancomycin to optimize release.

F127 solutions were created at concentrations 20-30 wt% and incubated until gelation. Determination of degradation rate under laminar flow required a chamber designed to mimic lumbar cerebrospinal fluid (CSF) in the spinal canal and a syringe system to input fluid across the chamber. A ratio of 5:1 PL to deionized (DI) water was desired to further replicate spinal conditions. A chamber was designed in Solidworks and 3D-printed with High Resolution UV-curing resin on a Formlabs SLA 3D printer and designed for rheometric use [Figure 1]. Due to fluctuations in CSF flow rate (depending on body position, e.g. sleeping or walking), degradation patterns were tested at multiple rates ranging from 0.1 ml/min to 2 ml/min. After flow testing, the remaining gel was liquified and reincubated to return to a homogeneous state and tested rheologically using a peltier plate equipped Bohlin Gemini HR rheometer [Figure 2]. UV-Vis spectroscopy was performed on gels before and after flow and spectral peak areas were compared to confirm gel quantity differences. Counterintuitively, F127 degradation possessed a negative linear correlation with flow rate; in theoretical terms, the phenomena may be explained by the inability of F127 micelles to swell up at high rates due to the high surface liquid velocity, whereas at low flow rates less physical forces impede the swelling of micelles to the top, where they are carried out by the fluid.

X-ray visibility of F127 is essential for observing degradation patterns for *in vivo* conditions. F127 solutions were created accordingly with amounts of Iohexol, an FDA approved injectable iodine contrast agent². Using a high resolution X-RAY WorX imaging machine provided by VJ Technologies, we quantitatively determined the degradation pattern of the gel under flow and visualize a concentration gradient after degradation [Figure 4]. Deionized water flow was applied across the gel in the chamber for 30 minutes at 0.1 mL/min, yielding a 230 count difference between the bottom and top of the gel after 15 minutes. Visualization confirms degradation results in a concentration gradient rather than a homogeneous spread of micelles in the F127 solution. Further analysis verified that at a higher flow of 1ml/min, the degradation occurred at a much slower rate, with the water penetrating a millimeter into the gel surface, resulting in a 60 count difference after 15 minutes.

To prepare for drug delivery under flow, vancomycin stock solution (supplied by Stony Brook Hospital) was diluted to a concentration of 200µg per mL of DI water, as done so in literature,³ and added to 30 wt% F127 Solution. As before, all samples were analyzed under a Thermo Scientific UV-Vis spectrophotometer to obtain baseline spectral peaks. Flow was applied to the sample at 0.1, 0.5, 0.75, and 1 mL/min of DI water. Resultant excess output flow and gel were analyzed under and analyzed using UV spectroscopy. Through the UV-vis absorption graphs, we were able to observe the vancomycin spectral peak decrease as a function of flow.

Future research objectives consist of performing additional flow tests to solidify trends and statistically analyze current UV-Vis data, as well as possible simulations of F127 under flow using molecular dynamics software to visualize micellization vs. flow at a molecular scale and further understand the underlying the morphology and kinetics of F127, and ultimately providing key information to be incorporated into developing a (solution for FBSS).



Figure 1:
Flow chamber

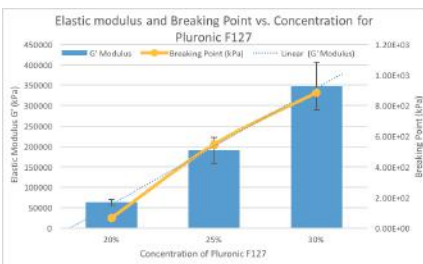


Figure 2:
Pluronic elastic modulus calibration curve

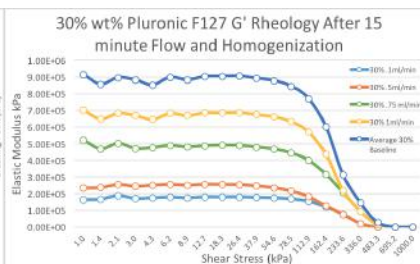


Figure 3:
F127 baseline G' vs wt%



Figure 4:
X-ray image of flow chamber

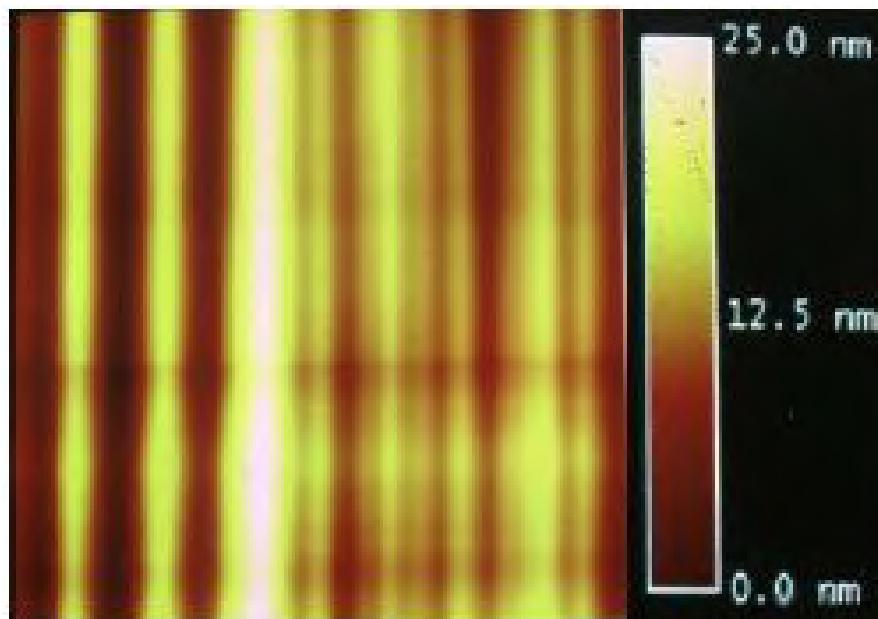
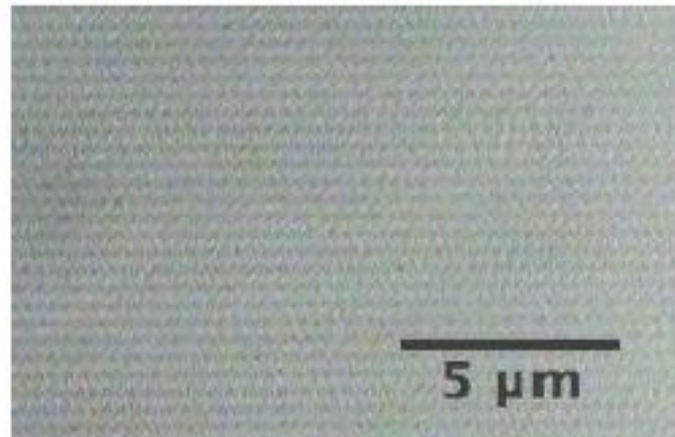
¹Hom, K., Patrizio, D., & Sugimoto, D. (2016, May). Development and Analysis of Pluronic Gels For Scar Prevention [Abstract]. Journal of Undergraduate Chemical Engineering Research, 67-74

²Lusic, H., & Grinstaff, M. W. (2013). X-ray-Computed Tomography Contrast Agents. Chemical Reviews Chem. Rev., 113(3), 1641-1666. doi:10.1021/cr200358s

³Sultana, N., Naveed, S., & Arayne, S. (2013). Development and Validation of a Simple and Efficient RPLC Method for Analysis of Captopril, Metformin, Pioglitazone and Glibenclamide in API, Formulations and Human Serum. Analytical & Bioanalytical Techniques, 04(07). doi:10.4172/2153-2435.1000257

Session VII: Separating DNA on Surfaces

Graduate Students: Julia Budassi



Utilization of Laser Interference Lithography as a Novel Method for Synthesizing Sub-micron Soft Gratings for Applying Interference Cutting Enzymes to Surface-absorbed DNA

Junyu Liang,¹ Adam Richter,² Will Burnett,³ Demian Zuric,³ Junaid Khan,³ Donald Liu,³ Julia Budassi,³ Jonathan Sokolov³

¹Guangdong Experimental High School, Guangzhou, Guangdong, China; ²Munster High School, Munster, IN;

³Dept. of Materials Science and Engineering, Stony Brook University, Stony Brook, NY

While next generation sequencing (NGS) methods hold promise for improving the current state of sequencing, all NGS methods¹ are hindered by the fact that separate DNA fragments are not sequenced in their genomic order. Previous research aimed at developing a sequencing method where the order of the DNA fragments is maintained is based on a soft lithographic technique to apply cutting enzymes to linearized DNA on surfaces.² Successful development of this method would allow for many ambiguous regions of DNA, such as areas with repeated sequences, to be more easily sequenced. This method involves slowly removing a polymethyl methacrylate (PMMA) coated silicon wafer from a solution of DNA, allowing the DNA to be stretched and aligned onto the wafer. Then, a polydimethylsiloxane (PDMS) stamp created via soft lithography and coated with a DNase 1 solution is used to cut the DNA on the surface of the wafer while maintaining its order. However, creating a PDMS stamp with soft lithography based on standard optical patterning yields strands of DNA ≥ 5 kbp, which are often too long to be effectively amplified with PCR. This study describes an alternate method, laser interference lithography, to create an enzyme coated stamp that has the ability cut DNA into smaller fragments (1-3 kbp). In this technique, the standing wave pattern that exists at the intersection of two coherent laser beams is used to expose a photosensitive layer.³

We performed a series of experiments testing different parameters to find the best way to create a pattern etched on a silicon wafer from which a PDMS stamp can be generated. After being cut and cleaned, 1cm by 1cm [100] silicon wafers were soaked in hydrofluoric acid to create a hydrophobic surface against water. Then, we spun photoresist solution (PFI-88 dissolved in propylene glycol methyl ether acetate in a 2:1 volume ratio) onto the silicon wafers at 1,750 RPM for 30 seconds. The adhesion of the photoresist to the wafer was strengthened by baking the samples at 110°C for 90 seconds. Next, the samples were exposed to a 405nm laser light using a Lloyd mirror configuration.³ After different trials, we found the best photoresist exposure time to be 122 seconds. Afterwards, we developed the grating pattern by soaking the sample in potassium hydroxide (1% by weight) for 30 seconds. The pitch of the pattern was found to be $0.41 \pm 0.04 \mu\text{m}$ (Figure 1). The grating pattern was etched into silicon wafer substrates by Reactive Ion Etching (RIE) using SF_6 as a process gas. Atomic Force Microscopy (AFM) was used to measure the surface topography of the developed photoresist pattern and the derived RIE pattern on silicon. The depth of the silicon grating was found to be $33 \pm 3 \text{ nm}$ (Figure 2), sufficiently deep to be used for producing PDMS stamps to fragment surface-absorbed DNA.

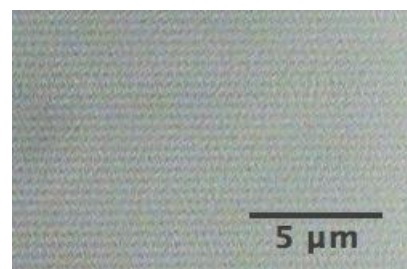


Figure 1: Developed photoresist pattern under optical microscope

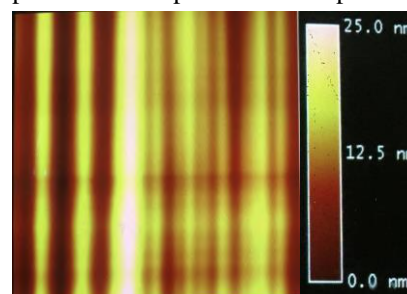


Figure 2: Etched silicon wafer pattern under AFM. Image size is 5cm by 5cm.

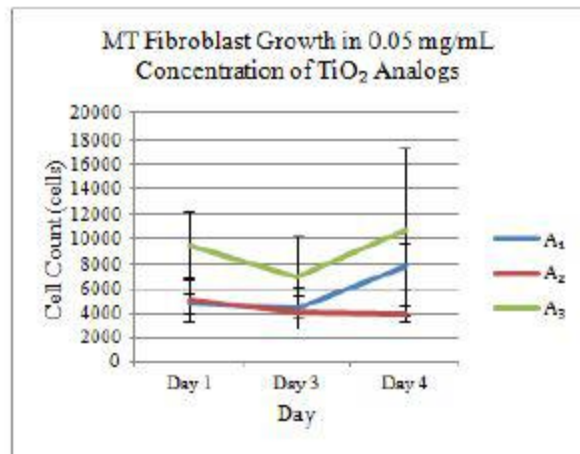
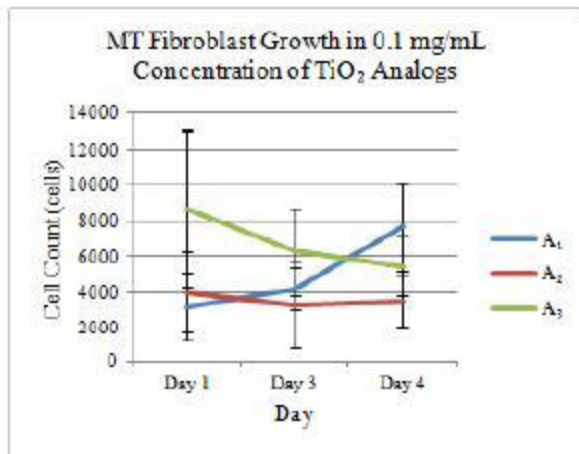
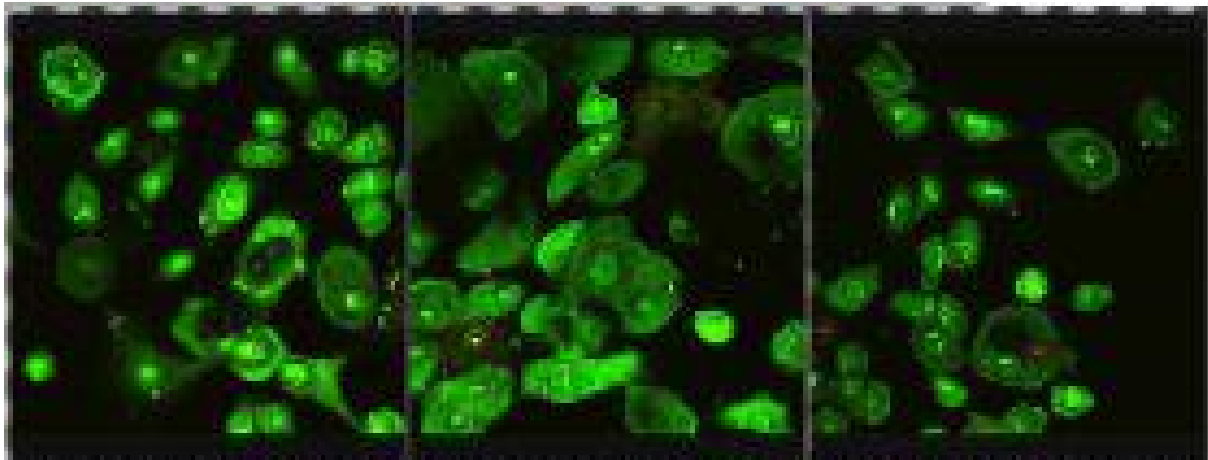
[1] Goodwin, S., McPherson, J. D. and McCombie, W. R. (2016). Coming to Age: Ten Years of Next-generation sequencing technologies, *Nature Reviews Genetics* 17, 333-351.

[2] Auerbach, A., Budassi, J., Shea, E., Zhu, K. and Sokolov, J. (2013) Controlled Enzymatic Cutting of DNA Molecules Adsorbed on Surfaces Using Soft Lithography, *Bulletin of the APS*, 58(1) and Cho, N. H., (2016) Ordered DNA Fragmentation and Amplification for Sequencing Applications, *The 5th Euro Biosensor Conference*, Valencia, Spain.

[3] Wolferen, H. V., & Abelmann, L. (2011). Laser Interference Lithography (T. C. Hennessy Pp., Ed.). In *Lithography: Principles, Processes, and Materials* (pp. 133-148). Nova Science.

Session VIII: Nanotoxicology

Graduate Students: Fan Yang, Yan Xu



The Effects of Titanium Dioxide Nanoparticle Exposure on Keratinocyte and U937 Cell Susceptibility to Bacterial Infection

Natalie Tan¹, Sharon Chao², Yan Xu³, Dr. Tatsiana Mironava³, Dr. Miriam Rafailovich³, Abigail Wax⁴
1 Herricks High School, 100 Shelter Rock Road, New Hyde Park, NY 11040 2 Stuyvesant High School, 345 Chambers Street, New York, NY 10282 3 Department of Materials Science and Engineering, Stony Brook University, Stony Brook, NY 11794 4 University of Pennsylvania, Philadelphia, PA 19104

Titanium dioxide (TiO₂) nanoparticles (NP) form a characteristic white pigment and are used in paints, inks, rubbers, cosmetics, toothpastes, sunscreens, and food products [1]. Their ubiquity in consumer products highlights their effects on human contact, specifically keratinocytes, which constitute 90% of the epidermis and act as barriers to environmental damage [2]. A past study found that 500 µg/mL UV-irradiated TiO₂ NP inhibited the growth of methicillin-resistant *Staphylococcus aureus* (*S. aureus*) isolates [1]. However, this concentration is too high for commercial use and UV radiation causes chronic damage to human skin. Moreover, TiO₂ NPs' potential as an ingredient in antibacterial creams jeopardizes humans internally, especially the immune system. U937 is a model cell line used to study monocytes, which participate in pathogenesis by engulfing microbes. *S. aureus* is a gram-positive bacteria that is found in the skin and nostrils of 20% of humans and causes an array of diseases. Thus, we hypothesized that the NP-exposed keratinocytes and U937 cells would not die but rather exhibit morphological damage and reduced cellular function as increased and decreased *S. aureus* infection, respectively.

Anatase and rutile TiO₂ NP were studied under the scanning electron microscope and characterized by zeta potential, x-ray diffraction, and dynamic light scattering for surface charge, chemical arrangement, and particle size. Keratinocytes and U937 cells were washed with DPBS and, after trypsinization, were plated in 6-well culture plates using KGM and RPMI supplemented with 10% FBS, respectively, and counted on a hemacytometer. After 24 hours of incubation, cells were exposed to 0.1 mg/mL anatase and rutile TiO₂ NP solutions and incubated again for 24 hours. Intracellular LDH levels were measured. Other cultures were infected by *S. aureus* provided by Dr. Marcia Simon, which were incubated with DMEM supplemented with 10% FBS for keratinocytes, at MOI 1000. NP-exposed bacteria-infected cells were washed with Triton X-100 and sent to Dr. Stephen Walker for colony counting or stained with LIVE/DEAD and studied under the confocal microscope.

Our results confirmed the composition of the anatase and rutile TiO₂ NP, which were approximately 100 and 20 nanometers in size, respectively. Relative to water, the surface charges of the anatase and rutile TiO₂ NP in RPMI supplemented with 10% FBS greatly decreased due to albumin adsorption and particle attraction and stability, while anatase TiO₂ NP formed larger agglomerates than their rutile counterparts. Such measurements were unable to be taken in KGM due to high instability. The U937 cell growth curve similarities compared to our control indicate that cell proliferation is unaffected by NP exposure. Anatase and rutile TiO₂ NP-exposed U937 cells ingested approximately 30% and 14%, respectively, less bacteria than our control, which suggests that NP either decrease phagocytosis and therefore cellular function or occupy space otherwise taken up by consumed *S. aureus* (**Figure 1**). However, the numbers of bacteria ingested per cell for our control and anatase and rutile TiO₂ NP-exposed keratinocytes were all less than one, and confocal micrographs illustrate a few dead cells and no internalized bacteria for the TiO₂ NP-exposed keratinocytes (**Figure 2a, 2b, 2c**). We concluded that either 24 hours of incubation with TiO₂ NP caused cell death or *S. aureus* infection instigated apoptosis, thus either centrifuging and aspirating out the supernatant, vigorous shaking and washing with DPBS, or Triton X-100 vortexing discarded of the dead cells with high infection and left only the few unaffected cells for observation.

In the future, we hope to conduct transmission electron microscopy, confocal microscopy with Alexa Fluor and Propidium Iodide staining, U937 cell differentiation to M1 macrophages, atomic force microscopy, extracellular LDH assay, and ROS measurements to assess uptake of TiO₂ NP, vacuole formation, penetration of nuclei and mitochondria, morphology, intercellular connections, specifically-functioned cell response, relative modulus, broken membranes, and oxidative stress.

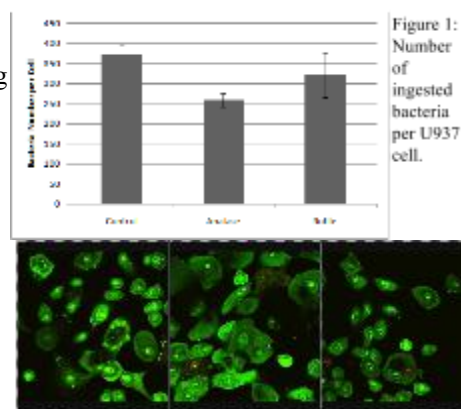


Figure 2: Confocal microscopy of LIVE/DEAD-stained a. control and b. anatase and c. rutile TiO₂ nanoparticle-exposed keratinocytes.

1. Jesline A, John NP, Narayanan PM, Vani C, Murugan S. 2015. Antimicrobial activity of zinc and titanium dioxide nanoparticles against biofilm-producing methicillin-resistant *Staphylococcus aureus*. *Applied Nanoscience* 5:157-162.
2. 7. McGrath JA; Eady RAJ; Pope FM. (2004). "Anatomy and Organization of Human Skin". In Burns T; Breathnach S; Cox N; Griffiths C. *Rook's Textbook of Dermatology* (7th ed.). Blackwell Publishing. p. 4190.

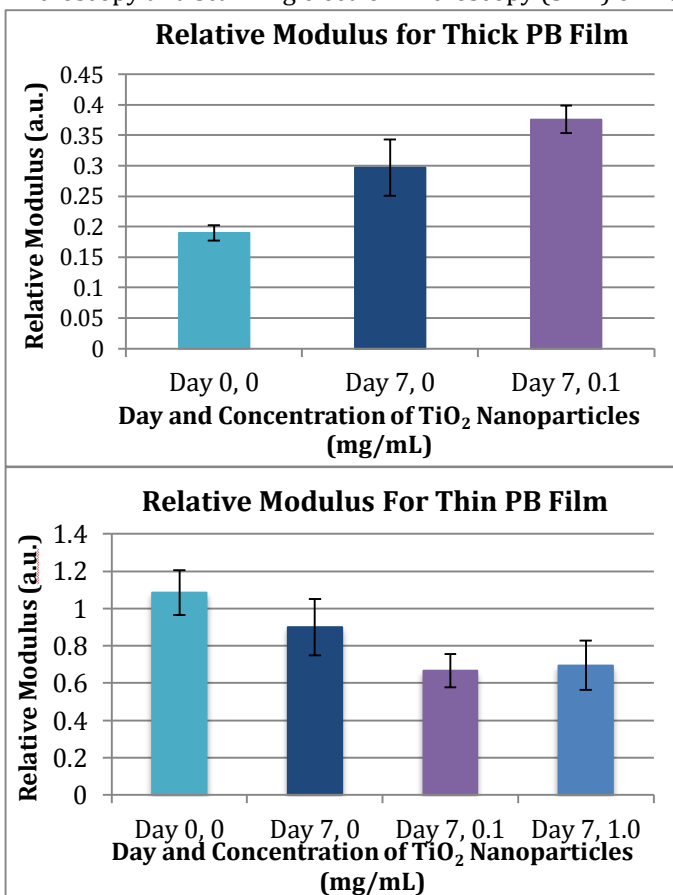
The Effects of Different Concentrations of TiO₂ Nanoparticles on Dental Pulp Stem Cells (DPSCs) Plated on Thin and Thick Polybutadiene Films

Vaidehi Patel, Half Hollow Hills High School East
Ya-Chen Chuang, Stony Brook University

Titanium Dioxide nanoparticles are used in bone implants, as well as in dental implants due to their mechanical properties as well as their good biocompatibility. Previous studies, however, have shown that TiO₂ nanoparticles at higher concentrations have an adverse effect on mesenchymal stem cells (MSCs)¹.

DPSCs (strain AX3) were plated onto HF-etched silicon wafers (1 cm x 1 cm), which had been spun cast with two different concentrations of polybutadiene in toluene: 3 and 20 mg/mL. On Day 0 (before the nanoparticles were added), cell count was taken using a hemacytometer, and atomic force microscopy (AFM) was also done to measure the relative modulus of the DPSCs. On Day 1, three concentrations of the TiO₂ nanoparticles were added to the cells: 0, 0.1, and 1.0 mg/mL. On Days 2, 5, and 7, cell count was done using the hemacytometer, and on Day 7, AFM was done. Afterwards, the cells were stained with Alexa Fluor 488 Phalloidin and DAPI, dilactate in order to see the actin and DNA, respectively, when performing confocal microscopy on the cells.

As seen in Figure 1 and 2 below, analysis of the AFM from Days 0 and 7 shows that after adding the nanoparticles, the relative modulus for the cells on the thin film becomes softer, and the relative modulus for the cells on the thick film becomes harder. It still isn't clear as to why this phenomenon occurred; further research into this area is needed. Below, Figure 3 shows the results of the cell count from Days 0, 2, 5, and 7. The graph shows that as the concentration of TiO₂ increases, the negative effects on the DPSCs seems to increase. In fact, after Day 5, the nanoparticles really seem to start to have an adverse effect on the cells, as the DPSCs continuously decrease. In addition, it seems that the thin or thick polybutadiene films do not seem to make a significant difference in their impact on DPSC growth. As for future research, we still have to conduct confocal microscopy and scanning electron microscopy (SEM) on Day 21, as well as further data analysis.



Figures 1 and 2: These graphs depict the results of the AFM from DPSCs on both thick and thin polybutadiene (PB) films.

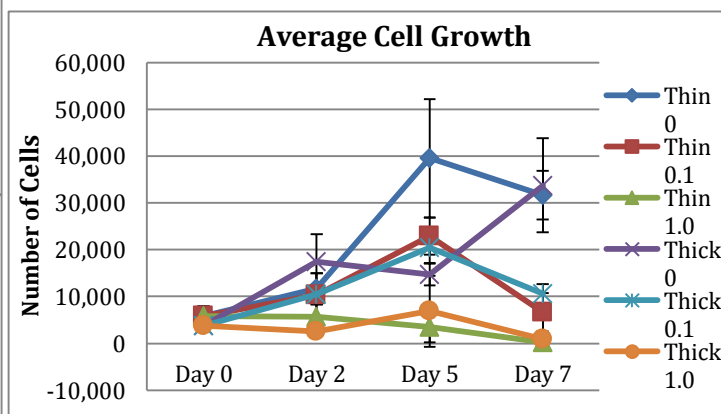


Figure 3. This graph depicts the change in the number of DPSCs over the course of 8 days.

1. Cai, K., Hou, Y., Li, J., Chen, X., Hu, Y., Luo, Z., ... Lai, M. Effects of Titanium Nanoparticles on Adhesion, Migration, Proliferation, and Differentiation of Mesenchymal Stem Cells. *International Journal of Nanomedicine*. 2013; 8.

Evaluating the Cytotoxic Response of Adult Human Dermal Fibroblasts to Hybrid Bismuth Oxyhalides of Varying Concentrations

Michael Peng¹, Fan Yang², Dr. Miriam Rafailovich², Dr. Tatsiana Mironava²

¹Campbell High School, Smyrna, GA, 30080; ²Department of Materials Science & Engineering, Stony Brook University, Stony Brook, 11790

Titanium dioxide (TiO₂) nanoparticles are known for their prevalence in a vast range of products such as cosmetics, paper, and paints in addition to their ability to be used as photocatalysts^[1]. However, their wide range of distribution raises questions as to their potential health effects. Studies have suggested that TiO₂ nanoparticles actually maintain a multitude of deleterious effects on organisms, causing respiratory tract cancer in rats and even inducing apoptosis in certain cell lines. In recent years, hybrid bismuth oxyhalides (BiOCl_xBr_{1-x}) have been suggested as a possible replacement for titanium dioxide both as a photocatalyst under visible light and as a possible technology for removing organic contaminants like toluene, benzene, and xylene from water^[2,3]. The purpose of this project was to determine whether three distinct variants of these materials (3% Bi⁰ doped BiOCl_{0.8}Br_{0.2}, 3% Bi⁰ doped BiOCl_{0.2}Br_{0.8}, and BiOCl_{0.8}Br_{0.2}), as TiO₂ analogs, possessed cytotoxic characteristics similar to those of titanium dioxide nanoparticles.

To test this, adult human dermal fibroblasts were plated in high-glucose DMEM, and the size of the particles was measured. After 24 hours of incubation, the cells were washed in DPBS, trypsinized, centrifuged, resuspended, and plated again into six 24-well plates, after which they were exposed to 0.8 mg/mL, 0.2 mg/mL, 0.1 mg/mL, and 0.05 mg/mL of each of the three TiO₂ analogs. Cell concentration in each of the test groups was measured over the course of six days with a hemocytometer to generate growth curves later compared to that of a control group grown in the same media without the analogs. After the 0.8 mg/mL and 0.2 mg/mL concentrations of all three materials were revealed to be quite toxic to the fibroblasts, six new batches of cells were plated in 0.1 mg/mL and 0.05 mg/mL concentrations of each of the analogs and later fixed with 3.7% formaldehyde for confocal microscopy to find any possibly morphological differences between cells exposed to the particles and cells without the particles. Additionally, after 3 days of exposure, two of the 24-well plates were washed with DPBS and plated into media without microparticles to evaluate cell recovery.

Our preliminary measurements indicate that the analogs' particles were all on the micro scale. Current results for the growth curves show that nearly all of the cells were killed by the 0.8 mg/mL and 0.2 mg/mL concentrations and that even the 0.1 mg/mL and 0.05 mg/mL concentrations were toxic to some degree. Cell concentration in these test groups remained relatively the same or even dropped over the course of three days (**Figure 1**), suggesting that the cells were dying relatively quickly following exposure. Even considering the large margin of error present in the data, the control group grew at a significantly more rapid rate than the analog-exposed cells. Due to the constraint of time, results for recovery and confocal microscopy have yet to be obtained. However, in the future, we would like to test even lower

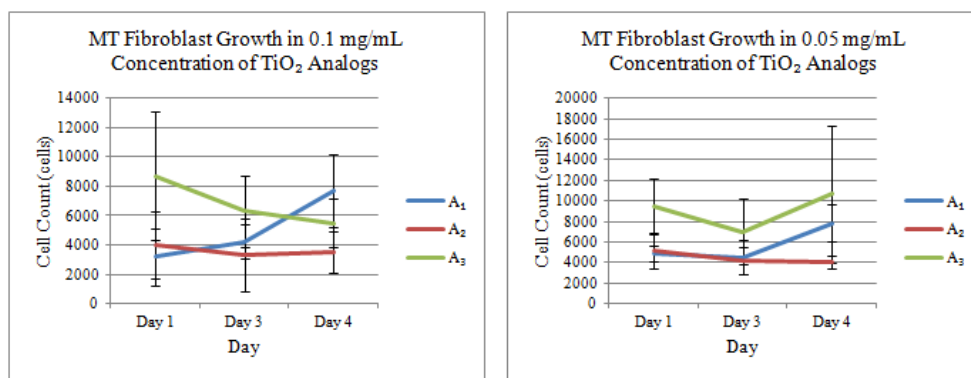


Figure 1. Growth curves for 0.1 mg/mL and 0.05 mg/mL concentrations

concentrations of the analogs and to compare their toxicity to corresponding concentrations of TiO₂.

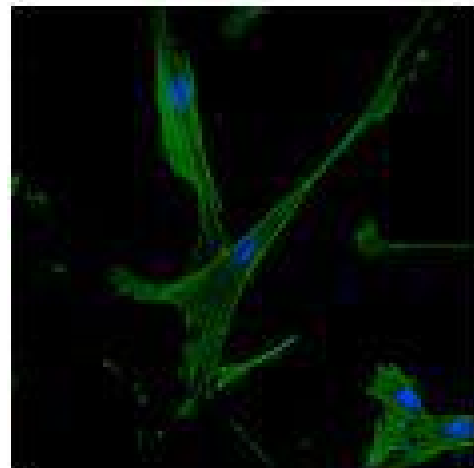
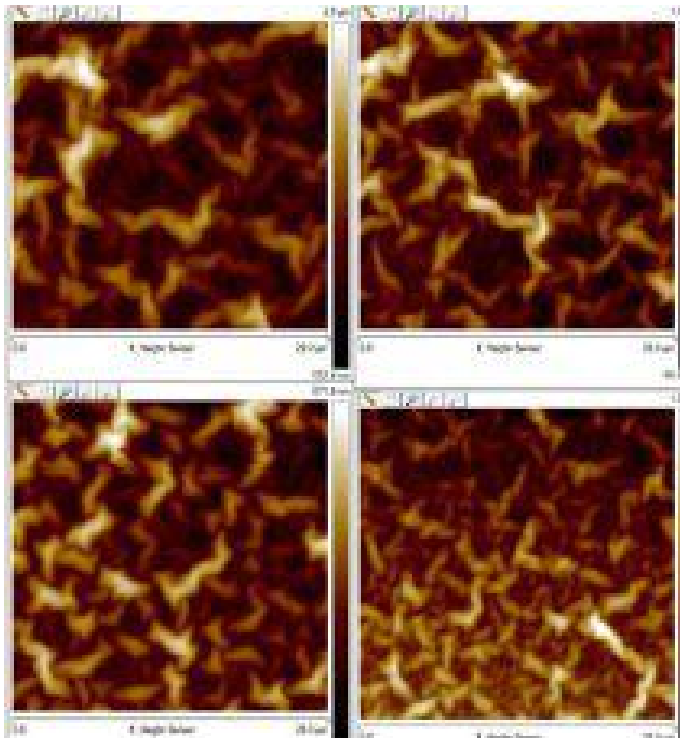
[1] Iavicoli, I., Leso, V., Fontana, L., & Bergamaschi, A. (2011). Toxicological Effects of Titanium Dioxide Nanoparticles: A Review of *in vitro* Mammalian Studies. *European Review for Medical and Pharmacological Sciences*, 15, 481-508.

[2] Gnyayem, H., Uvarov, V., Lahad, O., & Sasson, Y. (2015). Hybrid Bismuth Oxyhalides@Gypsum as Self-Cleaning Composites: Novel Aspects of Sustainable Photocatalytic Technology for Solar Environmental Cleanup. *RSC Advances*, 5, 66650-66656.

[3] Gnyayem, H., & Sasson, Y. (2015). Nanostructured 3D Sunflower-Like Bismuth Doped BiOCl_kBr_{1-x} Solid Solutions with Enhanced Visible Light Photocatalytic Activity as a Remarkably Efficient Technology for Water Purification. *The Journal of Physical Chemistry*, 119, 19201-19209.

Session IX: Cells on Natural and Electrospun Fibers

Graduate Students: Linxi Zhang, Kao Li, Vincent Ricotta



Effects of Cancerous Extracellular Matrix on Healthy Keratinocytes

Oliver Xu^{1,2}

Collaborators: Ya-Chen Chuang¹, Dr. Miriam Rafailovich¹, Dr. J. Sokolov¹

¹Garcia Program, Stony Brook University, 100 Nicolls Road, Stony Brook, NY 11790

²Edina High School, 6754 Valley View Road, MN 55439

The extracellular matrix (ECM) plays a role in regulating numerous cellular processes, whether through direct or indirect means. While usually highly regulated during the processes of embryonic development and organ homeostasis, the ECM becomes abnormal during diseases such as cancer. Such abnormal ECM may play a role in tumorigenesis, having been shown to be a direct factor in cellular transformation and metastasis¹. Cell elastic modulus is a fair indicator of cell physiology; lower elastic modulus has been linked to cancer². The purpose of the present study was to investigate the changes that resulted in healthy keratinocytes (DO33) when grown on the ECM of tumorous keratinocytes (SCC13), with a particular focus on elastic modulus and ECM morphology.

The ECM was created by first culturing cells over a spun-cast thin film of sulfonated polystyrene (SPS) at a density of approximately 60,000 cells per well. Once the ECM had been established, cells were killed by replacing culture media with phosphate buffered saline, and allowed to detach from the substrate. With the ECM isolated, an atomic force microscope was used to characterize the ECM fibers of both the cancer cells and the healthy cells. Regular keratinocytes were then plated onto the cancerous ECM samples, as well as ECM from healthy keratinocytes and SPS thin film as a control, at the same density of 60,000 cells per well. After 144 hours, the keratinocytes were taken to be examined via AFM.

The results indicated that cancerous ECM had altered morphology, with cancerous ECM having thinner ECM fibers (Figure 2). In addition, keratinocytes grown on the cancerous ECM had slightly lower relative elastic modulus compared to keratinocytes grown on healthy cell ECM, and a lower relative modulus compared to keratinocytes grown on SPS thin film (Figure 1). Similarly, the ECM developed by the healthy keratinocytes grown on cancerous ECM reflected slight morphological differences from the ECM developed by keratinocytes grown on healthy keratinocyte ECM or just bare SPS (Figure 2). Confocal microscopy of the keratinocytes is pending, and future research would include more testing to determine if the differences between the relative elastic modulus of the cells grown on different substrates are significant.

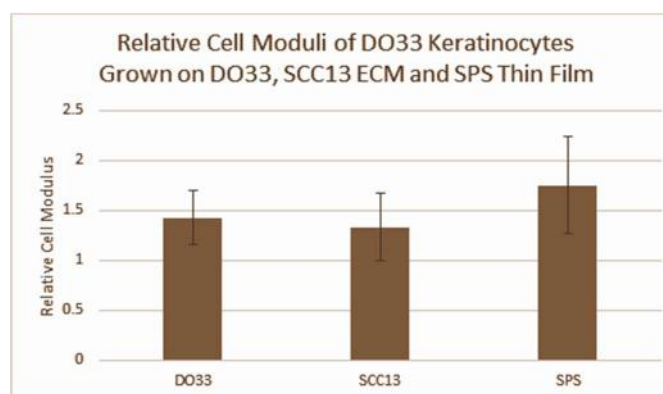


Figure 1. Relative elastic modulus of DO33 cells grown on various substrates.

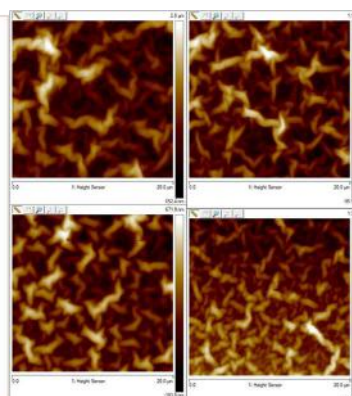


Figure 2. Counterclockwise from top right: AFM height sensor measurements of ECM of DO33 grown on SCC13 ECM, DO33 ECM, and SPS thin film; SCC13 ECM (bottom-right) for reference.

¹ Lu, P., Weaver, V., Werb, Z. (2012). The extracellular matrix: A dynamic niche in cancer progression. *Journal of Cell Biology* 196(4):395

² Pernodet, N., Jurukovski, V., Fields, J., Fields, A., Ramek, A., Tmirnav, T., Ghosh, K., Bernheim, T., Hall, K., Ge, S., Slutsky, L., Dorst, K., Simon, M. and Rafailovich, M. (2008). Detecting Cancer Cells in Normal Tissue by Scanning Force Modulation Microscopy. *Microscopy and Analysis* 22(2):5-8.

The Effect of Sulfonated Polystyrene and Graphene Oxide/Reduced Graphene Oxide Functionalized with Gold and Silver Nanoparticles on the Extracellular Matrices of Fetal Bovine Serum, Fibrinogen, and Dental Pulp Derived Cells

Rachel Sacks¹, Gila Schein¹, Rebecca Isseroff², Vincent Ricotta³, Dr. Miriam Rafailovich³

¹Hebrew Academy of the Five Towns and Rockaway, Cedarhurst, NY 11516

²Lawrence High School, Cedarhurst, NY 11516

³Stony Brook University, Stony Brook, NY 11794

The first step in tissue development revolves around the adsorption and organization of the extracellular matrix (ECM) proteins, such as, fibronectin and collagen. Therefore, advances to be made in tissue engineering are reliant on the interactions of cells with the ECM proteins. Previously, it was found that sulfonated polystyrene surfaces (SPS) stimulated the transition of fibronectin from monolayer to multilayer adsorption and that distinct protein networks were formed due to the increase in surface charge density, or the increase in negative charge from the available sulfonate ions provided by the SPS.¹ Here we seek to introduce SPS to our graphene oxide (GO) and reduced graphene oxide (rGO) metal salt solutions to observe whether the solutions have an effect on the lattice structures of the serum and ECM proteins. Thus far, these changes have been analyzed in protein media and will soon expand to pure fibrinogen and dental pulp derived cells.

GO was produced from graphite using a modified Hummers' method. We then functionalized GO with silver and gold nanoparticles by adding gold and silver salts in different concentrations, stirring overnight, and then reducing each using 20 mmol sodium borohydride, creating 10 different metal-reduced graphene oxide (rGO) samples. After drying and weighing, we created 3% solutions in SPS with a 33% degree of sulfonation, using DMF as the solvent. Each sample was dried on slides for Raman Spectroscopy and Scanning Electron Microscopy (SEM) to analyze the differences in the chemical disorder of the samples and to observe the size and distribution of nanoparticles, respectively. The rest of the solutions were spin casted onto Silicon wafers and annealed at 175 °C and 10 mTorr for 3 days. 3 wafers were cut for each of the 11 samples, where 2 were incubated with the 10% FBS protein serum and 1 was used to analyze polymer surface morphologies with the Atomic Force Microscope (AFM). The 22 wafers and serum were incubated at 37 °C, 5% Carbon Dioxide and 100% humidity. After 48 and 240 hours of incubation, the samples were removed from the serum media and analyzed under the AFM to measure the morphology of the adsorbed proteins. Using a scan size of 50x50 μm for the images, topographies of the samples and heights of the adsorbed proteins were compared. Protein structures were found to differ between the reduced and non-reduced graphene oxide solutions and between the silver and gold metalized solutions, as displayed in **Figure 1**.

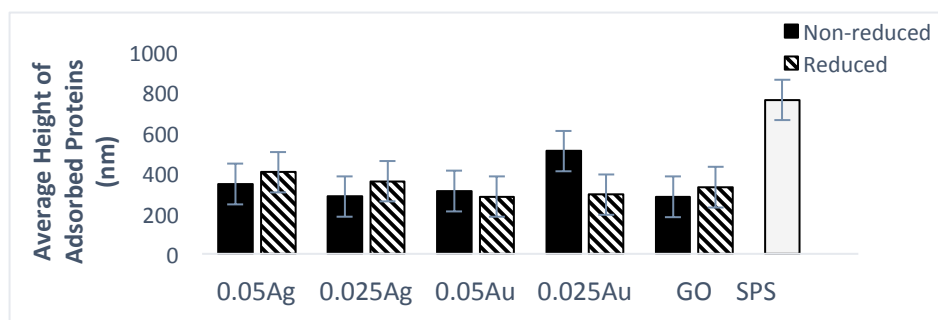


Figure 1. Different heights of the adsorbed proteins as observed with the AFM.

¹ Pernodet, N., Rafailovich, M., Xu, D., Yang, N-L., McLeod, K.(2003). Fibronectin Fibrillogenesis on Sulfonate Polystyrene Surfaces. *Wiley Periodicals, Inc.*, 64A(4), 684-692. doi: 10.1002/jbm.a.10394

A Comparison of the Biological and Mechanical Properties of Poly(4-Vinylpyridine) and Polystyrene Tissue Culture Plastic

Ben Davidson, Campbell High School, Marietta, GA
Linxi Zhang, Stony Brook University, Stony Brook, NY

Polystyrene, while useful for the manufacture of standard cell tissue culture plastic for its strength and inexpensiveness, is hydrophobic¹, leading to cell clumping and inadequate attachment to the surface of non tissue culture treated plates. With this in mind, the goal of this experiment was to compare the biological and mechanical properties of the polymer poly(4-vinylpyridine) (P4VP) and the polystyrene used in tissue culture plastic, the two of which are similar to each other. If P4VP, a similarly-priced material, proves to be equally or more strong than polystyrene and more conducive to cell growth, then it will be this group's recommendation to use P4VP, when appropriate, in the manufacture of tissue culture plastic.

The polystyrene used was of MWT 280 000 and the P4VP of MWT 150 000 – 200 000. Data collected on P4VP would be compared to known values for polystyrene, so in order to determine the concentration of P4VP most similar to the polystyrene used, solutions of P4VP dissolved in N,N-Dimethylformamide, 99.8% Anhydrous (DMF) were prepared at concentrations 1, 3, 5, 7 mg/mL. Solutions were spin-casted (at 2500 rpm, 1000 rpm/s, 30 s) on silicon wafers (two per concentration) and analyzed with ellipsometry to determine the concentration whose film thickness was closest to that of polystyrene. The 7 mg/mL concentration had average thickness of about 336 Å, quite close to polystyrene's approximately 330 Å, and so was selected for use in the rest of this experiment. A greater quantity of the solution was made and spin-casted on 30 silicon wafers (rinsed and washed appropriately) before being annealed for 8 hours at 150°C. These wafers were used to monitor the growth of fibroblast and endothelial cells, addressed later.

For mechanical testing, two samples of each material were prepared for rheology. The rheometer showed that polystyrene was about twice as strong as P4VP – however, the operator of the rheometer, Clement Marmorat, noted that as most all data points were in the order of magnitude of megapascals and that the samples were approximately solid at room temperature, rheology was a not very useful test. So, a tensile strength test was performed, which yielded that P4VP is about 151% as strong as polystyrene. Atomic force microscopy showed that on P4VP, endothelial cells were about 15% stiffer than on polystyrene, and fibroblasts were about 20% stiffer than on polystyrene.

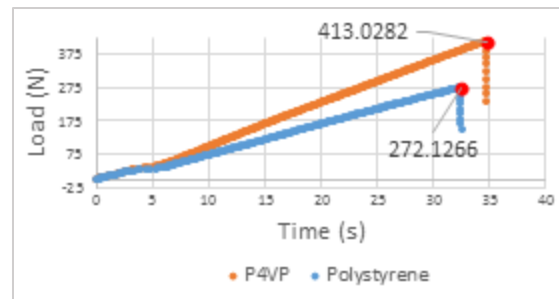


Figure 1: Tensile Strength

For biological testing, endothelial cells and fibroblasts were prepared in media and their growth monitored, with proper procedure for cell fixing and media change, for seven days. A confocal microscope was used to take pictures of cell growth on P4VP and polystyrene tissue culture plastic on days three and five. Two different densities of cells, 5000 per well (density one) and 10000 (density two) per well, were used for comparison. Cell counts revealed that on the whole, P4VP offered significant advantages over polystyrene for cell growth. For day three cells, P4VP changed cell growth, on average, by a factor of 0.487 and 1.560 for endothelial cells of densities one and two, respectively; by a factor of 2.098 and 1.779 for fibroblasts of densities one and two, respectively. For day five cells, P4VP changed cell growth, on average, by a factor of 1.119 and 1.298 for endothelial cells of densities one and two, respectively; by a factor of 0.345 and 0.493 for fibroblasts of densities one and two, respectively.

The experiment shows generally positive results for the proposal to replace polystyrene tissue culture plastic with P4VP. For future testing, it is advised to gather further samples and trials on cell growth as to confirm that P4VP increases cell growth by a significant factor in most cases. It may also be beneficial to confirm this with different types of cells over longer periods of time, depending on the type of research being performed.

¹ Faghiehnejad, A., & Zeng, H. (2012, January 27). Hydrophobic interactions between polymer surfaces: Using polystyrene as a model system. *Soft Matter*, (9), 2746-2759. doi:Hydrophobic interactions between polymer surfaces: using polystyrene as a model system

Effects of Electrospun P4VP Fiber Structure and Thin Film Composition on the Biom mineralization and Proliferation Rate of Dental Pulp Stem Cells

Mark Choi¹, Hong-Hsuan (Shannon) Chen², Linxi Zhang³, Miriam Rafailovich³

¹Mission San Jose High School, Fremont, CA 94539

²Saratoga High School, Saratoga, CA 95070

³Stony Brook University, Stony Brook, NY 11790

As the bioengineering field technologically advances, there has been increasing interest in dental pulp stem cells (DPSCs) as a method of dental tissue regeneration¹. DPSCs, which are multipotent and extensively proliferate, have been revealed as optimal for tissue reconstruction due to their relative accessibility and efficiency of extraction². This study evaluated the effect of different P4VP morphologies on the proliferation and differentiation of human dental pulp stem cells. A P4VP thin film was prepared as the control substrate, while P4VP/3% graphene and P4VP/3% graphene oxide thin films were tested to study the effect of these materials on stem cell differentiation. Different P4VP fiber diameters were obtained by varying the concentration of P4VP, with 17%, 25%, 30%, and 35% wt P4VP in 3mL DMF/ethanol solutions that had a 5:1 DMF:ethanol weight ratio. Well plates were prepared for 1, 4, and 7-day analysis in order to study cell proliferation and cell modulus. The effect of dexamethasone in cell media was studied by preparing two different plates for final 28-day analysis.

SEM images were taken to determine the diameter of the P4VP fibers (Figure 1). Confocal microscopy of 40x magnification was performed to view cell morphology, where the comparison of DPSCs growing on P4VP fibers with those growing on P4VP thin film reveals that the DPSCs grow linearly along the fiber structures (Figure 2). Cell counts from confocal microscopy images indicate that cells growing on P4VP thin film proliferated the least, while DPSCs on 25%wt P4VP microfibers and GO and G thin films proliferated the most (Figure 3). AFM results from the day 7 samples show an increase of cell modulus as concentration of P4VP solution increases, indicating the cells become stiffer as a result of the decreasing curvature of fibers (Figure 4). This holds true for the P4VP thin film, which resulted in the highest cell modulus. However, the cell modulus was lowest for the P4VP/GO and P4VP/G thin films, suggesting that the DPSCs responded to the GO and G additives.



Figure 1 3000x magnification of 35%wt P4VP fibers

After 28 days of incubation, SEM images with EDX will be taken to analyze the biom mineralization of DPSCs on each thin film and fiber substrate. Confocal images will also be taken to check cell protein expression.

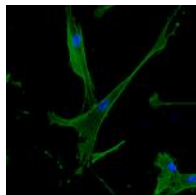


Figure 2
40x magnification of Day 1 DPSCs on 25%wt P4VP fibers.

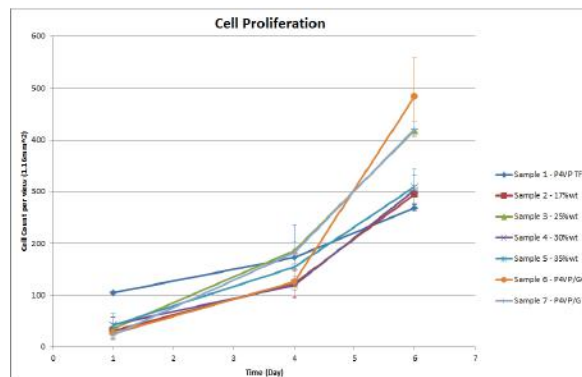


Figure 3
Proliferation of DPSCs on different substrates.

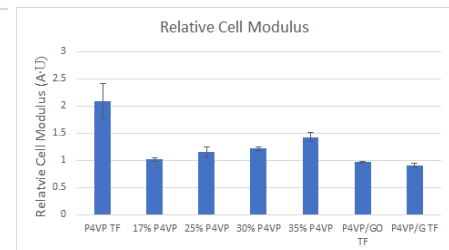


Figure 4
Relative cell modulus of DPSCs growing on different substrates, measured with AFM.

¹Dannan, A. (2009, June). Dental-derived Stem Cells and whole Tooth Regeneration: An Overview. *Journal of Clinical Medical Research*, 1(2), 63-71. doi:10.4021/jocmr2009.03.1230

²Graziano, A., d'Aquino, R., Laino, G., Papaccio, G. (2008). Dental pulp stem cells: a promising tool for bone regeneration. *Stem Cell Review*, 4(1), 65. doi: 10.1007/s12015-008-9013-5

The Effect of Fibronectin and P12 on Human Dermal Fibroblast Migration on PLA and PMMA Fibrillar Substrates

Tiffany Ding¹, Miriam Radinsky², Kao Li³, Miriam Rafailovich³

¹Emma Willard School, Troy, NY, ²Yeshiva University High School for Girls, Holliswood, NY, ³Stony Brook University, Stony Brook, NY

Dermal fibroblasts play a critical role in wound healing by depositing new extracellular matrix (ECM) in damaged areas. Consequently, facilitating the migration of dermal fibroblasts to sites of wound healing is a worthwhile topic of research. Previously, fibronectin-coated poly (methyl methacrylate) (PMMA) fibers were tested as a cell migration substrate.¹ However, polylactic acid (PLA) is known to have greater biocompatibility and was investigated as a cell migration substrate in this study.² Fibronectin is a glycoprotein that helps cells bind to collagen fibers in the ECM, and this study examined the effect of fibronectin on cell migration on PLA substrates. Additionally, the effect of a recently identified fibronectin-derived peptide that promotes cell survival, known as P12, was investigated.³

To test the viability of PLA fibers as a cell substrate, human dermal fibroblasts were cultured in medium and plated on 2 μm and 4 μm PLA fibers, with PLA thin film as a control. The cells proved to be capable of surviving on these substrates, and cell migration tracking using a MetaMorph-operated CoolSNAP HQ camera attached to a Nikon Diaphot-TMD inverted microscope showed that cells moved faster on the fibrillar surfaces. There was no significant difference between cell migration rates on the 2 μm and 4 μm fibers, so the 4 μm fibers were chosen for use in subsequent experiments due to their more consistent fiber diameter.

In order to determine the effect of fibronectin on cell migration, PLA substrates, both with and without fibers, were incubated in 30 $\mu\text{g/ml}$ fibronectin solution for 2 hours. Cells were suspended in agarose gel and deposited as a droplet in the center of each substrate. Cell migration was then monitored for 3 days using the aforementioned method. The results shown in Figure 1 indicate that the fibronectin initially increased cell migration rates on the PLA thin films, but not on the PLA thin films and fibers. With extended incubation, cell migration rates on the PLA thin films and fibers with fibronectin increased, while migration rates on the other substrates did not show significant change. However, cells on the PLA thin film and fibers with fibronectin did not show a preference for the fibers, so it is possible that fibronectin interactions with PLA fibers caused mechanical stretching of the fibronectin that decreased its integrin binding affinity.⁴ As a potential solution, ultraviolet-ozone surface treatment will be applied to the PLA fibers to increase their hydrophilicity, thereby increasing cell-fiber compatibility.

Following this procedure, the effects of P12 on cell migration on fibronectin-coated PMMA fibers were tested. 1mL 10 μM P12 was added to the cell medium before tracking the cell migration over 4 days. A sample without P12 acted as the control. The results demonstrate that P12 increases cell migration on fibronectin-coated PMMA substrates (Figure 2).

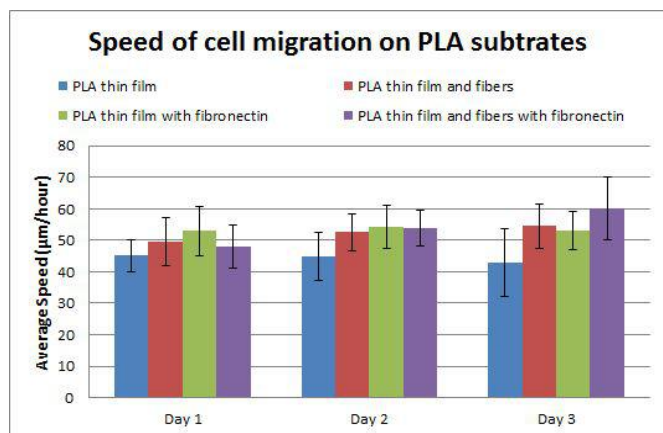


Figure 1. Cell migration rates on PLA substrates

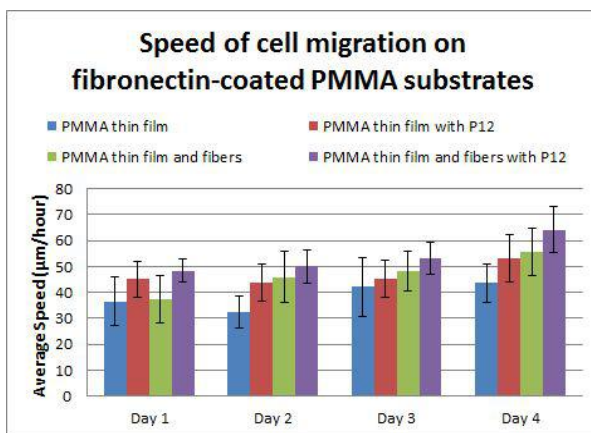


Figure 2. Cell migration rates on PMMA substrates

¹ Liu, Y., Franco, A., Huang, L., Gersappe, D., Clark, R. A., Rafailovich, M. H., Control of cell migration in two and three dimensions using substrate morphology. *Experimental Cell Research*, 315, 2544-2557. doi:10.1016/j.yexcr.2009.05.013

² Jahno, V. D., Ribiero, G. B., Santos, L. A., Ligabue, R., Einloft, S., Ferreira, M. R., Bombonato-Prado, K. F. (2007). Chemical synthesis and *in vitro* biocompatibility tests of poly (L-lactic acid). *Journal of Biomedical Materials Research*, 83A, 209-215. doi:10.1002/jbm.a.31210

³ Lin, F., Zhu, J., Tonnesen, M. G., Taira, B. R., McClain, S. A., Singer, A. J. (2013). Fibronectin Peptides that Bind PDGF-BB Enhance Survival of Cells and Tissue under Stress. *Journal of Investigative Dermatology*, 134, 1119-1127. doi:10.1038/jid.2013.420

⁴ Kramer, A., Craig, D. Thomas, W. E., Schulten, K., Vogel, V. (2002). A structural model for force regulated integrin binding to fibronectin's RGD-synergy site. *Matrix Biology*, 21, 139-147. doi:10.1016/S0945-053X(01)00197-4

GARCLA 2K16

Nicholas Zumba
 Justin Ng
 Kiran Shetty
 Antonis Camero
 Jesse Beatt
 Zhenhua Yang
 Nishant
 Helen Lin
 Yuyao Woo
 Paul the more
 Heron Habibi
 Sukrit Arora
 Alice
 William
 Susan Shukkar
 Bengov
 Michael Tang
 Shi Patel
 Aviva R. Samchou
 110925 1 2 2 2 16
 SHANNON CHEN
 Jon Scholov
 Allen Green
 Zvi Heimerwitz
 Bill Chen
 Miriam
 Ashwin Awasthi
 Josh Blaut
 Gila Schein
 Miriam Radinsky
 Rachel Sacks
 Aline Zh
 SHARON S HUANG
 Eric Han
 Benjamin George
 Ker de
 Yurkiatovich
 Jennifer Yu
 Peyton Michael Kao
 Janna Bukasi
 Winnie Hu
 Kamin
 Ryan
 Michael Kao
 Alex. Xu.
 Boana Mendon
 Alan W
 I 王浩浩
 81
 me sm 2016
 9 55
 7.0
 30
 (유중우)

We gratefully acknowledge support from:
 The National Science Foundation (NSF-Inspire Program)
 The Louis Morin Charitable Trust
 Crew of Osprey Fishing Fleet

